Thermoelectric transport in density-modulated two-dimensional electron gases

Der Fakultät für Physik
der Universität Duisburg-Essen
vorgelegte Dissertation
zur Erlangung des Grades
„Doktor der Naturwissenschaften“
von

Stephan Rojek, M.Sc.

Referent: Prof. Dr. Jürgen König
Korreferent: Prof. Dr. Tero Heikkilä
Disputation am 16.05.2018

Zusammenfassung

Longitudinale und transversale thermoelektrische Eigenschaften werden in verschiedensten strukturierten zweidimensionalen Elektronengasen analysiert. Um die thermoelektischen Charakteristiken, wie den Seebeck-Koeffizienten, zu untersuchen, wird oft auf einen Temperaturgradienten zurückgegriffen, der durch Joulsche Wärme erzeugt wird. In dem Fall heizt ein Strom lokal die Elektronen in dem zweidimensionalen Elektronengas. Durch Energiediffusion ist die Ortsabhängigkeit der Temperatur nicht trivial. In dieser Arbeit fokussieren wir uns auf Strukturen, deren Dimension mit der Energiediffusionslänge vergleichbar ist, und behandeln mesoskopische Eigenschaften der thermoelektrischen Spannung. Die Abhängigkeit von Systemlängen im Vergleich zu der Energiediffusionslänge wird im Detail analysiert. Wir diskutieren die thermoelektrischen Transporteigenschaften im Rahmen eines diffusiven thermischen Modells und studieren Situationen, in denen die Energiediffusionslänge und ihre Energieabhängigkeit gemessen werden kann. Diese Beschreibung basiert auf einer Quasigleichgewichts-Verteilungsfunktion mit ortsabhängiger Temperatur und ortsabhängigem chemischen Potential. Die thermoelektrischen Transportkoeffizienten werden in niedrigster Ordnung der Sommerfeld-Entwicklung bestimmt. In dieser Arbeit wird auch der Zusammenhang zu aktuellen Experimenten hergestellt, bei denen mesoskopische Effekte eine wichtige Rolle spielen.

Der Quasigleichgewichtsansatz innerhalb des diffusiven thermischen Modells ist ausreichend, solange die Energie, die durch die Elektronentemperatur repräsentiert wird, viel kleiner ist als die Fermi-Energie. Allerdings gibt es Situationen, in denen das Modell verallgemeinert werden muss, um die thermoelektrische Spannung angemessen zu beschreiben. Daher ist es wichtig, die Beiträge des Nichtgleichgewichts zur Verteilungsfunktion der Elektronen systematisch zu verstehen. Diese Arbeit präsentiert eine analytische Methode, diese Nichtgleichgewichtsbeiträge zu berechnen. Hierfür wird die Boltzmann-Gleichung mit einer Entwicklung in Energiemomente im Sinne von hydrodynamischen Gleichungen analytisch gelöst. Eine effektive Gleichung wird hergleitet, die sowohl elastische als auch inelastische Streuprozesse in einer Relaxationszeit-Approximation berücksichtigt. Die Nichtgleichgewichtsbeiträge zum elektrochemischen Potential werden im Rahmen einer systematischen Sommerfeld-Entwicklung berechnet. Entsprechend wird nicht nur das Äquivalent zum Temperaturprofil bestimmt, sondern auch die Profile höherer Energiemomente. In der niedrigsten Ordnung der Sommerfeld-Entwicklung ist die verallgemeinerte Theorie äquivalent zum Quasigleichgewichtsansatz. Allerdings verändert bereits die erste Korrektur die Mott-Formel für den Seebeck-Koeffizienten. Selbst für niedrige Temperaturen kann diese Korrektur signifikant sein, wenn die Elektronendichte durch externe Potentiale reduziert wird. Darüber hinaus erlaubt eine systematische Behandlung der Energiemomente ein besseres Verständnis der Transporteigenschaften im Nichtgleichgewicht, welches für mesoskopische Strukturen, wie diejenigen, die hier behandelt werden, essentiell ist.

Summary

Longitudinal and transverse thermoelectrics have been analyzed in various structured two-dimensional electron gases. To study the thermoelectric characteristics such as the thermopower, a temperature gradient often relies on Joule heating, where a current heats the electrons of the two-dimensional electron gas locally. Due to energy diffusion, the spacial dependence of the temperature is not obvious and it is challenging to access it experimentally. In this thesis, we focus on devices where the device dimensions are comparable to the energy diffusion length and study mesoscopic features of the thermoelectric voltage. The dependence on the device dimensions in comparison to the energy diffusion length is analyzed in detail. We discuss the thermoelectric transport properties within a diffusion thermopower model and study schemes to measure the energy diffusion length and its energy-dependence. That description is based on a quasi-equilibrium distribution function with spatially-dependent electron temperature and chemical potential. Thermoelectric response coefficients are calculated in lowest order of the Sommerfeld expansion. The relation to recent experiments where mesoscopic effects play an important role is shown in this thesis.

The quasi-equilibrium approach within the diffusion thermopower model is sufficient as long as the energy that corresponds to the electron temperature is much smaller than the Fermi energy. However, there are situations where that model has to be generalized for an appropriate determination of the thermoelectric voltage. It is therefore important to understand the non-equilibrium contributions to the electron distribution function systematically. This thesis presents an analytic method to calculate the non-equilibrium contributions to the electron distribution. For that, the Boltzmann equation is solved analytically in an expansion of energy moments in the manner of hydrodynamic equations. An effective equation is derived incorporating both elastic and inelastic scattering processes in a relaxation time approximation. The non-equilibrium contributions to the electrochemical potential are calculated within a systematic Sommerfeld expansion. Correspondingly, we calculate not only the equivalent to a temperature profile but the profiles of higher energy moments of the non-equilibrium distribution function as well. Actually, in lowest order of the Sommerfeld expansion, the generalized approach is equivalent to the quasi-equilibrium ansatz. The first correction modifies Mott's formula for the Seebeck coefficient. Even at low temperature, that correction can become significant if the electron density of the two-dimensional electron gas is reduced by an external potential. Moreover, the systematic treatment of the energy moments of the distribution function allows for a better understanding of the non-equilibrium transport characteristics which are important for mesoscopic device geometries as analyzed in this thesis.

Contents

Introduction

In 2009, Ganczarczyk *et al.* [1] presented measurements on a tunable rectifier realized in a two-dimensional electron gas. This experiment was actually the starting point and the motivation for this theoretical work. After some research, it was clear that mesoscopic length scales play an important role in such a device in the diffusive regime.

The concept of the rectifier is based on a thermoelectric effect. An input current increases the electron temperature locally which leads to a thermoelectric voltage perpendicular to the input current. This voltage results from the temperature difference between the transport channel and contact probes in transverse direction. The fact that the additional temperature is proportional to the square of the heating current (input) gives the opportunity to establish a rectification device. The thermoelectric voltage measured in transverse direction to the input current is therefore an unipolar output voltage. However, to get a finite output signal, the symmetry in transverse direction has to be broken. That is done by tuning the carrier density in that direction via top-gates. In the diffusive regime, where the device dimensions are larger than the elastic mean free path of the electrons, the carrier density influences both the temperature diffusion and the thermopower [2,3]. That kind of rectification device has the advantage that the rectification efficiency can be tuned via the carrier density. This is different from ballistic rectification [4–9] where the symmetry is broken by scatterers or the geometry of the transport channel itself. In the ballistic regime device dimensions are comparable to the elastic mean free path of the electrons. Although the temperature diffusion effects mentioned afore are not relevant in the ballistic regime, thermoelectric effects in general can influence the results in the ballistic regime, too [10–13]. Breaking the symmetry by taking advantage of hot-electron thermopower of quantum point contacts is another possibility to break the symmetry [14, 15].

In this thesis, we focus on the diffusive limit. Although that incorporates device dimensions that are much larger than the elastic scattering length, the energy diffusion length can be comparable to the length scales of the device geometry. The energy diffusion length is the length scale on which the temperature of the electrons varies. Therefore, the temperature profile perpendicular to the input current might not be trivial depending on the device geometry. In fact, it turns out that the determination of the temperature profile is necessary to explain the thermoelectric voltage when the device dimensions are comparable to the energy diffusion length. To study the thermoelectric transverse voltage depending on the characteristics of the temperature profile, we use a thermopower diffusion model in

this thesis. The results by Ganczarczyk *et al.* can be discussed in that framework. The results have been published in collaboration in Ref. [2].

However, such a tunable rectification device is only one example for systems where temperature diffusion and the corresponding mesoscopic length scales are important aspects. In general, the challenge of efficient electronic refrigeration and power generation has lead to a rising interest on thermoelectrics [16, 17] and, especially, mesoscopic structures show promising features for various device concepts [18, 19]. There is a recent interest on quantum thermoelectrics [20] and energy harvesting with quantum dots [21], too. Besides that rather general interest in mesoscopic thermoelectricy, longitudinal and transverse thermoelectrics have been analyzed in different structures within a two-dimensional electron gas [22–28]. To analyze the thermoelectric characteristics such as the thermopower, a temperature gradient often relies on Joule heating, where a current heats the electrons of the two-dimensional electron gas locally [22, 25, 29–31]. In such a case, the spacial dependence of the temperature is not obvious and it is challenging to access it experimentally in a diffusive regime [32]. Here again, the energy diffusion length is the relevant length scale. To understand and describe the mesoscopic effects that correspond to that length scale is one goal for this thesis.

To discuss these mesoscopic features, the device concept by Ganczarczyk *et al.* is generalized in this thesis. In particular, we allow for an arbitrary potential variation in transverse direction and thereby tuning the local electron density of both the heating channel (with a finite heating current) and the voltage probes perpendicular to the input current. We discuss thermoelectric transport properties within a diffusion thermopower model and propose schemes to measure the energy diffusion length and its dependence on the electron density. In this model the thermoelectric transverse signal is given by both, a non-trivial temperature profile that results from energy diffusion and a modulation of the thermopower. The energy diffusion length depends on the local electric potential, too. A gradient of the electron temperature in combination with a local thermopower contributes to the thermoelectric transverse voltage. That description is based on a quasi-equilibrium distribution function with spatially dependent temperature and chemical potential [18, 33, 34]. Thermoelectric response coefficients are calculated in lowest order of the Sommerfeld expansion. During the theoretical research for this thesis, the here presented results were published in Ref. [35]. The relation to recent experiments are pointed out in this thesis.

Although the quasi-equilibrium approach within the diffusion thermopower model suits for the description in a certain regime, there are situations where that model has to be generalized for an appropriate determination of the thermoelectric voltage. It is therefore important to understand the non-equilibrium contributions to the electron distribution function. To do that systematically, the description by a local electron temperature and a local chemical potential only is not sufficient. Hence, a large part of this thesis is about an analytic method to calculate systematically the non-equlibrium contributions to the electron distribution. For that, the

Boltzmann equation is solved analytically in an expansion of energy moments in the manner of hydrodynamic equations [36–40]. An effective deterministic equation is derived incorporating both elastic and inelastic scattering processes in a relaxation-time approximation. The non-equilibrium contributions to the electrochemical potential are calculated within a systematic Sommerfeld expansion which leads to corrections of the Mott's representation of the thermopower [41]. Correspondingly, we calculate not only the equivalent to a temperature profile but the profiles of higher energy moments of the non-equilibrium distribution function as well. Actually we find, that in lowest order of the Sommerfeld expansion the generalized approach is equivalent to the previous mentioned quasi-equilibrium ansatz.

This thesis is divided into three parts. The first part (Chap. 1) contains an introduction to semi-classical transport in a two-dimensional electron gas. Afterwards we present the device geometries we focus on and discuss in the second part (Chap. 2) the mesoscopic characteristics of thermoelectric transverse voltage by means of the diffusion thermopower model. For that part we use the quasi-equilibrium description only. In the third part of the thesis (Chap. 3), we derive the generalized Boltzmann equation approach beyond quasi-equilibrium and discuss higher-order contributions, especially in the context of the Sommerfeld expansion.

1 Semiclassical heat and charge transport in two-dimensional electron gases

Semiclassical transport in bulk materials is usually described by well approved theory, see e.g. Ref. [34]. However, the focus is often on thermal and electric linear response to externally applied gradients of the electrochemical potential or temperature.

Low-dimensional structures incorporate the advantage to engineer the potential landscape by modern growth and etching techniques [18]. Thereby, those systems allow for a continuous crossover from bulk characteristics to the ballistic regime, where the size of the transport channel is small compared to the elastic mean free path of electrons. Different mesoscopic length scales define the validity of a semiclassical approach and the transport characteristics [42]. Finite size effects regarding the size of the semiconductor structure have to be taken into account which demands a calculation of the position-dependent electron distribution function [33]. This part of the thesis is an introduction to semiclassical transport theory and to transport characteristics in low-dimensional structures. Those aspects are crucial for the later discussion and analysis in this thesis. This section is primarily based on Refs. [18, 33, 42–44].

In particular, this work presents a drift-diffusion approach to a non-equilibrium state in a two-dimensional electron gas (2DEG) realized, e.g., in a AlGaAs/GaAs heterostructure. Although we focus on a certain geometry, the concept of this semiclassical transport approach can, in principle, be extended to other mesoscopic structures.

1.1 Two-dimensional electron gas in a semiconductor heterostructure

The advance of low-dimensional structures in semiconductor systems started in the 1970s [43]. One of the first fundamental realizations of superlattices in a semiconductor heterostructure by epitaxial growth was reported by Esaki and Tsu [45]. They studied negative-differential conductivity and Bloch oscillations. A first review from a theoretical point of view is given by Ando *et al.* [46].

In principle, low-dimensional systems in semiconductor structures are based on potential modulations. Charge carriers are confined in one or more directions by potential barriers [44]. If the size of the confined region is of the order of the Fermi wave length, the quantization of the momentum according to the confined direction in space leads to quantized energy bands characterized by a large spacing. At low temperatures, the charge carriers occupy the ground state only and a finite continuous momentum is restricted to the unconfined directions in space. In the following, we discuss the two-dimensional realization of an electron system.

Semiconductors are characterized, amongst other criteria, by the direct energy gap of their band structure. Thus, combining different semiconductors in a heterostructure allows for an engineering of the band structure. Layers of semiconductor materials with a thickness given by a certain number of atoms can be grown epitaxially on top of each other. The most common epitaxial growth techniques are the molecular beam epitaxy and the metal-organic chemical vapor deposition, see, e.g., Refs. [47] and [48], respectively. The application of epitaxial growth allows for a continuation of the semiconductors crystal structure, since the crystal symmetry is unchanged. To minimize the number of defects, the difference between the lattice constants of the semiconductor materials has to be small. Regarding those constrains, the most striking combination of cubic-compound semiconductor materials is given by GaAs and AlAs. Both materials are characterized by nearly the same lattice constant (with deviations of about 0.15% only) but the energy gap differs crucially, i.e. 1.42 eV for GaAs and 2.16 eV for AlAs [43]. In fact, $Al_xGa_{1-x}As$ allows for band-gap engineering of the corresponding layer in dependence of the fraction x of Ga replaced by Al. Figure 1.1 (a) illustrates a possible potential profile in growth direction z. The band gap E_g for GaAs is sketched to be smaller than the band gap of $Al_xGa_{1-x}As$ accordingly.

One layer with a smaller band gap (e.g. GaAs) confined by layers of a larger band gap (e.g. $Al_xGa_{1-x}As$) forms a quantum well for electrons in the conduction band (CB) and for holes in the valence band (VB). The motion of electrons (holes) is quantized in growth direction. The energy of electrons in the conduction band can be described by

$$\epsilon = \epsilon_n + \frac{p_x^2 + p_y^2}{2\,m} \quad , \tag{1.1}$$

with momentum $\boldsymbol{p} = (p_x, p_y)$ in two-dimensions. Due to the description by the effective mass m, the quantum well forms a two-dimensional electron gas (2DEG) for each energy band ϵ_n. That is shown in Fig. 1.1 (b) where dark gray shows states which are occupied by electrons. If the confining potential barriers are sufficiently strong or if the thickness of the layer is sufficiently low and also the temperature is low, the groundstate $n = 0$ with respect to the motion in growth direction contributes to transport dominantly. Therefore, throughout this thesis, we consider the lowest band only and use the parabolic dispersion relation $\epsilon = \left(p_x^2 + p_y^2\right)/(2\,m)$. The subbands $n > 0$ are assumed to be empty.

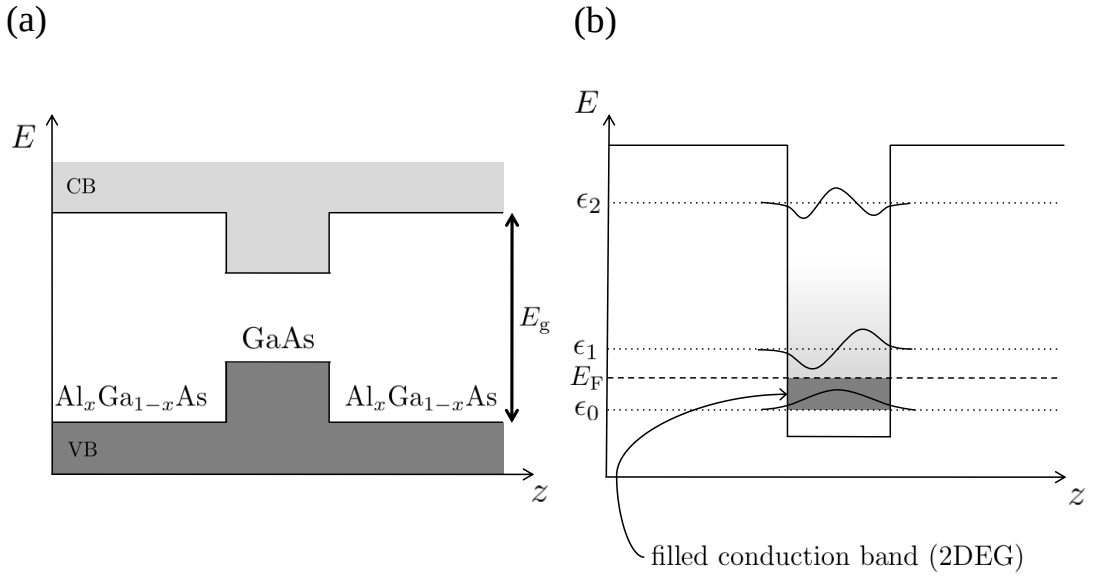

Figure 1.1: A sketch of the origin of 2DEGs in a AlGaAs/GaAs heterostructure: (a) A layer of GaAs is embedded in a $Al_xGa_{1-x}As$ structure with growth in z-direction. Filled electronic states are indicated by dark gray and empty states in the CB are light gray. (b) The edge of the groundstate is indicated by ϵ_0. The edges of the following subbands of higher energy are ϵ_1 and ϵ_2 (inspired by Refs. [43, 49]).

In principle, the shape of the confining potential can be different from the one sketched in Fig. 1.1 (a). In AlGaAs structures, a 2DEG can be realized by a potential well of triangular shape, see Fig. 1.2 (a). The lower band edge of the lowest subband of the 2DEG is given by ϵ_0 (see Fig. 1.2 (b)). In addition, Figure 1.2 (a) introduces the concept of modulation-doping. On the left hand side a Si-doped layer of $Al_xGa_{1-x}As$ is separated from the undoped GaAs layer by an un-doped spacer of $Al_xGa_{1-x}As$. Thereby, Si^+-ions are spatially separated from the 2DEG, where simultaneously the number of free charge carriers is enhanced. Due to the spacer, scattering effects on those ionized impurities are reduced and high mobilities are possible [50].

In general, the description of transport within a 2DEG has much in common with those of 3D bulk systems, although there are crucial differences, e.g. the density of states, which is proportional to $\sqrt{E}$ for 3D while being constant with respect to energy in two dimensions. We discuss the semi-classical approach for transport and scattering processes in Sec. 1.4.

In case of $Al_xGa_{1-x}As$, the charge carriers are scattered by

- optical phonons,

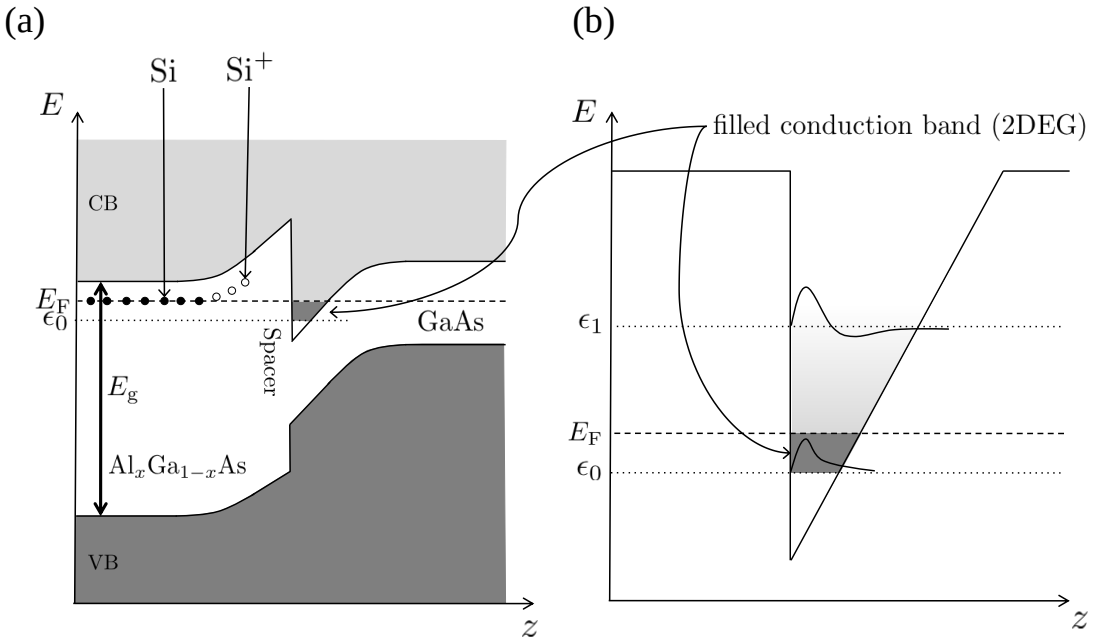

Figure 1.2: A sketch of the origin of 2DEGs in AlGaAs/GaAs heterostructures based on a triangular potential: (a) A modulation-doped $Al_xGa_{1-x}As$/GaAs heterostructure forms a triangular quantum well. Filled electronic states are indicated by dark gray and empty states in the CB are light gray. (b) The edge of the groundstate is indicated by ϵ_0. The edge of the following subband of higher energy is ϵ_1 (after Harris *et al.* [44]).

- acoustic phonons arising from deformation potentials,
- acoustic phonons by piezoelectric scattering,
- remote impurity scattering,
- background impurities,
- roughness of the interface between GaAs and AlGaAs,
- subband transitions,
- and electron-electron interaction.

The influence on the mobility of the different kinds of scattering events depending on the temperature has been studied by Walukiewicz *et al.* [51]. In this work, structures within 2DEGs realized in semiconductor heterostructures (AlGaAs/GaAs structures in particular) are the backbone of the presented analysis. Those structures are realized by potential barriers within the 2DEG which are created by top gates.

1.2 Thermoelectricity

Linear response coefficients can describe how electric and thermal properties in a solid state environment react on externally applied gradients of the temperature and the electrochemical potential. Conceptional different settings give rise to various effects. In 1821 (published in 1822) the Seebeck effect has been discovered [52]. Two different temperatures at the ends of a current free wire, which result in a temperature difference ΔT, give rise to a finite voltage ΔV. The voltage is proportional to the temperature difference times the thermopower, i.e. the Seebeck coefficient $S = \Delta V/\Delta T$. A current carries both, charge and energy. The relation between the charge and heat current density is given by the Peltier coefficient Π [53]. Thereby, a finite voltage leads to a heat current. The two effects are related by the Kelvin-Onsager relation $\Pi = ST$ at temperature T. However, the Joule heating, which is quadratic in the applied voltage, will dominate over the linear Peltier effect in most cases. The Thomson effect describes the heat production per volume based on Joule heating and heat currents. For further discussion of thermoelectric effects, e.g. in case of an applied external magnetic field which gives rise to the Nernst and Ettinghausen effects, we refer to Ref. [54], since magnetic fields are not considered in this thesis. In addition, there is a new and rising interest in Spin caloritronics, which describes coupling between thermal and spin dependent transport, e.g., the spin Seebeck effect [55]. Recent experiments showed a large spin accumulation due to a temperature gradient [56] (spin Seebeck) and a spin-dependent Peltier effect [57].

From point of application, the potential of a material based on its material parameters is described by the figure of merit

$$ZT = \frac{S^2 \sigma T}{\kappa} \quad , \tag{1.2}$$

where σ is the electric conductivity and κ the total thermal conductivity (at zero charge current) of both the lattice and the charge carriers. A good thermoelectric material is characterized by a large Seebeck coefficient, high electrical conductivity to minimize Joule heating and low thermal conductivity to maintain a large temperature gradient. Materials that show a large ZT of the order of one are Bi_2Te_3 and $Si_{1-y}Ge_y$. A promising direction to improve the figure of merit are nanostructures of those materials. See Refs. [17] and [16] and References therein for further reading. Recently, Hung *et al.* [58] analyzed the influence of quantum effects on the thermoelectric performance in low-dimensional semiconductors. Low-dimensional mesoscopic structures in various types of materials provide, first, the ability to establish a bunch of different device concepts [18, 19] and, secondly, a large figure of merit [17]. Possible device applications are electronic refrigerators, thermometers, radiation detectors and distribution controlled transistors.

To characterize thermoelectric properties, the determination of thermoelectric transport coefficients is the objective of many theoretical approaches for various

materials and systems. In 1928, Sommerfeld studied thermoelectric phenomena based on a free-electron theory using the Fermi-Dirac statistics and determined expressions for the electrical conductivity, the thermal conductivity and the Thomson coefficient in metals based on the elastic mean free path [59, 60]. Later, the modeling of thermoelectric coefficients was extended to semiconductors and low-dimensional systems. Different scattering processes in context of the Boltzmann equation and non-equilibrium effects were analyzed. An overview on theoretical models (also from a historical point of view) can be found in Ref. [16].

1.3 Rectification: from the ballistic to the diffusive regime

When the characteristic length scales of the geometry are smaller than the electron mean free path, the motion of electrons can be described in terms of a billiard model, i.e., the electrons are scattered at the boundaries of the transport channel only. Since lithography allows for fabricating such electronic structures, ballistic rectification devices represent a promising concept for application. A feature of ballistic rectifiers, in contrast to pn-junctions, is the fact that those devices can work without potential barriers within the transport channel which leads to full-wave rectification. A large efficiency is, therefore, a great advantage of such electronic geometries.

A ballistic rectifier introduced by Song *et al.* [4] consists of a triangular scatterer in direction of a current which results from an applied voltage between source and drain (see Fig. 1.3 (a)). The scatterer is oriented in such a way that the symmetry perpendicular to the current is broken. The electrons are ballistically scattered at the triangular shaped barrier. Thereby, as indicated by the arrows in Fig. 1.3 (a), the electrons move preferably to the upper terminal which leads to a potential difference between the lower and upper terminal. The output voltage is independent of the current's direction which leads to rectification. Similar effects due to ballistic behavior are observed at asymmetric cross junctions [9, 61] or Y-shaped three terminal devices as shown in Fig. 1.3 (c) [5].

However, the rectification mechanism of devices with asymmetric structure is not necessarily of pure ballistic nature described by a billiard-like model. That has been studied, e.g., by analyzing a device where the central, symmetry-breaking scatterer forms four channels of different size between input and output terminals [8, 62–64]. In this case, the symmetry is broken by tuning the width of these channels as indicated by Fig. 1.3 (b). The width can be controlled by either a shifted, central scatterer or by gate voltages (G1-G4). The corresponding transport characteristics within the channels can range from diffusive to quantized transport. Fleischmann and Geisel [62] proposed that the energy dependence of the number of current-carrying modes leads to a nonlinear rectification signal. That has been studied

experimentally in Refs. [8, 63, 64] and is related to the studies of rectification at three-terminal junctions [5–7, 65–67]. Hieke *et al.* [5] measured the potential at the third terminal (for an applied source-drain voltage in push-pull manner) in structures as shown in Fig. 1.3 (c) where ballistic contributions and contribution from the energy dependence of the modes can be seen [65]. Therefore, structures without a ballistic contribution have been analyzed, especially for different length scales of the device geometry [66].

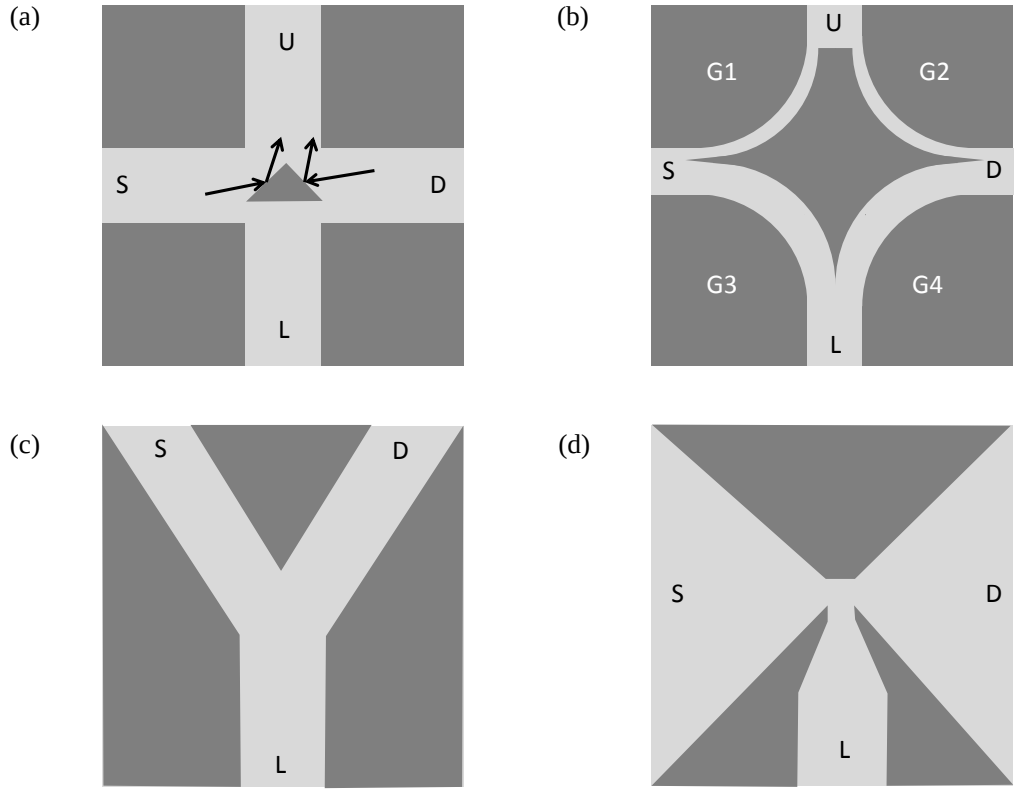

Figure 1.3: (a) Ballistic rectification at a triangular scatterer (after de Haan *et al.* [64]). An applied voltage at source (S) and drain (D) leads to a unipolar output voltage between the lower (L) and upper (U) terminal. (b) The symmetry of the device is broken by tuning the width of the channels connecting input and output terminals. That is done by either shifting the central scatterer or by gate voltages G1-G4 (after de Haan *et al.* [63, 64]). (c)-(d) Three terminal devices with different geometry (after Hieke *et al.* [5] and Irie *et al.* [66]).

Nonlocal thermal rectification effects in a ballistic device, as shown in Fig. 1.3, have been analyzed by Matthews *et al.* [13]. However, thermoelectric effects yield the opportunity for rectification in a diffusive regime as well. Reference [2] studies a transverse rectifier in a two-dimensional electron gas where the unipolar output

voltage is measured perpendicularly to the input current. By Joule heating, the current gives rise to a temperature difference between the contacts and the region with the applied source-drain current. Gates modulate the electron-density and, thereby, the thermopower, which breaks the symmetry in this case and leads to a unipolar output voltage. We discuss the corresponding diffusion thermopower model in detail in Sec. 2.1. However, understanding the contributions to the transverse voltage beyond a temperature description, which holds in quasi-equilibrium only, is a key motivation to this work.

1.4 Semiclassical transport theory

This section is an introduction the commonly used semiclassical transport theory based on the Boltzmann equation which is described from different point of views in many textbooks. That section is the starting point of the introduction to the model and theory discussed in this thesis.

In this thesis, we consider devices where mesoscopic length scales that fall between the macroscopic and atomic scale play an important role. Since the device dimensions are assumed to be much larger than the Fermi wave length, a semiclassical approach is applicable. In a semiclassical regime, the energy distribution of the electrons is well defined by means of the Boltzmann equation. In an equilibrium state, the energy distribution is given by the Fermi-Dirac statistic,

$$f_{\mathrm{F}}(\epsilon, \mu, T_{\mathrm{e}}) = \frac{1}{1 + \exp\left(\frac{\epsilon - \mu}{k_{\mathrm{B}} T_{\mathrm{e}}}\right)} \quad , \tag{1.3}$$

where ϵ is the energy of the electrons, μ the chemical potential and T_e the temperature of the electron system. The electron system is coupled to the system of phonons with the lattice temperature T_{ph}. Those phonons are coupled to other phonon systems, e.g. substrate phonons, and the environment. In a non-equilibrium state all those temperatures depend on the energy transfer between the systems. For a macroscopic sample in thermal equilibrium those temperatures adapt to each other, i.e. $T_{\mathrm{e}} = T_{\mathrm{ph}}$, even in case of a position-dependent potential profile which leads to a position-dependent temperature according to the Seebeck effect. For a mesoscopic system, on the other hand, the situation is different in the sense that the position-dependent electron temperature can deviate from the lattice temperature. The temperature can only be defined in the *quasi-equilibrium* limit, where the dominating contribution of the distribution function takes the form of a Fermi-Dirac statistic.

It is assumed, that the properties of the electron system can be described by a chemical potential $\mu(\boldsymbol{r})$ and an electron temperature $T_e(\boldsymbol{r})$ only. Both depend on the position $\boldsymbol{r}$. Thus, the energy distribution in a mesoscopic system is characterized by $f_{\mathrm{F}}(\epsilon, \mu(\boldsymbol{r}), T_e(\boldsymbol{r}))$. Note that bold parameters like $\boldsymbol{r}$ indicate vector

quantities. In case that the position-dependent temperature equals to the phonon temperature, $T_e = T_{\mathrm{ph}}$, we refer to the thermal equilibrium by the term *local equilibrium*. In a non-equilibrium state with finite charge and heat currents, the electron distribution differs from the distribution function $f_{\mathrm{F}}(\epsilon, \mu(\boldsymbol{r}), T_{\mathrm{e}}(\boldsymbol{r}))$.

In the following, we introduce the derivation of the Boltzmann equation, which is in first place a differential equation for the electron distribution. Studying certain energy moments of the energy-resolved equation reduces the complexity of the equation and leads to observables like currents, energy and particle density. The most challenging part of the equation is the collision term. We discuss different scattering processes from a rather general point of view. Based on the linearized Boltzmann equation and a corresponding relaxation time approximation, we refer again to famous thermoelectric relations. The following sections are close to the description by Jacoboni [43] and Heikkilä [42]. See also Ref. [18].

1.4.1 Boltzmann equation

We consider a gas of electrons (as classical quasi-particles) with the distribution function $f(\boldsymbol{r}, \boldsymbol{p}, t)$, $\boldsymbol{p} = (p_x, p_y, p_z)$ for three dimensions. Then $f(\boldsymbol{r}, \boldsymbol{p}, t)\,\mathrm{d}\boldsymbol{r}\,\mathrm{d}\boldsymbol{p}$ is proportional to the number of particles in the volume $\{\mathrm{d}\boldsymbol{r}, \mathrm{d}\boldsymbol{p}\}$ around $\{\boldsymbol{r}, \boldsymbol{p}\}$ at time t. Thus, for a d-dimensional system of electrons the particle density is given by

$$n_{\mathrm{e}}(\boldsymbol{r}, t) = 2 \int \frac{\mathrm{d}\boldsymbol{p}}{(2\pi\hbar)^d} f(\boldsymbol{r}, \boldsymbol{p}, t) \quad , \tag{1.4}$$

including the spin degree of freedom. In fact, the distribution function $f(\boldsymbol{r}, \boldsymbol{p}, t)$ incorporates the necessary information to determine observables of the electron system. Thus, we aim to determine the distribution function (under suitable approximations). Collisions in a time interval $\mathrm{d}t$ change the distribution function. One collision can instantaneously change the momentum of a particle and by that the corresponding distribution function. That can be described in terms of an equation by

$$\frac{\mathrm{d}f(\boldsymbol{r}, \boldsymbol{p}, t)}{\mathrm{d}t} = I_{\mathrm{coll}}[f] \quad , \tag{1.5}$$

where $I_{\mathrm{coll}}[f]$ is the collision integral. Considering the total time dependence of f, the Boltzmann equation reads

$$\frac{\partial f(\boldsymbol{r}, \boldsymbol{p}, t)}{\partial t} + \boldsymbol{v} \cdot \frac{\partial f(\boldsymbol{r}, \boldsymbol{p}, t)}{\partial \boldsymbol{r}} + \boldsymbol{F} \cdot \frac{\partial f(\boldsymbol{r}, \boldsymbol{p}, t)}{\partial \boldsymbol{p}} = I_{\mathrm{coll}}[f(\boldsymbol{r}, \boldsymbol{p}, t)] \quad , \tag{1.6}$$

with velocity $\boldsymbol{v}$ and force $\boldsymbol{F}$. The collision integral $I_{\mathrm{coll}}[f(\boldsymbol{r}, \boldsymbol{p}, t)]$ is an integral over all possible scattering events. In general, the collision integral is a combination of a certain scattering process minus the reversed process. Both terms are scaled by

the probability that the 'in' state of the scattered electron is occupied and the 'out' state is empty at the same time. The latter accounts for the Pauli principle. The collision integral reads

$$I_{\mathrm{coll}}[f(\boldsymbol{r},\boldsymbol{p},t)] = -2\int \frac{\mathrm{d}\boldsymbol{p}'}{(2\pi\hbar)^d}\left[P(\boldsymbol{p},\boldsymbol{p}')f_{\boldsymbol{p}}(1-f_{\boldsymbol{p}'}) - P(\boldsymbol{p}',\boldsymbol{p})f_{\boldsymbol{p}'}(1-f_{\boldsymbol{p}})\right] \quad , \quad (1.7)$$

with $f_{\boldsymbol{p}} = f(\boldsymbol{r},\boldsymbol{p},t)$. The scattering rate $P(\boldsymbol{p},\boldsymbol{p}')$ from momentum state $\boldsymbol{p}$ to $\boldsymbol{p}'$ has to be calculated for each type of scattering process and depends on the electron distribution f as well, e.g., for electron-electron scattering. Due to Eq. (1.7), the Boltzmann equation is a nonlinear integro-differential equation. Thus, solving the full Boltzmann equation is in general not an easy task and numerical iterations or Monte Carlo techniques where the distribution function is expanded in a set of basis functions are used. For an introduction, we refer to Ref. [68].

A common approximation to solve the Boltzmann equation analytically is given in the linear regime, where the perturbation of the equilibrium distribution function is weak. Hence, a linearization of the Boltzmann equation with respect to, e.g., an applied electric field or temperature gradient, is applicable. The linearized Boltzmann equation is discussed in many textbooks that deal with transport phenomena and is a common basis for the derivation of thermoelectric transport coefficients. Section 1.4.3 gives a short overview on transport phenomena based on the linearized Boltzmann equation. The collision integral is treated in terms of a relaxation time approximation (Sec. 1.4.2). However, that approach is valid for bulk materials in a linear regime only. In a diffusive regime, where elastic and inelastic scattering processes have to be distinguished, a more profound treatment of the distribution function and the collision integral is necessary, as will be discussed in this thesis. For even smaller device dimensions, quantum transport models have to be applied like the non-equilibrium Green's function formalism [16]. Since the difference between inelastic and elastic scattering processes is important for the the mesoscopic transport characteristics in the diffusive regime, we study the contributions of this scattering processes to the collision integral in the following section.

1.4.2 Scattering and the collision integral

The collision integral is often calculated for the relevant scattering processes only. That is an advantage for low-temperature transport since most of the phonon scattering processes can be neglected in that limit. We discuss the characteristics of the collision integral from the following perspective: If the electronic system is in an equilibrium state, the collision integral vanishes. The other way around, if the electronic system is out of equilibrium, scattering mechanisms drive a non-equilibrium function to the local-equilibrium function as long as the collision integral is finite. The local-equilibrium function $f_{\mathrm{l.e.}} = f_{\mathrm{F}}(\epsilon, \mu(\boldsymbol{r}), T_{\mathrm{e}}(\boldsymbol{r}))$ depends on the local chemical potential and local temperature. The latter depends on the energy exchange with the lattice. Different types of scattering mechanism operate on

different length scales. Thus, in non-equilibrium, the different types of scattering define regimes where the distribution function shows characteristics that depend on the dominating scattering processes. The collision integral can be seen as the sum of contributions from different scattering processes.

For the scattering process between two electrons, e.g., there is no coupling with another system. Although different momentum states within the electron system are mixed, the electron-electron interaction conserves the total energy and the total momentum of the two electrons. Therefore, that type of scattering has minor influence on the transport in the diffusive regime. However, it is an important scattering process in the ballistic regime, where the motion of single electrons is relevant.

For the diffusive regime under consideration, we distinguish between two types of scattering: *elastic scattering* and *inelastic scattering*. Elastic scattering processes conserve the energy of the scattered electron. However, the momentum direction is changed due to a collision with impurity atoms or crystal defects. By inelastic scattering we refer to scattering processes where the energy of the scattered electrons are changed. That is the case for electron-phonon scattering. In this thesis, we define inelastic processes by the condition that the change of energy is $k_B T$ or larger [69]. The collision integral can then be written as

$$I_{\text{coll}}[f(\boldsymbol{r},\boldsymbol{p},t)] = I_{\text{el}}[f(\boldsymbol{r},\boldsymbol{p},t)] + I_{\text{inel}}[f(\boldsymbol{r},\boldsymbol{p},t)] \quad , \tag{1.8}$$

where each term has the form of Eq. (1.7). In the following, the characteristics of a few key scattering processes are introduced.

Elastic scattering

The elastic collision integral results from, e.g., scattering on impurity atoms. Thereby, the electrons are scattered on the Coulomb potential of ionized impurities. The scattering by neutral impurities is much weaker due to the short range interaction. The imperfections of alloys can be modeled as impurity potentials, too.

The kernel $P(\boldsymbol{p},\boldsymbol{p}')$ (see Eq. (1.7)) depends on the potential of the scatterer. If we assume, that the time between two scattering events is sufficiently large, the scattering rate is given by Fermi's Golden Rule. However, the Coulomb potential of the ionized impurity is screened by the free charge carriers of the system. The screening length, on the other hand, depends on the electron density. Thus, to find a solution for the distribution function is, in principle, a self-consistent problem.

In case that the scattering potential does not depend on the direction of the electron's momentum, the kernel P is symmetric with respect to $\boldsymbol{p}$ and $\boldsymbol{p}'$. Since the mass of the impurity atom is much larger than the mass of the electron, we have $|\boldsymbol{p}| = |\boldsymbol{p}'|$ for a spherical Fermi surface. Therefore, the total elastic collision integral vanishes if the distribution function is isotropic in momentum space, $f(\boldsymbol{r},\boldsymbol{p},t) = f(\boldsymbol{r},p,t)$ with $p = |\boldsymbol{p}|$. Hence, elastic scattering on impurities or lattice defects leads to a randomization of the electrons' momentum. Due to elastic relaxation, the

non-equilibrium distribution function will become independent of the momentum's direction.

For low temperatures the elastic scattering is the dominating type of all scattering processes that take place. Therefore, for a weak perturbation of the equilibrium state, e.g. by an electric field, the part of the equilibrium function that depends on the momentum's direction is weak as well. The dominating part of the distribution function depends on the electron energy only. However, the latter always leads to vanishing currents. Therefore, the contributions to the distribution function depending on the momentums direction are essential for the analysis of a non-equilibrium state.

Inelastic scattering

In most materials there are acoustic and optical phonons which are more or less relevant for scattering with electrons depending on the temperature. At low temperatures and small voltages, which is the regime studied in this thesis, the scattering with optical phonons can be neglected. Scattering processes with acoustic phonons, on the other hand, are relevant for the determination of the inelastic collision integral in that regime. At room temperature, scattering with optical phonons are the dominating inelastic scattering events. The acoustic phonons carry a small amount of energy and, thus, can be approximately described as elastic scatterers at high temperature. In principle, there are two kinds of scattering potentials that are associated with phonons. That are the deformation potential and the piezoelectric potential (for acoustic phonons) or polar potential (for optical phonons). The deformation potential results from the changing lattice parameter which in turn influences the band structure. In addition, the dislocation of an ionized atom leads to a piezoelectric potential. Kreschuk *et al.* found that this is the main energy relaxation process at Helium temperature for a 2DEG in an AlGaAs/GaAs heterostructure [70].

Inelastic scattering is, in general, a process where an electron of energy ϵ is scattered to a state with energy $\epsilon + \hbar\omega$. For scattering of an electron with the deformation potential of an acoustic phonon, we have

$$I_{\mathrm{inel}}[f_\epsilon] = -\int \mathrm{d}\omega\; K_{\mathrm{e-ph}}(\epsilon,\omega)\left\{\left[f_\epsilon\left(1-f_{\epsilon-\hbar\omega}\right)-f_{\epsilon+\hbar\omega}\left(1-f_\epsilon\right)\right]\left(n_{\hbar\omega}+1\right)\right.$$
$$\left.-\left[f_{\epsilon-\hbar\omega}\left(1-f_\epsilon\right)-f_\epsilon\left(1-f_{\epsilon+\hbar\omega}\right)\right]n_{\hbar\omega}\right\}\quad, \tag{1.9}$$

where f_ϵ is the distribution function with electron energy ϵ. The kernel $K_{\mathrm{e-ph}}(\epsilon,\omega)$ describes the transition rate for the scattering with a phonon of energy $\hbar\omega$. In case of a low-dimensional system the phonons are usually strongly coupled to the phonons of the substrate. The latter can be seen as a large reservoir of bosons in equilibrium. Due to the strong coupling, the phonon distribution function is a

Bose-Einstein function with

$$n_{\hbar\omega} = \frac{1}{\exp\left(\frac{\hbar\omega}{k_B T_0}\right) - 1} \quad , \tag{1.10}$$

where T_0 is the temperature of the substrate. In this case, the inelastic collision integral vanishes for $f_\epsilon = f_{\mathrm{F}}(\epsilon, \mu(\boldsymbol{r}), T_0)$ which represents the local-equilibrium function under the influence of electron-phonon scattering.

The influence of inelastic scattering processes leads to the local-equilibrium state. That is due to the coupling of the electron system to the phonon system, which is assumed to be in a local-equilibrium state in first place. As long as the inelastic mean free path is large compared to the characteristic length scale of the low-dimensional structure, we are in a diffusive regime, where the inelastic scattering can be treated perturbatively. On a macroscopic length scale, where the device geometry exceeds the inelastic mean free path, the distribution function is in a thermal equilibrium with the phonon system. Hence, the distribution tends to a Fermi function with a position-dependent chemical potential and a temperature that is equal to the temperature of the phonon system.

Relaxation-time approximation

If the deviation of the distribution function from equilibrium is small, the collision integrals introduced in the previous section can often be treated in terms of a relaxation-time approximation. Therefore close to equilibrium, the local-equilibrium function $f_{\mathrm{l.e.}}$, with $I_{\mathrm{coll}}[f_{\mathrm{l.e.}}] = 0$, is corrected by a non-equilibrium term δf. The latter is small compared to $f_{\mathrm{l.e.}}$. We can expand the collision integral and get

$$I_{\mathrm{coll}}[f_{\mathrm{l.e.}} + \delta f] \approx \left(\frac{\partial I_{\mathrm{coll}}}{\partial f}\right)_{f=f_{\mathrm{l.e.}}} \delta f = -\frac{\delta f}{\tau} \quad , \tag{1.11}$$

which defines the relaxation time τ. The relaxation time τ is the typical time scale for the relaxation of a non-equilibrium contribution of the distribution function. Since the collision integral is energy dependent, the relaxation time is energy dependent, too. The corresponding length scale is given by $v_{\mathrm{F}}\tau(\epsilon_{\mathrm{F}})$ where the index F denotes the Fermi velocity and the energy at the Fermi level, respectively. In principle, a specific relaxation time can be defined for different types of scattering processes. The Matthiessen's rule,

$$\tau^{-1} = \sum_j \tau_j^{-1} \quad , \tag{1.12}$$

leads to the total relaxation time.

1.4.3 Linearized Boltzmann equation

In the following, we do not distinguish between different scattering processes for the sake of simplicity. Hence, we write the Boltzmann equation in relaxation-time approximation as

$$\boldsymbol{v} \cdot \frac{\partial f(\boldsymbol{r},\boldsymbol{p})}{\partial \boldsymbol{r}} + \boldsymbol{F} \cdot \frac{\partial f(\boldsymbol{r},\boldsymbol{p})}{\partial \boldsymbol{p}} = I_{\text{coll}}[f(\boldsymbol{r},\boldsymbol{p})] \quad . \tag{1.13}$$

Here, we study a stationary situation, where the characteristics of the system are assumed to be constant in time. Thus the distribution function depends on $\boldsymbol{r}$ and $\boldsymbol{p}$ only. We assume that an electronic system is close to a local equilibrium, where $f_{\text{l.e.}} = f_{\text{F}}(\epsilon, \mu(\boldsymbol{r}), T(\boldsymbol{r}))$ is the local-equilibrium function with $I_{\text{coll}}[f_{\text{l.e.}}] = 0$. A weak, externally applied electric field $\boldsymbol{E}$ causes a small deviation of the distribution function f from the local equilibrium. Thus we have

$$f = f_{\text{l.e.}} + \delta f \quad . \tag{1.14}$$

For weak perturbation of the equilibrium, the collision integral can be expressed in terms of the relaxation-time approximation, see Sec. 1.4.2. The Boltzmann equation in relaxation-time approximation is given by

$$\frac{\partial f}{\partial \boldsymbol{r}} - e\boldsymbol{E} \cdot \frac{\partial f}{\partial \boldsymbol{p}} = -\frac{f - f_{\text{l.e}}}{\tau} \quad , \tag{1.15}$$

with the electron charge $-e$ and the relaxation time τ. In general, the relaxation time τ depends on the energy of the electrons. We assume that the variation of electron temperature, $T_e(\boldsymbol{r})$, is weak compared to the temperature. As long as we consider a macroscopic sample, the inelastic scattering leads to a local equilibrium of the phonon and electron temperature. We consider the lowest order contribution to the Boltzmann equation with respect to the externally applied electrical field E, the variation of the chemical potential $\mu(\boldsymbol{r})$ and the variation of the temperature $T(\boldsymbol{r})$. Hence, δf is linear with respect to the gradient of an external electric potential, a chemical potential or the electron temperature. Therefore, the term $\nabla \delta f$ where $\frac{\partial}{\partial \boldsymbol{r}} = \nabla$ can be neglected. That is a suitable approximation on a macroscopic length scale. The Boltzmann equation transforms in

$$\left(-e\nabla\phi - \frac{\epsilon - \mu}{T}\nabla T\right) \boldsymbol{v} \frac{\partial f_{\text{l.e.}}}{\partial \epsilon} = -\frac{\delta f}{\tau} \quad , \tag{1.16}$$

where ϕ is the electrochemical potential with $\nabla\phi = \nabla\mu/(-e) + \boldsymbol{E}$. The correction δf reads then

$$\delta f = \tau \left(\left(-e\nabla\phi + \frac{\epsilon - \mu}{T}\nabla T \right) \boldsymbol{v} \frac{\partial f_{\text{l.e.}}}{\partial \epsilon} \right) \quad , \tag{1.17}$$

with $m\boldsymbol{v} = \boldsymbol{p}$. In non-equilibrium, nonvanishing charge and heat current densities are given by

$$\begin{aligned}\boldsymbol{j} &= -2\,e \int \frac{\mathrm{d}\boldsymbol{p}}{(2\pi\hbar)^d}\, \boldsymbol{v}\, \delta f \\ &= -2\,e \int \frac{\mathrm{d}\boldsymbol{p}}{(2\pi\hbar)^d}\, \tau \left(-e\nabla\phi - \frac{\epsilon-\mu}{T}\nabla T \right) \boldsymbol{v}^2 \frac{\partial f_{\text{l.e.}}}{\partial \epsilon} \quad , \qquad (1.18)\\ \boldsymbol{j}^q &= 2 \int \frac{\mathrm{d}\boldsymbol{p}}{(2\pi\hbar)^d}\, (\epsilon-\mu)\, \boldsymbol{v}\, \delta f \\ &= 2 \int \frac{\mathrm{d}\boldsymbol{p}}{(2\pi\hbar)^d}\, \tau \left(-e\nabla\phi - \frac{\epsilon-\mu}{T}\nabla T \right) (\epsilon-\mu)\, \boldsymbol{v}^2 \frac{\partial f_{\text{l.e.}}}{\partial \epsilon} \quad . \qquad (1.19)\end{aligned}$$

With the definition

$$\mathcal{L}_n = 2 \int \frac{\mathrm{d}\boldsymbol{p}}{(2\pi\hbar)^d}\, \tau\, (\epsilon-\mu)^n\, \boldsymbol{v}^2 \frac{\partial f_{\text{l.e.}}}{\partial \epsilon} \qquad (1.20)$$

the current densities can be written as

$$\boldsymbol{j} = e^2 \mathcal{L}_0 \nabla\phi + e\mathcal{L}_1 \frac{\nabla T}{T} \quad , \qquad (1.21)$$

$$\boldsymbol{j}^q = -e\mathcal{L}_1 \nabla\phi - \mathcal{L}_2 \frac{\nabla T}{T} \quad . \qquad (1.22)$$

The charge and heat currents result from finite gradients of the electrochemical potential or electron temperature. The response coefficients can be taken from Eqs. (1.21) and (1.22). That is first of all the electric conductivity σ

$$\boldsymbol{j} = \sigma \boldsymbol{E} \quad , \qquad (1.23)$$

with $\sigma = e^2\mathcal{L}_0$ for constant temperature. Similarly, the thermal conductivity is the linear response of the heat current density to an applied temperature gradient. In setups with vanishing charge currents, the gradient of the electrochemical potential yields

$$\nabla\phi = S\nabla T \quad , \qquad (1.24)$$

where $S = -\mathcal{L}_1/(eT\mathcal{L}_0)$ is the Seebeck coefficient or thermopower, see Sec. 1.2. That means, a temperature difference leads to a voltage in a closed system, where no charge currents are present. However, allowing for a finite heat current in that system,

$$\boldsymbol{j}^q = \kappa \nabla T \quad , \qquad (1.25)$$

the thermal conductivity reads $\kappa = (\mathcal{L}_2 + e\mathcal{L}_1 S)/T$. In Sec. 1.2 the Peltier coefficient Π was introduced as well. It relates the charge and the heat current densities to

each other. For a vanishing temperature gradient, the Peltier coefficient is given by

$$\boldsymbol{j}_q = \Pi \boldsymbol{j} \quad , \tag{1.26}$$

with $\Pi = -\mathcal{L}_1/(e\mathcal{L}_0) = ST$. This identity is the Kelvin-Onsager relation (see Sec. 1.2) [71, 72].

In principle, the coefficients $\mathcal{L}_i$ can be calculated in terms of a Sommerfeld expansion where the lowest order with respect to $k_B T/\epsilon_\mathrm{F}$ is considered. Since the Sommerfeld expansion is a key aspect of the theoretical approach in this thesis, we do not go into detail at this point but refer later to this section.

The linearized Boltzmann equation presented in this section is valid in case that the geometry of the electronic system is based on macroscopic length scales where the mean free path is small compared to the device dimensions. In addition, the gradients of the temperature and the electrochemical potential are weak. That is the case for d-dimensional bulk materials. For this linear transport theory, we assume that the transport is governed by elastic scattering on impurities where energy dissipation vanishes due to a local thermal equilibrium. However, that does not hold in the diffusive regime. There, energy dissipation, i.e. electron-phonon interaction, has to be treated explicitly. Since this thesis deals with mesoscopic effects in a diffusive regime, the separation of inelastic and elastic processes on different length scales is a crucial aspect. That is shown in the next part of this thesis. We study an all-electric setup where a current creates a temperature profile in a density-modulated two-dimensional electron gas. Due to regions of different temperature, thermoelectric effects contribute to the transport characteristics of the electron gas. In that context, the discussion deals first of all with mesoscopic diffusion thermopower.

2 Mesoscopic diffusion thermopower in two-dimensional electron gases

The content of this part has been published in Ref. [35] and is reprinted with permission from S. Rojek and J. König, Phys. Ref. B **90**, 115403 (2014). Copyright 2017 by the American Physical Society. Additional comments and adjustments of the notation in accordance to this thesis were made.

Originally this work was motivated by a device concept published by Ganzarczyk *et al.* [2]. Therein, tunable transverse rectification in a density-modulated two-dimensional electron gas has been demonstrated. The density modulation is induced by two surface gates. The gates are aligned parallel on top of a narrow stripe of a 2DEG. An input current is running parallel to both gates through the 2DEG. A transverse voltage in the direction of the density modulation is observed, i.e. perpendicular to the applied source-drain voltage. The polarity of the transverse voltage is independent of the polarity of the source-drain voltage, demonstrating rectification in the device as introduced in Sec. 1.3. It is shown that the transverse voltage depends on the applied source-drain voltage quadratically and on the density modulation non-monotonically. The experimental results are discussed in the framework of a diffusion thermopower model. The theoretical approach presented therein can be derived from the theoretical model discussed in this thesis. The understanding of mesoscopic effects on thermoelectric transport characteristics has contributed to the discussion shown in Ref. [2]. However, the profound understanding of the mesoscopic effects, that have to be taken into account to model such a device, go beyond the content of Ref. [2]. Therefore, the analysis in this part of the thesis is a generalization that focuses on different mesoscopic aspects in similar device concepts. Furthermore, there is fundamental interest in studying thermoelectric effects since they provide insight into underlying transport mechanisms. The information derived from heat and charge transport is beyond that contained in measurements of electric conductivity only. This especially applies to mesoscopic devices [18, 19], where sample size and geometry affect transport, while, for bulk systems, only a few material parameters are relevant. Two-dimensional electron gases are particularly suited for fundamental studies because the variety of possible structures and the possibility to tune the carrier density by gate voltages allow for controlling mesoscopic aspects of charge and heat transport. In particular, one can

reach the regime in which the energy diffusion length becomes comparable to the size of the system, such that mesoscopic effects for heat transport are expected.

For 2DEGs realized in a semiconductor heterostructure, the momentum relaxation time, τ_e, that determines the mobility of the charge carriers, is mostly based on elastic scattering processes for typical low-temperature measurements. The corresponding elastic scattering length or elastic mean-free path $l_\mathrm{e} = v_\mathrm{F}\tau_\mathrm{e}$, where v_F is the Fermi velocity, marks the separation between ballistic and diffusive transport of the electrons. For device dimensions L larger than l_e, transport is diffusive with diffusion constant $D = v_\mathrm{F}^2\tau_\mathrm{e}/2$ (in two dimensions). An important length scale for heat transport results from the inelastic or energy-relaxation time, τ_i, given by scattering processes in which the energy transfer between electrons and lattice exceeds $k_\mathrm{B}T$. This introduces the energy diffusion length $l = \sqrt{D\tau_\mathrm{i}}$ as a length scale, on which the local energy density of the charge carriers spatially varies in a stationary situation [73–77].

Since at a low temperature we have $\tau_\mathrm{e} \ll \tau_\mathrm{i}$, it is possible to realize devices with $l_\mathrm{e} \ll L \lesssim l$, for which heat transport behaves mesoscopically while charge transport does not. This regime, that we want to address in this thesis, is distinctively different from macroscopic thermoelectric devices but also from nanoscale systems [26,78–86], in which energy quantization and Coulomb charging are important, and from the ballistic or quasi-ballistic regime [87–93], in which charge transport behaves mesoscopically [94]. The calculations are based on a noninteracting-electron picture. This is in contrast to recent experimental studies of diffusion thermopower in strongly correlated systems, e.g., those displaying the fractional quantum Hall effect [95–97] or low-concentration samples with unconventional metallic phases [29, 98, 99].

As introduced in Sec. 1.2, a temperature gradient can drive an electric current, or, for open electric contacts, generate a finite voltage between the contacts. The strength of this thermopower is characterized by the Seebeck coefficient $S = U/\Delta T$, where U is the voltage generated by a temperature difference ΔT between two contacts. The Seebeck coefficient is a useful quantity whenever the temperature of the two contacts are given as a boundary condition. While this is the case in many experimental setups involving macroscopic systems, the situation may be different for mesoscopic samples in which temperature gradients appear as a consequence of Joule heating by local electric currents. To be more specific, we will consider devices as sketched in Fig. 2.1: metallic gates, with a length in x-direction that is much larger than the width, modulate the electric potential of a 2DEG in y-direction. Thereby, an electric current I_x, driven through the 2DEG in x-direction, heats up the electron system which, in turn, generates a perpendicular output voltage U_y.

In such a mesoscopic all-electric setup, heat generation and heat diffusion have to be treated on the same footing, i.e., the local temperature is not a priori known but needs to be determined self-consistently. Therefore, it is more natural to characterize the thermopower by relating the output voltage U_y to the input heating

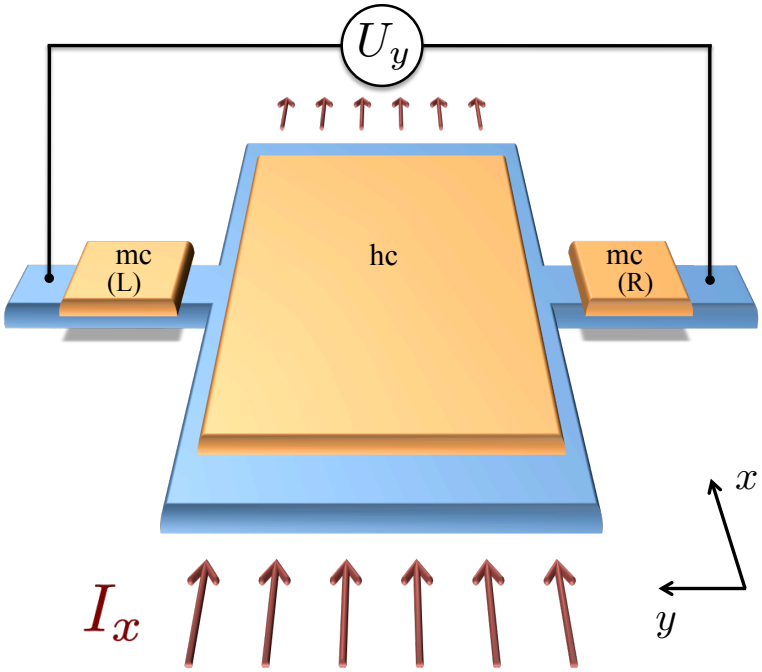

Figure 2.1: Schematic picture of a transverse thermoelectric rectifier. The carrier density of a 2DEG (blue region) is given by the potentials $V_{\mathrm{mc}}^{\mathrm{L}}$, $V_{\mathrm{mc}}^{\mathrm{R}}$, and V_{hc} locally controlled by voltages applied to top gates. An applied current I_x heats up the electrons in the heating channel (hc). The transverse, thermoelectric output voltage U_y depends on the gate voltages applied to the gates on top of the modulation channels (mc) on the left (L) and right (R) hand side. Reprinted with permission from [35]. Copyright 2017 by the American Physical Society.

current or voltage rather than to a temperature difference. As we will see later, a convenient measure of the device's performance is the dimensionless quantity

$$s = \frac{eU_y}{\omega} \quad , \tag{2.1}$$

where ω is the application of energy per electron provided by the heating current, I_x. For devices for which all relevant geometric lengths exceed the energy diffusion length, s is just a number determined by material parameters. In the mesoscopic regime, however, s depends on various geometric lengths such as the width of region heated by an applied current (heating channel), the width of regions with a modulated charge density (modulation channel), the distance between heating and modulation channels, and the width of the potential steps at the edges of modulation channels.

The aim of this part of the thesis is to discuss the influence of the energy diffusion

length on the thermoelectric output voltage generated by the input heating current for devices as sketched in Fig. 2.1 and experimentally realized in, e.g., Refs. [2, 3, 100]. For practical reasons, the voltage contacts are spatially separated from the heating channel, i.e., the voltage contacts remain at base temperature. Therefore, a finite output voltage can occur only if the reflection symmetry with respect to the x-axis is broken, e.g., by placing a modulation channel on one side only. Since the unipolar output voltage, U_y, is independent of the input current's direction, the studied setups effectively act as transverse rectifiers.

The underlying mechanism of this rectification, diffusive thermopower, is different from ballistic rectification in samples with dimensions small compared to the elastic mean free path l_e. Those ballistic rectifiers work with symmetry-breaking scatterers [4, 13] or asymmetric cross junctions [9, 61]. It is, furthermore, different from hot-electron thermopower of quantum point contacts [11, 14], which sometimes enhances the rectification signal in ballistic rectifiers [10, 12]. Another source of a nonlinear output signal is related to the number of current-carrying modes in channels connecting input and output terminals. An asymmetry in the mode numbers may be influenced by the position of a central scatterer and/or gate voltages. This and related mechanisms have been discussed for both four- [8, 62–64] and three-terminal [5–7, 65–67] devices in the range from diffusive to quantized transport.

2.1 Diffusion thermopower model

The diffusion thermopower model is based on a semiclassical approach to thermoelectric transport [34] (see Sec. 1.4). An applied electric current provides additional energy for the electronic system within the heating channel (the case of more than one heating channel is addressed later in Sec. 2.1.5). The excess energy diffuses perpendicularly, since we assume translational invariance in x-direction, i.e., all quantities only depend on the position in y-direction. In a steady state, the distribution of the excess energy is described by a temperature profile $T(y)$ with a maximum somewhere in the heating channel. For spatially well-separated voltage contacts, the temperature decreases towards the base temperature of the lattice, $T(y) \to T_0$ for $y \to \pm\infty$. The local temperature gradient induces a voltage gradient proportional to the Seebeck coefficient $S(y)$, which yields the total voltage drop

$$U_y = \int_{-\infty}^{\infty} \mathrm{d}y \; S(y) \; \partial_y T(y) \quad . \tag{2.2}$$

The contributions from regions with positive and negative temperature gradients compensate each other for a setup which is symmetric in transverse direction. In this case, U_y vanishes. An applied gate voltage on either side of the heating channel

breaks this symmetry by modulating the charge density, leading to a finite U_y. The density modulation changes the local Seebeck coefficient $S(y)$, which explicitly enters Eq. (2.2). Moreover, the heat diffusion within the electronic system and from electrons to the lattice are modified by the gate voltage via the energy dependence of τ_e and τ_i, which, in turn, affects the temperature profile and, thereby, indirectly U_y.

For determining the temperature profile in the most general case, we allow for an arbitrary y-dependence of the potential profile. That can be used to model changes, e.g, in the potential profile at the edges of the modulation channels.

2.1.1 Heat balance equation

To derive the temperature profile, we identify the processes which change the local heat density in the electronic system. First, heat is generated by Joule heating $\mathbf{j}\cdot\mathbf{E}$ (power per area), where $\mathbf{j}$ is the charge current per unit length in the 2DEG and $\mathbf{E}$ the electric field. Second, heat is transferred from the electronic system to the lattice, which we treat as a reservoir with fixed temperature T_0. Phenomenologically, this process can be modeled by $c_V(T-T_0)/\tau_\mathrm{i}$ for small temperature difference $\delta T = T - T_0$, where c_V is the heat capacity per unit area and τ_i the energy-relaxation time of the electrons taken at the Fermi level [74, 101]. The latter accounts for scattering processes with energy transfer of $k_\mathrm{B}T$ or more, which, at low temperature, are mainly given by scattering with acoustic phonons [69], see Sec. 1.4.2. Scattering processes with smaller energy transfer do not affect the local temperature but, still, charge and energy diffusion and, thereby, the charge current, $\mathbf{j}$, and heat current, $\mathbf{j}^q$, per unit length. As a result, we get

$$\nabla\cdot\mathbf{j}^q = \mathbf{j}\cdot\mathbf{E} - c_V\frac{\delta T}{\tau_\mathrm{i}} \quad , \tag{2.3}$$

for the heat balance equation.

Translation invariance in x-direction implies $\mathbf{j}^q = \mathbf{j}^q(y)$ and, thus, $\nabla\cdot\mathbf{j}^q = \partial j_y^q/\partial y$. Furthermore, for open voltage contacts electric current is flowing in x-direction only, i.e., $\mathbf{j} = (j_x, 0, 0)$, which yields the Joule heating $\mathbf{j}\cdot\mathbf{E} = j_x E_x$, where E_x is the electric field that drives the electric current in x-direction. To eliminate the current densities in Eq. (2.3), we make use of the linear-response relations

$$j_x = \sigma\, E_x \quad , \tag{2.4}$$

$$j_y^q = -\kappa\,\frac{\partial T}{\partial y} \quad , \tag{2.5}$$

which define the (two-dimensional) electric and thermal conductivity σ and κ, respectively. That leads to a differential equation for the temperature profile

$$T - \frac{l^2}{\kappa}\frac{\partial}{\partial y}\left(\kappa\frac{\partial T}{\partial y}\right) = T_\mathrm{bulk} \quad , \tag{2.6}$$

where the energy diffusion length

$$l = \sqrt{\frac{\kappa\tau_\mathrm{i}}{c_V}} \tag{2.7}$$

defines the length scale on which the temperature profile varies (see Refs. [2,75] for diffusive temperature differential equations in case of a constant carrier density). The inhomogeneity

$$T_\mathrm{bulk} = T_0 + \frac{\omega}{c_V/n_\mathrm{e}} \tag{2.8}$$

is the temperature the electrons would acquire in a bulk sample much larger than the energy diffusion length l. Here, n_e is the electron density and

$$\omega = \frac{\sigma\tau_\mathrm{i}E_x^2}{n_\mathrm{e}} \tag{2.9}$$

is readily identified as the energy increase per electron provided by the heating current (σE_x^2 is the power density due to Joule heating and τ_i is the characteristic time on which the electrons gain energy before they are scattered inelastically). We remark that $l(y)$, $\kappa(y)$, $\sigma(y)$, and $E_x(y)$ are, in general, y-dependent. In the case of l, κ, and σ that results from the charge-density modulation. The externally applied electric field, on the other hand, is constant within the heating channels, but vanishes outside. Any temperature dependence of l, κ, and σ can be neglected in Eq. (2.6) because we restrict ourselves to linear order in δT and quadratic order in E_x.

2.1.2 Boundary conditions

Since the differential equation for the temperature, Eq. (2.6), is of second order, two boundary conditions are needed. Far away from the heating channels, $y \to \pm\infty$, the temperature remains at base temperature, $T \to T_0$.

Sharp edges of the modulation and the heating channels divide the integration range due to discontinuities in the potential or the inhomogeneity T_bulk. In this case, the solutions of the differential equation on the left and right hand side of the interface need to be matched. This is achieved by making use of two conditions: the heat current entering the interface from one side is (i) equal to the heat current leaving the interface from the other side and (ii) equal to the heat current flowing through the interface. The first condition leads to the continuity of $\kappa\,(\partial T/\partial y)$.

The heat current through the interface, which enters the second condition, is driven by a temperature difference across the interface. (This discontinuity of the temperature at the interface is accompanied by a jump in the electrochemical potential since for open voltage contacts there is no charge current flowing through the interface.) As derived in Ref. [2], the size of this temperature jump is in

general much smaller than the temperature variation within the 2DEG and can be neglected. This can be interpreted in the following way: The heat current through the interface is carried by ballistic electrons and, therefore, only limited by the finite transmission probability $|t|^2$ for an incoming electron to pass the interface [102–104]. The heat conductivity in the 2DEG, on the other hand, is limited by elastic scattering, characterized by the scattering length l_e. The length scale associated with the temperature gradient driving the heat current, however, is the energy diffusion length l and, thus, much larger. As a consequence, the temperature jump at the interface is parametrically given by a factor of $l_\mathrm{e}/(l|t|^2)$ smaller than the temperature change in the 2DEG and, therefore, negligible (unless $|t|^2 \lesssim l_\mathrm{e}/l$). In conclusion, we demand, as the second matching condition, the temperature T to be continuous at the interface.

2.1.3 Sommerfeld expansion

The thermopower diffusion model presented above contains the linear transport coefficients σ and κ and the specific heat capacity c_V. At low temperature, $k_\mathrm{B}T_0 \ll \epsilon_\mathrm{F}$, it is sufficient to determine them to lowest order in the Sommerfeld expansion [33, 34]. We express the results by making use of the density of states $\rho = m/\pi\hbar^2$ for free electrons with effective mass m and of the diffusion constant $D = \epsilon_\mathrm{F}\tau_\mathrm{e}(\epsilon_\mathrm{F})/m$ at the Fermi energy (both for two-dimensional systems), and obtain

$$\sigma = e^2 \rho\, D \quad , \tag{2.10a}$$

$$\kappa = \rho \frac{\pi^2}{3} k_\mathrm{B}^2 T_0\, D \quad , \tag{2.10b}$$

$$c_V = \kappa / D \quad , \tag{2.10c}$$

and from this, we derive

$$l = \sqrt{D\,\tau_i} = \sqrt{\frac{\epsilon \tau_\mathrm{e}(\epsilon)\tau_\mathrm{i}(\epsilon)}{m}}\bigg|_{\epsilon=\epsilon_\mathrm{F}} \quad , \tag{2.11a}$$

$$S = -\frac{\pi^2}{3}\frac{k_\mathrm{B}^2 T_0}{e}\frac{\partial \ln\left(\epsilon\tau_\mathrm{e}(\epsilon)\right)}{\partial\epsilon}\bigg|_{\epsilon=\epsilon_\mathrm{F}} \quad , \tag{2.11b}$$

$$\omega = \frac{(eE_x l)^2}{\epsilon_\mathrm{F}} \quad . \tag{2.11c}$$

Equation (2.11b) is the Mott formula for the thermopower in a two-dimensional electron gas [41]. The y-dependent charge carrier density enters l, S, and ω via the Fermi energy $\epsilon_\mathrm{F}(y)$, measured relatively to the lower subband edge. In order to express all results in dimensionless quantities, we choose the case of vanishing gate voltages (which yields $V_\mathrm{hc} = V_\mathrm{mc} = 0$) as a reference, and denote the corresponding Fermi energy by $\epsilon_{\mathrm{F},0}$. Similarly, l, n_e, and ω taken at this energy fixes the reference quantities l_0, $n_{\mathrm{e},0}$, and ω_0. The quantity s_0 is defined as eU_y/ω_0.

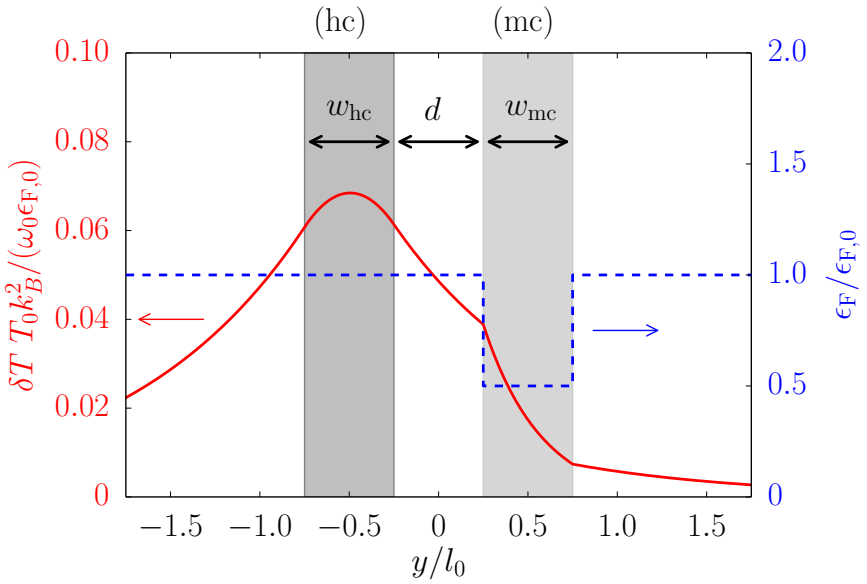

Figure 2.2: Setup consisting of one heating (hc) and one modulation (mc) channel in a distance $d = l_0/2$ from the heated region. The width of both is $w_{\mathrm{hc}} = w_{\mathrm{mc}} = l_0/2$. The red, solid line marks the temperature difference to the base temperature, T_0. The local Fermi energy is depicted by the blue, dashed line. Reprinted with permission from [35]. Copyright 2017 by the American Physical Society.

2.1.4 Gate-voltage dependent thermopower

A generic setup for addressing mesoscopic diffusion thermopower is shown in Fig. 2.2 consisting of one heating channel (hc) of width w_{hc} and one modulation channel (mc) of width w_{mc}. The modulation channel is separated from the heating channel by a distance d. Between the modulation and the heating channel, the carrier density remains unchanged and no electric field is applied, $E_x = 0$. The blue, dashed line (right y-axis) in Fig. 2.2 depicts the profile of the Fermi energy. The resulting temperature profile is marked by the red, solid line (left y-axis).

Within the Sommerfeld expansion (see Sec. 2.1.3), the values of τ_{e} and τ_{i} and their derivatives at the local Fermi energy are needed. We model the full energy dependence of the relaxation times [44, 51, 105] by power laws $\tau_{\mathrm{e}} = \tau_{\mathrm{e},0}\,(\epsilon/\epsilon_{\mathrm{F},0})^{\alpha_{\mathrm{e}}}$ and $\tau_{\mathrm{i}} = \tau_{\mathrm{i},0}\,(\epsilon/\epsilon_{\mathrm{F},0})^{\alpha_{\mathrm{i}}}$. The values $\tau_{\mathrm{e},0}$ and $\tau_{\mathrm{i},0}$ of the relaxation times at reference energy $\epsilon_{\mathrm{F},0}$ will, of course, enter the transverse voltage U_y. By expressing all our results in terms of the proper dimensionless quantities, however, the values of $\tau_{\mathrm{e},0}$ and $\tau_{\mathrm{i},0}$ completely drop out. They only need to be specified when comparing to experimental data. For the exponents, we take $\alpha_{\mathrm{e}} = 0.88$ and $\alpha_{\mathrm{i}} = 1.45$, that were experimentally determined for the device used in Ref. [2], but as we demonstrate below, a variation of α_{e} or α_{i} leads to only small quantitative corrections.

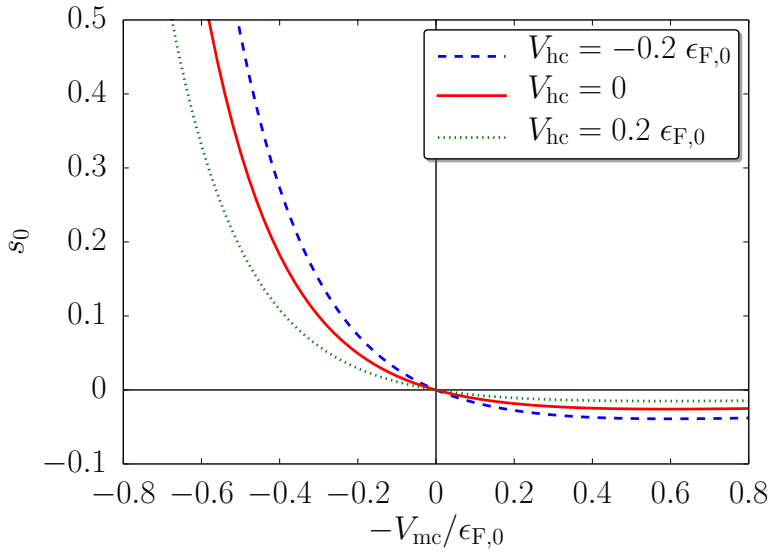

Figure 2.3: Dependence of s_0 on the electrostatic potential V_{mc} in the modulation channel for three different values of the potential V_{hc} in the heating channel. Referring to the setup in Fig. 2.2, we set $w_{\mathrm{hc}} = w_{\mathrm{mc}} = l_0/2$ and $d = 0$. Reprinted with permission from [35]. Copyright 2017 by the American Physical Society.

In Fig. 2.3 we show s_0 as a function of the potential V_{mc} that the electrons experience in the modulation channel due to the external gate voltage. For clarity, we study the case of vanishing gap ($d = 0$) between heating and modulation channel and a fixed channel width first. Those mesoscopic aspects are addressed in Sec. 2.2. The results shown in Fig. 2.3 are calculated for the setup in Fig. 2.2 with $w_{\mathrm{hc}} = w_{\mathrm{mc}} = l_0/2$ and $d = 0$. (The potential in the heating channel, V_{hc}, and the modulation channel, V_{mc}, are obtained from the applied gate voltage by multiplying with the electron charge $-e$ and a device-dependent lever factor.) For vanishing potential in the modulation channel, $V_{\mathrm{mc}} = 0$, the setup is spatially symmetric and the transverse voltage vanishes accordingly. A positive modulation potential V_{mc} decreases the Fermi energy, $\epsilon_{\mathrm{F}} = \epsilon_{\mathrm{F},0} - V_{\mathrm{mc}}$, and, thus, the carrier density n in the modulation channel, which leads to an enhanced Seebeck coefficient S there. That results in a positive s_0, which diverges close to the depletion of the 2DEG in the modulation channel (for $V_{\mathrm{mc}} \to \epsilon_{\mathrm{F},0}$). For an enhanced carrier density, on the other hand, s_0 becomes negative since the Seebeck coefficient in the modulation channel is reduced compared to the ungated region of the 2DEG on the opposite side of the heating channel. The solid (red) line in Fig. 2.3 depicts s_0 for the absence of a modulation of the carrier density within the heating channel. For comparison, the dashed (blue) line and dotted (green) line in Fig. 2.3 represent results with a finite potential within the heating channel. Since the applied voltage that drives

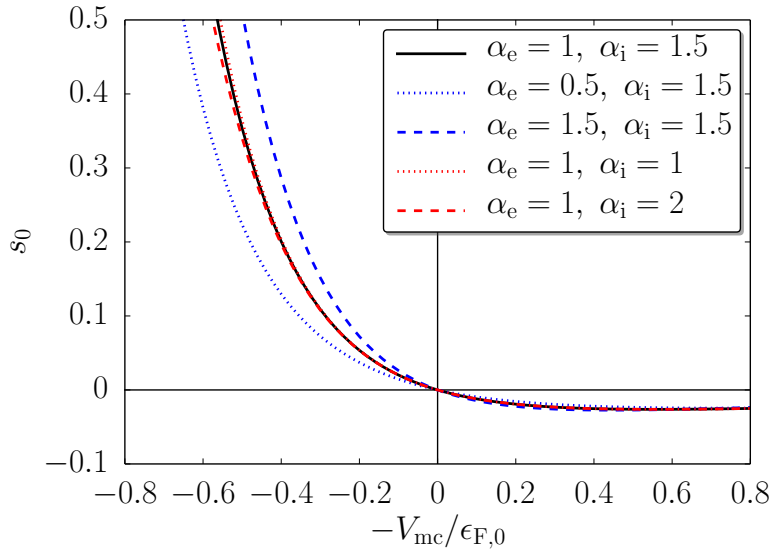

Figure 2.4: Dependence of s_0 on the electrostatic potential in the modulation channel V_{mc} comparing different α_e and α_i. Referring to the setup in Fig. 2.2, we set $w_{\mathrm{hc}} = w_{\mathrm{mc}} = l_0/2$ and $d = 0$. Reprinted with permission from [35]. Copyright 2017 by the American Physical Society.

the current in x-direction is kept constant, the density modulation in the heating channel influences the current and, thereby, the energy acquired by the electrons. That leads to a larger amplitude of s_0 for negative V_{hc} and vise versa. For the following discussion (except when discussing smeared potential steps in Sec. 2.2.4), we set $V_{\mathrm{hc}} = 0$, which yields $s = s_0$.

In Fig. 2.4, we compare the results for five different sets of exponents α_e and α_i (using again $w_{\mathrm{hc}} = w_{\mathrm{mc}} = l_0/2$ and $d = 0$). We find that the variation of s_0 is small even for the large range of chosen α_e (from 0.5 to 1.5) and α_i (from 1 to 2). This shows that the specific values of the exponents are of minor importance.

2.1.5 Multiple heating channels

Almost entirely throughout this thesis, we consider setups with only one heating channel. By this, we avoid structures that are experimentally more difficult to realize and control. But, more importantly, the restriction to one heating channel only is motivated on the theoretical ground by the linear structure of the differential equation Eq. (2.6) with respect to ω. If there are several heating channels, the total temperature increase is just the sum of the individual temperature increases $\delta T_j(y) = T_j(y) - T_0$ that would arise if only heating channel j was carrying an electric current while all other channels were kept current free. Therefore, considering only one heating channel does not define a conceptual restriction.

The transverse rectifier studied in Ref. [2] is an example of a device with effectively two heating channels since electric current was passed through two connected, parallel 2DEG stripes with different carrier densities. As stated above, the total output voltage is, in this case, the sum of the voltages generated by the heating currents in the individual channels. Furthermore, this is an example of the case that heating and modulation channel coincide, while for most of the results shown in this part of the thesis we assume the heating channel not to be gated.

2.2 Mesoscopic effects

In order to discuss mesoscopic aspects of the diffusion thermopower, we consider a suitable reference in the macroscopic regime first. For this, we study an ungated device, $V_{\mathrm{hc}} = V_{\mathrm{mc}} = 0$, with a wide heating channel, $w_{\mathrm{hc}} \gg l_0$. Then, the voltage drop between a position deep inside the heating channel and a contact far outside leads to the result

$$s_0 = 1 + \alpha_{\mathrm{e}} \quad , \tag{2.12}$$

which depends only on one, material-specific parameter α_{e}. To derive Eq. (2.12), we first determine the temperature increase deep inside the heating channel. For this we use Eq. (2.8) together with Eq. (2.10c) to get

$$T_{\mathrm{bulk}} - T_0 = \frac{3\,\omega\,\epsilon_{\mathrm{F},0}}{\pi^2 k_{\mathrm{B}}^2 T_0} \quad . \tag{2.13}$$

Since the Seebeck coefficient

$$S = -\frac{\pi^2}{3}\frac{k_{\mathrm{B}}^2 T_0}{e}\frac{1+\alpha_{\mathrm{e}}}{\epsilon_{\mathrm{F},0}} \tag{2.14}$$

is constant in space, the integration in Eq. (2.2) is trivial and leads to Eq. (2.12).

Device geometries as depicted in Fig. 2.1, however, in which the transverse voltage is measured spatially separated from the heating channel, can not access the individual voltage drop between heating channel and left or right contact. Instead, the difference between the contributions from the left and the right hand side is measured, which immediately yields $s_0 = 0$ in case of a symmetric device. Here, the modulation channel with $V_{\mathrm{mc}} \neq 0$ on the right side of the heating channel breaks the left/right symmetry. To remain in the macroscopic limit, we take $w_{\mathrm{mc}} \gg l$ and set $d = 0$. If the electron density in the modulation channel is reduced, the Seebeck coefficient is increased there, i.e., the contribution from the right part of the device to the thermopower dominates over the one from the left, so that $s_0 > 0$ (see Fig. 2.3). We remark that the contribution from the modulation channel to the total transverse voltage, $S\Delta T$, depends on the temperature difference $\Delta T = T_{\mathrm{i}} - T_0$ between the temperature T_{i} at the heating-/modulation-channel interface and the base temperature T_0. The interface temperature, T_{i}, which differs

from T_{bulk} reached deep inside the heating channel, depends on V_{mc} via (in the macroscopic regime)

$$\frac{T_{\mathrm{i}} - T_0}{T_{\mathrm{bulk}} - T_0} = \frac{1}{1 + (1 - V_{\mathrm{mc}}/\epsilon_{\mathrm{F},0})^{(1+\alpha_{\mathrm{e}}-\alpha_{\mathrm{i}})/2}} \quad . \tag{2.15}$$

To determine the temperature T_{i} at the interface at $y = 0$ between an infinitely wide heating channel and infinitely wide modulation channel at finite potential V_{mc}, we need to solve the differential equation Eq. (2.6) for $y < 0$ and $y > 0$ separately,

$$T(y) = \begin{cases} T_{\mathrm{bulk}} + (T_{\mathrm{i}} - T_{\mathrm{bulk}}) \exp(y/l_0) & \text{for } y < 0 \\ T_0 + (T_{\mathrm{i}} - T_0) \exp(-y/l) & \text{for } y > 0 \end{cases} \quad , \tag{2.16}$$

where l and l_0 are the energy diffusion lengths in the modulation and the heating channel, respectively. As explained in Sec. 2.1.2, not only T but also $\kappa(\partial T/\partial y)$ has to be continuous. Making use of Eqs. (2.10b) and (2.11a), we obtain

$$(T_{\mathrm{bulk}} - T_{\mathrm{i}})\, \epsilon_{\mathrm{F},0}^{(1+\alpha_{\mathrm{e}}-\alpha_{\mathrm{i}})/2} = (T_{\mathrm{i}} - T_0)\, (\epsilon_{\mathrm{F},0} - V_{\mathrm{mc}})^{(1+\alpha_{\mathrm{e}}-\alpha_{\mathrm{i}})/2} \quad , \tag{2.17}$$

which is equivalent to Eq. (2.15).

For $V_{\mathrm{mc}} = 0$, the interface temperature is just the arithmetic mean $T_{\mathrm{i}} = (T_{\mathrm{bulk}} + T_0)/2$, and in the limit of an almost depleted modulation channel, $\epsilon_{\mathrm{F},0} - V_{\mathrm{mc}} \ll \epsilon_{\mathrm{F},0}$, the interface temperature T_{i} approaches T_{bulk}.

The V_{mc} dependence of the Seebeck coefficient in the modulation channel is given by $\epsilon_{\mathrm{F},0}/(\epsilon_{\mathrm{F},0} - V_{\mathrm{mc}})$, i.e., it becomes large in the limit of an almost depleted modulation channel. In this case, the contributions to the transverse voltage outside the modulation channel can be neglected. Setting, furthermore, $T_{\mathrm{i}} \approx T_{\mathrm{bulk}}$, we find that

$$s_0 \approx \frac{1 + \alpha_{\mathrm{e}}}{1 - V_{\mathrm{mc}}/\epsilon_{\mathrm{F},0}} \tag{2.18}$$

diverges when approaching full depletion. After the replacement $T_{\mathrm{i}} \approx T_{\mathrm{bulk}}$, we calculate s_0 by making use of Eqs. (2.13) and (2.14). But, in order to take the gate voltage in the modulation channel into account, we replace in Eq. (2.14) $\epsilon_{\mathrm{F},0}$ by $\epsilon_{\mathrm{F},0} - V_{\mathrm{mc}}$. This immediately yields Eq. (2.18).

In the mesoscopic regime, the measured diffusion thermopower depends on the geometric lengths of the device. First, once the width of the heating channel becomes comparable to the energy diffusion length, $w_{\mathrm{hc}} \sim l_0$, the maximum of the temperature profile within the heating channel is substantially smaller than the value T_{bulk} reached in the macroscopic limit. Thus, the interface temperature T_{i} is smaller and the transverse voltage, too. Second, a modulation-channel width comparable to the energy diffusion length, $w_{\mathrm{mc}} \sim l$, has the effect that the temperature cannot fully drop to the base temperature T_0 in the modulation channel. This also leads to a reduction of s_0. Third, the energy diffusion also defines the length scale on which heating and modulation channel can be separated without loosing the

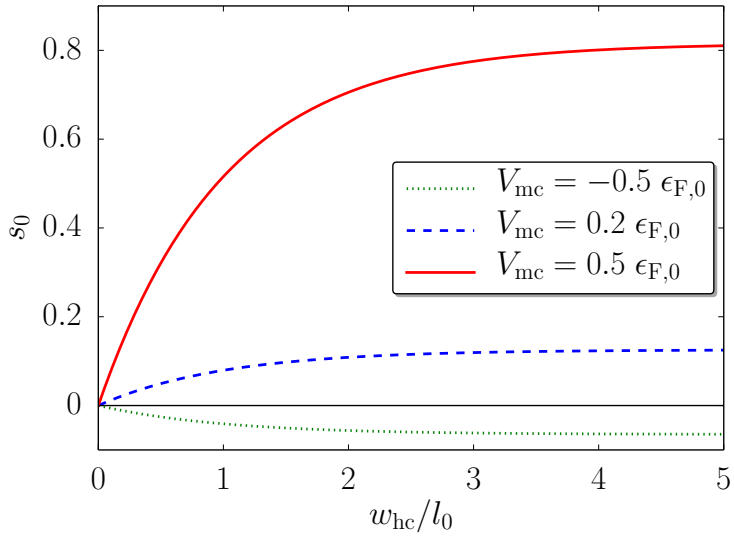

Figure 2.5: Dependence of s_0 on the width of the heating channel w_{hc} for the potential V_{mc} in the modulation channel. Referring to the setup in Fig. 2.2, we set $w_{\mathrm{mc}} = l_0/2$ and $d = 0$. Reprinted with permission from [35]. Copyright 2017 by the American Physical Society.

transverse voltage: as long as $d \lesssim l_0$, the electrons in the modulation channel will experience a temperature gradient and s_0 will be finite. A fourth mesoscopic effect is associated with the variation of the charge-carrier density on a length λ for smeared potential steps.

2.2.1 Heating-channel width

First, we discuss the role of the heating-channel width. For this, we consider a device with $d = 0$ (no space between heating and modulation channel) and fixed potential V_{mc}. As we stated before, we restrict the results presented here to the case $V_{\mathrm{hc}} = 0$. The energy diffusion length sets the scale of spatial temperature variations. Explicitly, the vanishing potential in the heating channel fixes the energy diffusion length there. As an important consequence, the maximal possible value T_{bulk} of the temperature in the heating channel can only be asymptotically reached if the heating-channel width w_{hc} is large compared to the energy diffusion length. In the opposite limit, the maximum of the electron temperature in the heating channel is much lower than T_{bulk}. This means that the temperature drop across the modulation channel and, therefore, also the transverse voltage is reduced.

This reasoning is consistent with the results shown in Fig. 2.5, where the dependence of s_0 on w_{hc} is depicted for $w_{\mathrm{mc}} = l_0/2$ (and $d = 0$): For $w_{\mathrm{hc}} \lesssim l_0$, the transverse voltage and, thus, s_0 is reduced. In case of vanishing V_{hc}, the

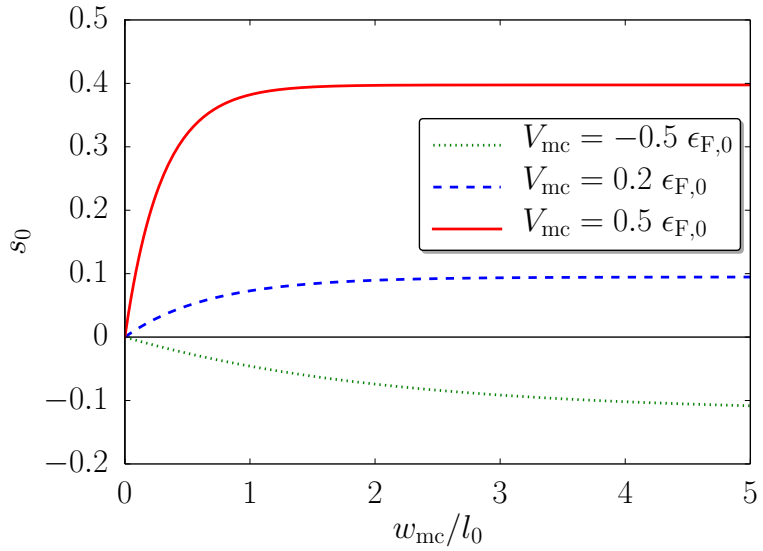

Figure 2.6: Dependence of s_0 on the width of the modulation channel w_{mc} for the potential V_{mc} in the modulation channel. Referring to the setup in Fig. 2.2, we set $w_{\mathrm{hc}} = l_0/2$ and $d = 0$. Reprinted with permission from [35]. Copyright 2017 by the American Physical Society.

functional dependence of s_0 on w_{hc} is exactly given by the exponential relation $s_0(w_{\mathrm{hc}}) = s_0(\infty)\,[1 - \exp(-w_{\mathrm{hc}}/l_0)]$.

The heating-channel width should be compared with the energy-diffusion length of the heating channel. The latter could be tuned via a nonvanishing V_{hc}. For a positive V_{hc}, the energy diffusion length is reduced such that the suppression of U_y is less severe for a fixed value of w_{hc}. However, also the energy ω decreases, and this has a much stronger effect on s_0 than the reduction of l.

2.2.2 Modulation-channel width

Next, we discuss the dependence of s_0 on the modulation-channel width w_{mc} while keeping the heating-channel width fixed.

Again, we take $d = 0$ (no space between heating and modulation channel) and $V_{\mathrm{hc}} = 0$. The finite potential V_{mc} in the modulation channel fixes the energy diffusion length there. In Fig. 2.6, we show the w_{mc} dependence of s_0 for $w_{\mathrm{hc}} = l_0/2$. We, again, find an exponential behavior.

The relevant length scale is the energy diffusion length, l, in the modulation channel. For $w_{\mathrm{mc}} \gg l$, the temperature profile is such that the temperature at the right edge of the modulation channel already reaches the base temperature T_0. A large temperature drop within the modulation channel is accompanied by a large value of s_0. For $w_{\mathrm{mc}} \lesssim l$, this temperature drop is reduced and s_0 is smaller.

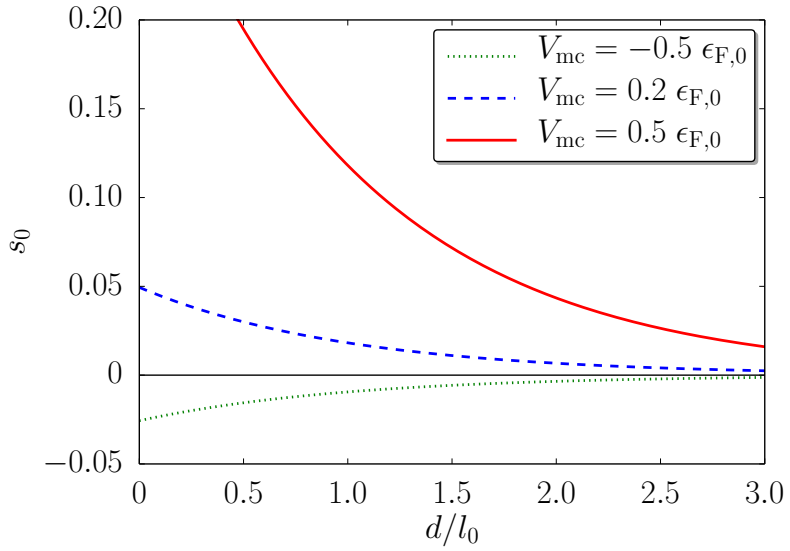

Figure 2.7: Dependence of s_0 on the distance d between heating and modulation channel for different potentials V_{mc} in the modulation channel. Referring to the setup in Fig. 2.2, we set $w_{\mathrm{hc}} = w_{\mathrm{mc}} = l_0/2$. Reprinted with permission from [35]. Copyright 2017 by the American Physical Society.

The fact that the energy diffusion length l in the modulation channel depends on the potential V_{mc} can be clearly seen in Fig. 2.6. For positive values of V_{mc} (decreased electron density) the energy diffusion length l becomes smaller than the reference l_0, for negative values of V_{mc}, l is larger.

2.2.3 Heating-/modulation-channel distance

Not only the widths of heating and modulation channel matter, but also their separation d from each other. For separations d much larger than the energy diffusion length l_0, the elevated temperature in the heating channel drops down to base temperature before reaching the beginning of the modulation channel. As a consequence, there is no temperature drop across the modulation channel, and the transverse voltage vanishes. A finite s_0 requires $d \lesssim l_0$. This is illustrated in Fig. 2.7 for different values of V_{mc}.

2.2.4 Sharpness of the potential step

Another length that may be relevant in some devices is the width on which a potential step is smeared. So far, we have always assumed sharp steps. To investigate the role of a finite step width, we construct a smooth potential profile which

changes on a characteristic length λ. As an example, we take

$$V(y) = V_{\mathrm{mc}} \frac{\tanh(2\,y/\lambda) + 1}{2} \tag{2.19}$$

in the range $-6\,l_0 < y < 6\,l_0$ depicted in panel (a) of Fig. 2.8. Here, V_{mc} is the height and λ the width of the step. The modulation and heating channel are kept at a constant width of $w_{\mathrm{hc}} = w_{\mathrm{mc}} = 6\,l_0$, which allows for a variation of λ on an appropriate range without side effects.

Figure 2.8 (b) shows the dependence of s_0 on λ for different step heights V_{mc}. Again, we find an exponential dependence of s_0 on a length scale given by the energy diffusion length. The finiteness of the step width influences s_0 in different ways. First, the energy diffusion length l is changed over a region of length λ across the interface, which, in turn, influences the temperature profile. Second, the Seebeck coefficient S becomes y-dependent. Third, the amount of excess energy ω provided by the heating current is modified at the edge of the heating channel. The combination of the three gives rise to the behavior displayed in Fig. 2.8 (b). For negative values of V_{mc}, the effect on ω dominates and the amplitude of s_0 gets larger with increasing λ. For positive values of V_{mc}, on the other hand, the effects on S and l are more important and s_0 decreases as function of λ.

2.2.5 Additivity

In order to amplify the output transverse voltage, one may want to put n devices (each consisting of one heating and one modulation channel) in series (similarly as it is done for electron ratchets [77, 106, 107] or in the context of state-dependent diffusion [108]). Then the important question arises, whether the n devices simply add, i.e., whether the total output voltage is just n times the voltage of a single device.

To answer this question, we model a structure as shown in the inset of Fig. 2.9. For each single device, we choose $w_{\mathrm{hc}} = w_{\mathrm{mc}} = l_0/2$ and $d = 0$. Neighboring devices are separated by an ungated and current-free channel of the length a. The applied electrical field E_x driving the heating current is the same in all devices. As discussed in Sec. 2.1.5, there is a superposition principle for the heating currents: the profile of the total temperature increase is just the sum of the temperature-increase profile δT_j due to device $j = 1, \ldots, n$. We find that for $a \gg l_0$, the total s_0 is just n times the result for a single device, i.e., additivity holds. Neighboring devices do not influence each other since the increased temperature due to heating in device j has already dropped down to base temperature T_0 before reaching the neighboring devices $j \pm 1$ (see dashed line in Fig. 2.9 which shows the minimum value δT_{min} of the temperature increase in between neighboring devices). This is different for $a \lesssim l_0$. In this case, the temperature profiles generated by neighboring devices influence each other, and the overall performance is reduced. In the extreme limit $a = 0$, the total performance is independent of the number n of devices. This can be

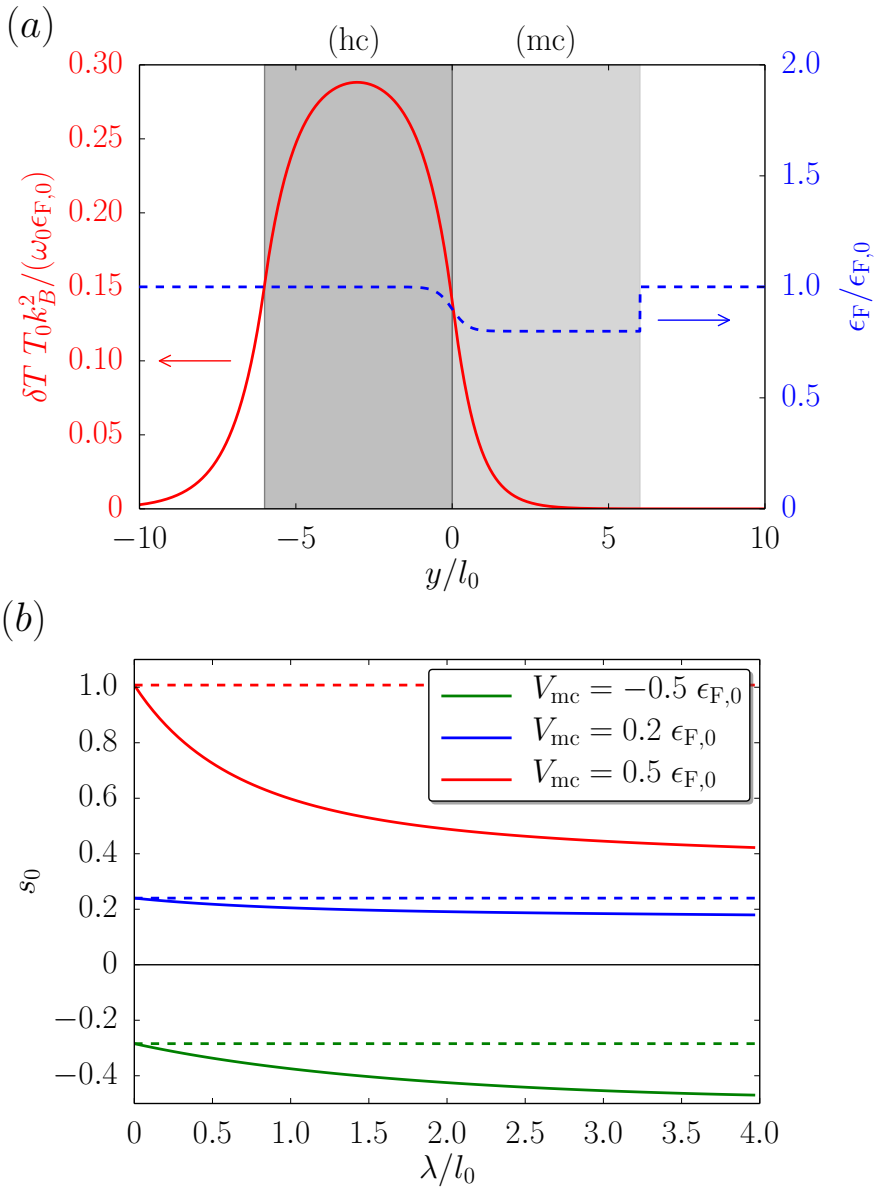

Figure 2.8: Dependence of s_0 on the sharpness of the potential step between modulation and heating channel. The width of the channels is set to $w_{\mathrm{hc}} = w_{\mathrm{mc}} = 6\,l_0$ and the distance $d = 0$. (a) The step of the Fermi energy at the heating-/modulation-channel interface is shown by the blue dashed line. The potential $V(y)$ is taken from Eq. (2.19). The red line marks the temperature difference, $\delta T(y)$, to the base temperature, T_0. For (a) we use $V_{\mathrm{mc}} = 0.2\,\epsilon_{\mathrm{F},0}$ and $\lambda = l_0/2$. (b) The dashed lines mark s_0 for a sharp step potential for different potentials V_{mc} in the modulation channel. The solid lines depict the influence of the step width λ. Reprinted with permission from [35]. Copyright 2017 by the American Physical Society.

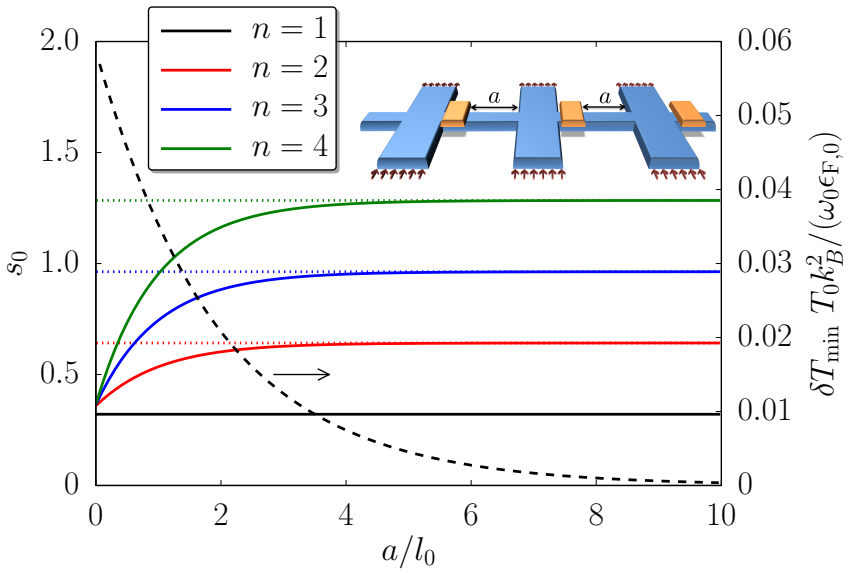

Figure 2.9: The solid lines mark s_0 for n devices as function of a. The black, dashed line show the minimum temperature value between the devices, also as function of a. The inset depicts an example consisting of three devices (with $w_{\mathrm{hc}} = w_{\mathrm{mc}} = l_0/2$ each), separated by a distance a. Reprinted with permission from [35]. Copyright 2017 by the American Physical Society.

easily understood by observing that the devices in the middle build a symmetric potential landscape of the modulation channels such that only the edge devices contribute, which is equivalent to $n = 1$.

2.3 Relation to recent experiments

The output voltage measured in Ref. [2] as a function of two gate voltages could only be explained by including the mesoscopic effects due to finite heating- and modulation-channel widths as compared to the energy diffusion length. This was, actually, the motivation for the systematic study of the mesoscopic aspects presented here.

But there is also an earlier measurement of the diffusion thermopower in a 2DEG realized in a GaAs/AlGaAs heterostructure [3], in which mesoscopic effects due to the finite modulation-channel width may play a role. Chickering *et al.* found a dependence of the thermopower on temperature and electron density that is compatible with the Mott formula.

For temperatures $T_0 \lesssim 2\,\mathrm{K}$, the absolute value of the thermopower was, however, reduced by about 20% as compared to what they expected in their analysis. Thereby, they did not take mesoscopic effects into account.

In the following we discuss a calculation of the device used in Ref. [3] by means of the model introduced so far. The potential profile that accounts for the data in Fig. 2 of Ref. [3] for $\Delta(1/n_\mathrm{e}) = 4.9 \times 10^{-12}\,\mathrm{cm}^2$ at 2 K is shown in Fig. 2.10 (a). Here, $\Delta(1/n_\mathrm{e})$ is the difference of the reciprocal carrier density between the right and left modulation channel. The dark gray region in Fig. 2.10 (a) indicates the narrow heating channel of width $w_\mathrm{hc} = 60\,\mu\mathrm{m}$. Two modulation channels (light gray) of width $w_\mathrm{mc} = 300\,\mu\mathrm{m}$ are placed left and right of the heating channel. We are able to identify the momentum-relaxation time $\tau_{\mathrm{e},0} = 0.126\,\mathrm{ns}$ from the electric conductivity under the assumption that the energy-relaxation time $\tau_{\mathrm{i},0}$ is much larger. In this case we can set the exponent α_e to the corresponding value, $\alpha_\mathrm{e} = 0.9$, used by Chickering *et al.*. Unfortunately, the value for $\tau_{\mathrm{i},0}$ and α_i are not known for this experiment. For the exponent α_i, we take the same value as determined in Ref. [2]. As discussed previously, the effects of that parameter are of minor importance.

In panel (a) of Fig. 2.10, we show the calculated temperature profile if we assume $\tau_{\mathrm{i},0} = 100\,\tau_{\mathrm{e},0}$, which is close to the ratio found for the device in Ref. [2]. The fact that the temperatures on the outer edges of the modulation channels have not yet reached base temperature indicates that mesoscopic corrections due to a finite modulation-channel width have to be expected. Mesoscopic effects due to the finite heating-channel, on the other hand, are not relevant for the 20% deviation of the measured thermopower since Chickering *et al.* measured the average temperature in the heating channel instead of calculating T_bulk from the heating current. In panel (b) of Fig. 2.10, we compare the results of Ref. [3] for $\Delta(1/n_\mathrm{e}) = 4.9 \times$

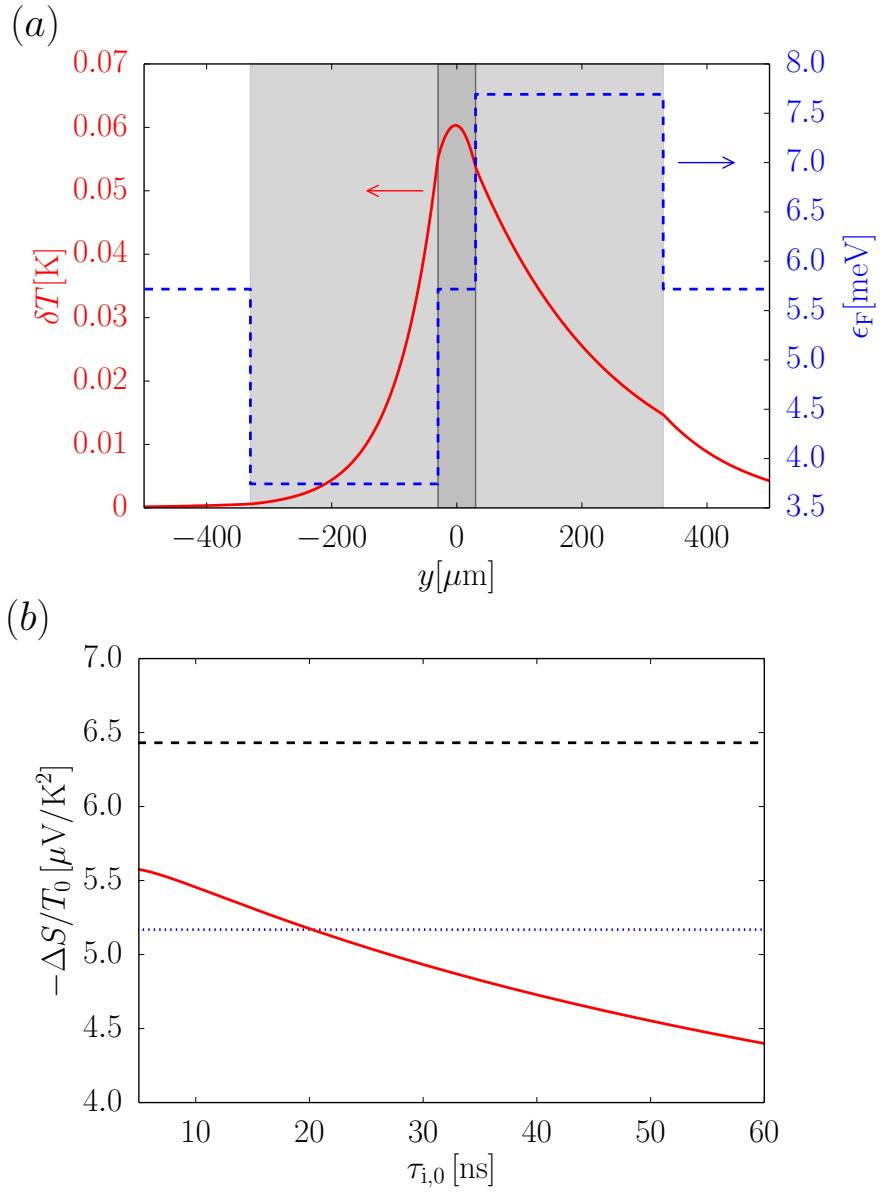

Figure 2.10: Results for a setup consisting of one heating channel of width $w_{\mathrm{hc}} = 60\,\mu\mathrm{m}$ and two neighboring modulation channels of widths $w_{\mathrm{hc}} = 300\,\mu\mathrm{m}$ each. The calculations are done for $T_0 = 2\,\mathrm{K}$ and $\tau_{\mathrm{e},0} = 0.126\,\mathrm{ns}$ (extracted from the mobility in Ref. [3]). (a) The red, solid line marks the profile of δT and the local Fermi energy is depicted by the blue, dashed line. We choose $\tau_{\mathrm{i},0} = 100\,\tau_{\mathrm{e},0}$ for the energy-relaxation time. (b) The black, dashed and the blue, dotted lines represent the theoretical and measured results for thermopower divided by the lattice temperature obtained by Chickering *et al.* [3], respectively. The red, solid line accounts for mesoscopic effects. Reprinted with permission from [35]. Copyright 2017 by the American Physical Society.

$10^{-12}\,\mathrm{cm}^2$ at 2 K to the results of the calculation that includes mesoscopic effects based on the diffusion thermopower model. That is done in dependence of the unknown quantity $\tau_{\mathrm{i},0}$ which crucially influences the mesoscopic effects since the energy relaxation time enters the energy diffusion length. The black, dashed line in Fig. 2.10 (b) corresponds to the result determined by the Mott formula (2.11b). The difference of the thermopower in the right and left modulation channel, ΔS, is divided by the base temperature T_0. The blue, dotted line shows the measured $-\Delta S/T_0$, where the amplitude is reduced by about 20% compared to the dashed line. To include mesoscopic aspects, we calculate the transverse voltage and divide it by both T_0 and the average (measured) temperature in the heating channel which yields the red, solid line in Fig. 2.10 (b). We find a reduction of about 15% to 25% for realistic choices of the energy-relaxation time.

2.4 Measuring the energy diffusion length

For studying thermoelectric effects which are associated with the electron temperature and energy diffusion in 2DEGs, it is important to determine the energy diffusion length. To do so in an indirect way, one may measure the momentum and the energy relaxation times τ_{e} and τ_{i}. This may be an easy task for τ_{e} (since it is related to the electrical conductivity), but determining τ_{i} is more challenging. Our analysis, however, suggests that transverse thermoelectric rectifiers realized in 2DEGs are ideal systems to directly access the energy diffusion length by systematically varying the width of heating or modulation channels or distances between them: the dependence of s (the mesoscopic analogon to the thermopower) on these lengths, calculated within the diffusion thermopower model, can be nicely approximated by exponential functions that depend on these lengths divided by the corresponding energy diffusion length l.

From the relation $l = v_{\mathrm{F}}\sqrt{\tau_{\mathrm{e}}\tau_{\mathrm{i}}/2}$ it is immediately clear that the energy diffusion length can be tuned by applied gate voltages via the energy dependence of the Fermi velocity and the relaxation times. Assuming that the energy dependences of v_{F} and τ_{e} are known, a systematic variation of the gate voltage fixing the potential in a modulation channel of a transverse thermoelectric rectifier allows for an investigation of the energy dependence of τ_{i} which may be more difficult to access by alternative methods.

A similar concept was applied by Billiald *et al.* [32]. They were able to determine the energy diffusion length and the dependence of the inelastic scattering on the electron density by measuring the thermoelectric voltage generated by a heated electron gas. The work by Billiald *et al.* was supported by the understanding of mesoscopic effects, which are discussed in this part of the thesis. They applied the diffusion themopower model introduced here and published the results in Ref. [35].

2.5 Magnitude of the output voltage

The magnitude of the electric voltage generated by a given temperature difference is characterized by the Seebeck coefficient S. For a 2DEG at low temperature, S scales linearly with temperature and is proportional to the inverse of the electron density, $S \sim T/n$. To characterize the performance of the all-electric devices studied in this thesis, however, we use the dimensionless quantity $s = eU_y/\omega$. Instead of relating the thermoelectric output voltage, U_y, to a temperature difference, which is not directly externally controlled but only appears indirectly as a consequence of electrical heating, we take as a reference the energy ω that is acquired per electron due to Joule heating. As can be seen from Eq. (2.12), s is a dimensionless quantity of order one that does not scale with temperature T or electron density n. This can also be understood in the following way: Since the electrons form a Fermi gas, the extra energy ω deposited on average per particle by Joule heating is not uniformly distributed to all electrons but only to some fraction $k_\mathrm{B}T/\epsilon_\mathrm{F} = \rho k_\mathrm{B}T/n_\mathrm{e}$ around the Fermi level. Therefore, the temperature increase due to Joule heating scales with $\omega n_\mathrm{e}/T$ (see also Eq. (2.8)), which compensates the T/n_e dependence of the Seebeck coefficient such that s is of order one.

The input parameter in experiments is not ω but the bias voltage or, equivalently, the electric field E_x driving the electric current which heats up the electrons. Therefore, it may be interesting to discuss the temperature and electron density dependence of ω for fixed E_x. As can be seen from Eq. (2.9) or (2.11c), ω scales with $n_\mathrm{e}^{\alpha_\mathrm{e}+\alpha_\mathrm{i}}$, independent of temperature.

How can the output voltage be maximized for given input voltage? The above mentioned compensation of the T/n_e dependence of the Seebeck coefficient with the $\omega n_\mathrm{e}/T$ dependence of the temperature increase due to Joule heating can be modified by choosing different electron densities n_hc and n_mc in the heating channel (responsible for the temperature increase) and the modulation channel (important for the thermoelectric voltage), respectively. For a depleted modulation channel, s is increased by a factor of $n_\mathrm{e,hc}/n_\mathrm{e,mc}$, see also Eq. (2.18) as well as Figs. 2.3 and 2.4.

An important message of Sec. 2.2 is that mesoscopic effects tend to reduce the output voltage. To prevent this reduction, the width of both the heating and the modulation channel should be larger than the energy diffusion length l (see Figs. 2.5 and 2.6). The distance between heating and modulation channel should, on the other hand, be smaller than l, see Fig. 2.7. And finally, for a series of multiple elements in the device, the distance between neighboring elements should be larger than l, see Fig. 2.9.

Furthermore, a series of elements as shown in Fig. 2.9 provide the possibility for increasing the output voltage because the output signal scales with the number of elements (if the distance is larger than l). That concept of additivity is certainly a tool for optimization. However, it requires the same number of heating channels and, thus, the total input current increases simultaneously for fixed input voltage.

This diffusion thermopower model allows for an appropriate description of the discussed mesoscopic effects in a low temperature regime. However, there are situations where a characterization of the electron system by a temperature profile and chemical potential only is not sufficient anymore. That is the case, e.g., when higher orders of the Sommerfeld expansion contributes significantly. Thus, for a systematic treatment of the low-temperature regime, the non-equilibrium distribution function of the electrons needs to be generalized. We present such a generalization in the next part of this thesis. Therein, the diffusion thermopower model used in this part can be identified in lowest order of the Sommerfeld expansion.

3 A Boltzmann equation approach beyond quasi-equilibrium

The theoretical approach that has been used in Section 2 is based on an electron distribution which differs only slightly from a Fermi function $f_{\mathrm{F}}(\epsilon, \mu(\boldsymbol{r}), T(\boldsymbol{r}))$ with a spatially dependent chemical potential and temperature. We have seen that the electron temperature T differs from the temperature T_0 of the environment and that the thermoelectric transverse voltage of the system depends on the electron temperature profile. However, the fact that the electron system can be described by a temperature in a non-equilibrium state (only) is not given necessarily. For the system discussed in Sec. 2, that is only the case at low temperature where $k_B T \ll \epsilon_{\mathrm{F}}$, which we will see later in this part of the thesis. If such an ansatz is applicable, we refer to this approximation of the non-equilibrium distribution function by the term *quasi-equilibrium* since the Fermi function takes the form of a local-equilibrium function with position-dependent chemical potential and position-dependent temperature.

In this chapter, we show that there are situations where the description by quasi-equilibrium has to be generalized for an appropriate determination of the thermoelectric voltage. We discuss an analytic method to solve the Boltzmann equation by means of an expansion of energy moments in the manner of hydrodynamic equations [36–40]. An effective, deterministic equation is derived incorporating both, elastic and inelastic scattering processes in a relaxation-time approximation. The non-equilibrium contributions to the electrochemical potential are calculated within a systematic Sommerfeld expansion which leads to corrections of the Mott's representation of the thermopower [41]. Correspondingly, we calculate not only the equivalent to a temperature profile, but the profiles of higher energy moments of the non-equilibrium distribution function as well.

The device geometry and diffusive regime studied here is the same as discussed in Chap. 2. Nevertheless, for a rigorous derivation of necessary balance equations, we need to start with a detailed description of the model in Sec. 3.1. Afterwards, we introduce and derive the semiclassical transport approach starting from the Boltzmann equation in Sec. 3.2. That approach supports basically the theory used in Chap. 2. However, the systematic expansion that leads to an effective solution for the relevant contributions of the electron distribution allows for a

better understanding of the thermoelectric relations and transport characteristics. Moreover, the approach described in the following can, in principle, be extended so that other device geometries in a semiclassical regime can be studied. Concluding the analytical derivation of the higher-order contributions to the transverse voltage, Sec. 3.3 discusses the profiles of the higher energy moments and the differences of the expected transverse voltage in comparison to a classic quasi-equilibrium model discussed in Chap. 2.

3.1 Model

We start with a detailed model for the device geometry studied in Chap. 2. Again, we consider a two-dimensional electron gas in the x-y-plane. A spatially confined region with respect to y is characterized by a finite electric field, which is applied externally. The latter points in x-direction only, $\boldsymbol{E} = (E_x, 0)$, and leads to the current density $\boldsymbol{j} = (j_x, 0)$ correspondingly. We assume that the y-component of the current density vanishes everywhere. The region of finite electric field works as a heating channel, where additional energy is transferred into the electronic system. The system is considered to be homogeneous in x. That approximation is valid as long as the characteristic length scales with respect to the transverse y-direction are small compared to the length of the device in x-direction. In principle, we may allow for multiple heating channels which are parallel aligned and connected transversally (see Sec. 2.1.5).

We aim for calculating the non-equilibrium contributions to the transverse voltage, U_y, which is defined by the difference of the electrochemical potential between $y = -\infty$ and $y = \infty$. The electrochemical potential,

$$\phi = -\frac{\Phi + \mu}{e} \quad , \tag{3.1}$$

consists of the electric, $-\Phi/e$, and the chemical potential, μ. While the spatial dependence of the potential Φ gives rise to an electric field, the gradient of the chemical potential μ is a diffusive force implicating the relation between the carrier density and the chemical potential in an equilibrium state, $n_e = \rho\mu$. Here and in the following, ρ labels the density of states in two dimensions. The infinitely long voltage probes at which the difference in the electrochemical potential is measured are independent of the non-equilibrium effects for $y = \pm\infty$. Especially in this case, the carrier density is independent of E_x and the chemical potential $\mu(-\infty) = \mu(\infty)$ do not change. Therefore, the transverse voltage, U_y, is purely given by the electric contribution, Φ.

In the 2DEG, the total energy of the charge carriers reads $\epsilon = \epsilon_p + \Phi(x, y)$, with $\epsilon_p = (p_x^2 + p_y^2)/2m$. We assume parabolic bands with the effective electron mass m and the momentum $\boldsymbol{p} = (p_x, p_y)$. The general potential $\Phi(x, y)$ consists of different contributions, which we write in form of a perturbation expansion in the applied

electric field E_x,

$$\Phi(x,y) = \Phi_0(y) + \Phi_1(x,y) + \Phi_2(y) + \mathcal{O}(E_x^3) \quad . \tag{3.2}$$

The first term, $\Phi_0(y)$, breaks the symmetry of the equilibrium state for E_x, and thereby allows for a finite transverse voltage in case of finite E_x. That external potential can be considered as generated by gates with tunable bias voltages. To guarantee homogeneity in x, $\Phi_0(y)$ varies with respect to y only. We distinguish between potential variations on a length scale smaller or larger than the elastic mean free path, l_e, of the electrons in the 2DEG. If the potential varies on a length scale smaller than l_e, we describe those variations by a step-function. Thereby, we define stripes where the potential changes on a length scale larger than l_e confined by potential steps. Still, the length of these stripes with respect to x is much larger than their extension in y, which allows for the assumption of a homogeneous potential in x. The thermoelectric voltage generated by a potential step [109] or periodic potential [106] has been analyzed in case of an externally applied temperature gradient. In contrast to those works, we study the effect of a finite current, j_x, as the source of energy and, on top, we allow for arbitrary variations of the potential.

For example, Fig. 2.1 shows a middle region with an applied electric field ($E_x \neq 0$). That electric field drives the current I_x through the heating channel. The potential $\Phi_0(y)$ is externally controlled by the top gates on top of the heating channel (hc) and on top of the modulation channels (mc).

The terms in Eq. (3.2) that follow Φ_0 describe contributions generated by the electric field E_x perturbatively. That includes the external electric potential that leads to E_x as well as self-consistent generated non-equilibrium contributions due to charge accumulations, which lead to y-dependent contributions to Φ. However, due to the symmetry of the system, U_y is independent of the sign of the applied electric field, E_x. Therefore, we expect the contributions to the transverse voltage to vanish in first order. In particular, that is described by the condition $\partial_y \Phi_1 = 0$ which can be derived consistently in terms of the method described in the following sections. The leading non-equilibrium contribution, $\Phi_2(y)$, is of second order. Although contributions of higher order can, in principle, be calculated, we choose to focus on the leading contribution.

In first order in E_x, the potential Φ_1 with $\nabla_x \Phi_1 = eE_x$ takes account of the applied electric field, E_x. Here, we demand that E_x is independent of x, otherwise a x-dependent force in first order breaks the homogeneity with respect to x. Additionally, E_x vanishes everywhere but not within the heating channels, where it takes a constant value. That piecewise constant functional behavior is depicted by the y-dependence of Φ_1 in Eq. 3.2.

3.2 Semiclassical transport approach beyond quasi-equilibrium

In this section, we describe a semiclassical method that allows for a systematic calculation of non-equilibrium contributions to the distribution function, which lead to the measured transverse voltage. First, the Boltzmann equation is formulated in terms of a relaxation-time approximation with respect to elastic and inelastic scattering (Sec. 3.2.1) to derive balance equations for each moment of energy (Sec. 3.2.2). After applying a transformation that accounts for conserved quantities of the setup under consideration (Sec. 3.2.3), we perform a perturbation expansion of the Boltzmann equation with respect to the applied electric field, E_x, up to second order (Sec. 3.2.4). The Boltzmann equation can be solved partially on an effective length scale, where variations of characteristic quantities are determined by a length scale much larger than the elastic mean free path (Sec. 3.2.5). Using the effective solution, the balance equations of the energy moments and the corresponding current densities can be formulated by the isotropic distribution function. Instead of studying the full energy dependence of the distribution function, we can formulate the electrochemical potential by those energy moments. Thereby, only the spatial profile of the energy moments have to be determined (Sec. 3.2.6). That can be done by a systematic Sommerfeld expansion of the effective balance equations (Sec. 3.2.7). The electrochemical potential is incorporated self-consistently. The lowest order of the Sommerfeld expansion is equivalent to a quasi-equilibrium description with a spatially dependent temperature and chemical potential. That finding and the resulting expression for the transverse voltage are discussed in Secs. 3.2.8 and 3.2.9. The first correction in the Sommerfeld expansion goes beyond that quasi-equilibrium description. In addition to temperature, contributions of higher energy moments have to be taken into account (Sec. 3.2.10).

3.2.1 Boltzmann equation in relaxation-time approximation: elastic and inelastic scattering

We study the device geometry under the condition that the characteristic dimensions are large compared to the elastic mean free path. Therefore, the framework lies beyond the ballistic regime and a kinetic drift and diffusion description is appropriate. In the stationary limit, the Boltzmann equation for the distribution function, $f(\boldsymbol{p}, \boldsymbol{r})$, with $\boldsymbol{r} = (x, y)$, reads

$$\boldsymbol{v} \cdot \nabla_{\boldsymbol{r}} f + \boldsymbol{F} \cdot \nabla_{\boldsymbol{p}} f = -\frac{f - \langle f \rangle}{\tau_e} - \frac{f - \hat{f}}{\tau_i} \quad , \tag{3.3}$$

where the left-hand side consists of the diffusive term (first) with $\boldsymbol{p}/m = \boldsymbol{v}$ and the drift term (second). The force, $\boldsymbol{F}$, on the electrons is given by $\boldsymbol{F} = -\nabla_{\boldsymbol{r}} \Phi$.

In Eq. (3.3), we formulated the collision integral of the Boltzmann equation in a relaxation-time approximation of elastic and inelastic scattering processes [74, 101, 110]. Analogously to Chap. 1 and Chap. 2, we define *inelastic* processes by the condition that the change of energy is $k_B T$ or larger [69] (see Sec. 1.4.2). These scattering events determine the inelastic relaxation time τ_i. The corresponding term on the right-hand side of Eq. (3.3) describes the relaxation of the general non-equilibrium distribution function, f, to the local-equilibrium distribution function, $\hat{f}$, for which the collision integral of the Boltzmann equation vanishes. On the other hand, scattering events accompanied by an energy transfer smaller than $k_B T$ constitute the first term on the left-hand side of Eq. (3.3) with the *elastic* relaxation time τ_e. For elastic processes, we neglect energy relaxation of the distribution function. Therefore, the elastic scattering events lead to an isotropic distribution regarding the momentum $\boldsymbol{p}$, $\langle f \rangle (p, \boldsymbol{r})$ with $p = |\boldsymbol{p}|$ [76, 77, 103]. Both, the elastic and inelastic relaxation time, depend on the kinetic energy of the electrons relative to the lower subband edge and therefore on $\epsilon_p = p^2/(2m)$ only.

The energy dependence and the amplitude of the elastic and inelastic relaxation time are considered as input parameter, which can be determined experimentally, see e.g. Ref. [2]. Therefore, we set aside the discussion of different contributions to those relaxation times and refer to Refs. [44, 51, 111] and to Sec. 1.4.2 for further reading instead.

Motivated by the ability to distinct the relaxation terms of the Boltzmann equation, we divide the distribution function $f = \hat{f} + \bar{f} + \tilde{f}$ into three parts:

- the local-equilibrium distribution $\hat{f}(p, \boldsymbol{r})$, for which both relaxation terms vanish,
- the isotropic non-equilibrium correction $\bar{f}(p, \boldsymbol{r})$,
- and corrections which accounts for the momentum's direction, $\tilde{f}(\boldsymbol{p}, \boldsymbol{r})$. We claim $\langle \tilde{f} \rangle = 0$, where $\langle \ldots \rangle = \int_0^{2\pi} \frac{\mathrm{d}\vartheta}{2\pi} \ldots$ is the angle average in momentum space.

In this thesis, we restrict the analysis to transport properties of the electronic system. The phonon system, which is coupled to the electron system via the inelastic scattering is kept in an equilibrium state at temperature T_0. That incorporates the assumption that energy transport in the substrate and energy transfer into the environment are fast compared to the inelastic relaxation time. Then, the local-equilibrium distribution reads [76, 77]

$$\hat{f} = \frac{1}{1 + \exp\left(\frac{\epsilon_p - \hat{\mu}}{k_B T_0}\right)} \quad , \tag{3.4}$$

with a local chemical potential, $\hat{\mu}(y)$. The chemical potential is allowed to vary with respect to y since the local-equilibrium state, for which the scattering term of

Eq. (3.3) vanishes, is not necessarily the equilibrium state, f_0, itself. For $E_x = 0$, the equilibrium distribution function takes the form of the Fermi function

$$f_0(p, y) = \frac{1}{1 + \exp\left(\frac{\epsilon_p - \epsilon_\mathrm{F}(y)}{k_B T_0}\right)} \quad , \tag{3.5}$$

with the Fermi energy ϵ_F.

For low temperatures the elastic scattering dominates over the inelastic processes, see, e.g. Refs. [69, 112] for GaAs. We assume $\tau_e \ll \tau_i$ accordingly. Thus, elastic scattering is the dominating process that leads to relaxation of the angle-dependent momentum. In addition, a much weaker contribution leads to the same contribution based on inelastic scattering processes. In the following, we consider the elastic scattering to incorporate the total angle-dependent relaxation, while inelastic scattering yields the relaxation of the isotropic distribution function to local-equilibrium. Thus, we can replace

$$-\frac{f - \langle f \rangle}{\tau_e} - \frac{f - \hat{f}}{\tau_i} \approx -\frac{\tilde{f}}{\tau_e} - \frac{\bar{f}}{\tau_i} \quad , \tag{3.6}$$

in Eq. (3.3).

3.2.2 Balance equations and moment method

The Boltzmann equation (3.3) is a balance equation for the distribution function which depends on momentum and space. Considering observable quantities, such as charge or heat currents, certain *moments* of the Boltzmann equation describe the corresponding balance equations. That concept, known as *moment method* [38, 43], leads to the hydrodynamic equations for semiconductors [36, 39, 101, 110] and generalizations or extensions of those [40, 113, 114]. Here, in addition to charge carrier density and heat, we consider balance equations that result from isotropic energy moments, $(\epsilon_p - \mu)^n$, of arbitrary order. The energy is measured with respect to the chemical potential μ and, thus, corresponds to the heat of the system. Since the particle number is conserved, both terms describe the same physical property. Correspondingly, the generalized current of the n-th energy moment in two dimensions is defined by

$$\boldsymbol{j}^{(n)} = \int \frac{\mathrm{d}^2 p}{2(\pi\hbar)^2} \, (\epsilon_p - \mu)^n \, \boldsymbol{v} \, \tilde{f} \quad . \tag{3.7}$$

A factor of two accounts for the spin degree of freedom. Here, $-e\,\boldsymbol{j}^{(0)}$ is the charge and $\boldsymbol{j}^{(1)}$ the heat current density. Multiplying the Boltzmann equation (3.3) by $(\epsilon_p - \mu)^n$ and integrating over the phase space of the momentum yields

$$\nabla_{\boldsymbol{r}} \cdot \boldsymbol{j}^{(n)} = -\boldsymbol{F} \cdot \int \frac{\mathrm{d}^2 p}{2(\pi\hbar)^2} \, (\epsilon_p - \mu)^n \, \nabla_{\boldsymbol{p}} f - \int \frac{\mathrm{d}^2 p}{2(\pi\hbar)^2} \, (\epsilon_p - \mu)^n \, \frac{\bar{f}}{\tau_i} \quad . \tag{3.8}$$

For $n \geq 1$ the force term can be related to the $(n-1)$-th current by

$$\int \frac{\mathrm{d}^2 p}{2(\pi\hbar)^2} \, (\epsilon_p - \mu)^n \, \nabla_{\boldsymbol{p}} f = -n \, \boldsymbol{j}^{(n-1)} \tag{3.9}$$

and, thus, that energy moment is of a hierarchic structure. The left-hand side of Eq. (3.8) describes diffusion of the corresponding energy-moment current density. The first term on the right-hand side is a source term driven by $\boldsymbol{F}$. The second term represents relaxation of the energy moment.

In the following, we aim for a relation of the generalized current, $\boldsymbol{j}^{(n)}$, to the isotropic part of the distribution function. Using Eq. (3.8), an effective balance equation for the isotropic part of the distribution function is derived in terms of a perturbation expansion in E_x. To get an expression for $\boldsymbol{j}^{(n)}$ we will consider Eq. (3.3) again.

3.2.3 Transformation to conserved equilibrium quantities

It is convenient to change the parameters of $f(p_x, p_y, x, y)$ to $f(\epsilon_0, p_x, y)$. To choose p_x as an independent parameter is self-evident since p_x is a conserved quantity due to the system's homogeneity in x. We account for the latter by neglecting the x-dependence of f. The energy, ϵ, is a conserved quantity as well. However, due to the perturbation expansion in E_x, that we aim for, we use the energy of the equilibrium state ($E_x = 0$), $\epsilon_0 = \epsilon_p + \Phi_0$, as an independent parameter. Thereby, the equilibrium distribution depends on ϵ_0 only

$$f_0 = f_0(\epsilon_0) = \frac{1}{1 + \exp\left(\frac{\epsilon_0 - (\Phi_0 + \epsilon_\mathrm{F})}{k_B T_0}\right)} \quad . \tag{3.10}$$

The sum of Φ_0 and ϵ_F represent the Fermi level with respect to ϵ_0 and is independent of y. In the following, we consider $f = f(\epsilon_0, p_x, y)$ and $\langle f \rangle = \langle f \rangle \, (\epsilon_0, y)$ if not stated otherwise. After the afore mentioned transformation, Equation (3.3) reads

$$v_y \left[\frac{\partial f}{\partial y} - \frac{\partial \Phi_2}{\partial y} \frac{\partial f}{\partial \epsilon_0} \right] - e E_x \left[\frac{\partial f}{\partial p_x} + v_y \frac{\partial f}{\partial \epsilon_0} \right] = -\frac{\tilde{f}}{\tau_e} - \frac{\bar{f}}{\tau_i} \quad . \tag{3.11}$$

The applied transformation leads to vanishing force terms in zeroth order in E_x. Moreover, we use the assumption, discussed in Sec. 3.1, that Φ_1 is a step-function with respect to y and thus $\frac{\partial \Phi_1}{\partial y} = 0$.

Note that the y-component of the velocity (and momentum) is a function of all parameters, $p_y/m = v_y = v_y(\epsilon_0, p_x, y)$, related by

$$\epsilon_0 = \epsilon_p + \Phi_0 = \frac{p^2}{2\,m} + \Phi_0 = \frac{p_x^2}{2\,m} + \frac{p_y^2}{2\,m} + \Phi_0 \quad . \tag{3.12}$$

The y-dependence originates from the zeroth order potential, Φ_0. The same argument applies for τ_e and τ_i, which depend on the kinetic energy of the charge carriers. Due to the transformation, ϵ_p is replaced by $\epsilon_0 - \Phi_0$, i.e., we write $\epsilon_p(\epsilon_0, y)$ and e.g. $\tau_e(\epsilon_0, y)$ accordingly.

3.2.4 Perturbation expansion in E_x

In the following, we perform a systematic perturbation expansion with respect to the applied electric field E_x. Therefore, we replace the non-equilibrium distribution functions by the sequence $f = f_0 + f_1 + f_2 + \mathcal{O}(E_x^3)$ and consider contributions up to second order in E_x. The same expansion is applied to all three parts of f: $\hat{f}$, $\bar{f}$, and $\tilde{f}$. The effective chemical potential of the local-equilibrium distribution, $\hat{f}$, is influenced by E_x as well. Since the inelastic scattering is energy-dependent, E_x, as source of energy, leads to a shift of the chemical potential. To be consistent, we expand $\hat{\mu}$ up to second order in E_x

$$\hat{\mu} = \epsilon_\mathrm{F} + \hat{\mu}_1 + \hat{\mu}_2 + \mathcal{O}(E_x^3) \quad , \tag{3.13}$$

where $\hat{\mu}_1(y)$ and $\hat{\mu}_2(y)$ are the first and second order contributions, respectively. Note, that the chemical potential μ contains not only $\hat{\mu}$ but has a contribution that arise from $\bar{f}$, too. The Fermi energy can be replaced by $\epsilon_\mathrm{F} = \epsilon_{\mathrm{F},0} - \Phi_0$. For $E_x = 0$, $\hat{f}$ becomes the equilibrium distribution, f_0. Expanding $\hat{f}$ up to second order in E_x yields

$$\hat{f} = f_0 - \hat{\mu}_1 f_0' - \hat{\mu}_2 f_0' + \frac{1}{2}\hat{\mu}_1^2 f_0'' + \mathcal{O}(E_x^3) \quad , \tag{3.14}$$

where $f_0' = \frac{\partial f_0}{\partial \epsilon_0}$ and $f_0'' = \frac{\partial^2 f_0}{\partial \epsilon_0^2}$, respectively.

First order

Both sides of Eq. (3.11) vanish for $E_x = 0$. Formulating this transformed Boltzmann equation in first and second order in E_x leads to conditional expressions for the first and second order contributions of f. In first order, we get

$$v_y \frac{\partial f_1}{\partial y} - eE_x v_x f_0' = -\frac{\tilde{f}_1}{\tau_e} - \frac{\bar{f}_1}{\tau_i} \quad . \tag{3.15}$$

As mentioned previously, $\partial_y \Phi_1$ vanishes since the leading contribution to the electrochemical potential depends on the applied electric field in second order. A similar argument applies for the isotropic contributions to the distribution function in first order. The source term of Eq. (3.15), $eE_x v_x f_0'$, is a odd function with respect to v_x and an even function with respect to v_y. Therefore, we assume the same for f_1. It follows that the isotropic part of f_1 vanishes, i.e., $\tilde{f}_1 = \bar{f}_1 = 0$ and $\hat{\mu}_1 = 0$. A rigorous derivation in the same manner as for the second order, which we present in the following, supports this statement. Therefore, Eq. (3.15) is an ordinary differential equation for $f_1(y) = \tilde{f}_1(y)$

$$\tilde{f}_1 + \lambda_y \frac{\partial \tilde{f}_1}{\partial y} = -\mathcal{E}_\mathrm{el} f_0' \quad , \tag{3.16}$$

with the conditional elastic mean free path $\lambda_y(\epsilon_0, p_x, y) = \tau_e v_y$ in direction y for a certain set of parameters, (ϵ_0, p_x, y). The conditional elastic mean free path in x-direction is defined accordingly: $\lambda_x(\epsilon_0, p_x, y) = \tau_e v_x$. Note that λ_x and λ_y are oriented quantities aligned with p_x and p_y, respectively. The energy gained by a single electron moving along λ_x under the influence of the electric field, E_x, is given by $\mathcal{E}_{\mathrm{el}}(\epsilon_0, p_x, y) = -eE_x\lambda_x$.

Second order

Second order in E_x, Eq. (3.11) reads

$$v_y\left[\frac{\partial f_2}{\partial y} - \frac{\partial \Phi_2}{\partial y} f_0'\right] - eE_x\left[v_x\frac{\partial f_1}{\partial \epsilon_0} + \frac{\partial f_1}{\partial p_x}\right] = -\frac{\tilde{f}_2}{\tau_e} - \frac{\bar{f}_2}{\tau_i} \quad . \tag{3.17}$$

In principle, all three contributions, $\hat{f}_2$, $\bar{f}_2$ and $\tilde{f}_2$, appear in this equation independently. However, considering the regime $\tau_i \gg \tau_e$ leads to the conclusion that $\langle f_2 \rangle$ is the dominating contribution with respect to τ_e/τ_i. The *nonisotropic* contribution, $\tilde{f}_2$, relaxes faster and, thus, is a small contribution compared to $\langle f \rangle$ in the steady state limit. Moreover, $\tilde{f}_2$ determines the current densities of all energy moments, $\boldsymbol{j}^{(n)}$. Aiming for a solution of the balance equations (3.8) motivates to rewrite Eq. (3.17) as an ordinary differential equation for $\tilde{f}_2(y)$

$$\tilde{f}_2 + \lambda_y\frac{\partial \tilde{f}_2}{\partial y} = -\mathcal{E}_{\mathrm{el}}\left(\frac{\partial f_1}{\partial \epsilon_0} + \frac{\tau_e}{\lambda_x}\frac{\partial f_1}{\partial p_x}\right) + \lambda_y\frac{\partial \Phi_2}{\partial y}f_0' - \frac{\tau_e}{\tau_i}\bar{f}_2 - \lambda_y\frac{\partial \langle f_2 \rangle}{\partial y} \quad . \tag{3.18}$$

By solving Eq. (3.18), the generalized current density $\boldsymbol{j}^{(n)}$ can be expressed by the isotropic parts of the distribution function. Thereby, Eq. (3.8) can be transformed into a self-consistent balance equation for those isotropic contributions. In addition, elastic and inelastic scattering and accordingly the mean free path of the individual collision processes define length scales of different order. We aim for an effective solution that allows for a systematic expansion in terms of elastic and inelastic scattering. The dominating contribution is derived in the following section.

3.2.5 Derivation of the effective balance equation

Equation (3.16) in first order in E_x has been studied for different semiconductor systems. In case of a piecewise constant potential Φ_0, that equation has been solved for thin metallic films [115,116] and wires [117,118]. There, however, the longitudinal current density, j_x, is calculated under the condition of $\tau_i \approx \tau_e$. That demands an exact calculation of the position dependence within the semi-classical approach. Neighboring ferromagnetic regions lead to the giant magnetoresistance [119, 120], which can be calculated in that manner as well [121–123].

In the following, we derive an effective solution for the distribution function that corresponds to the leading contribution in the limit of $\tau_e \ll \tau_i$. In terms of

the semi-classical model applied in this thesis, two different length scales define the order of the characteristic length on which properties of the system change. Those are the elastic, $l_e = [\tau_e v]_\mathrm{F}$, and the inelastic mean free path, $l_i = [\tau_i v]_\mathrm{F}$, with $v = |\boldsymbol{v}|$ and $[\ldots]_\mathrm{F}$ indicating the evaluation at the Fermi level. Thereby, the limit $\tau_e \ll \tau_i$ is equivalent to $l_e \ll l_i$. We aim for the leading solution of the distribution function with respect to the largest variation length that differs from the bulk solution. In a system where the energy relaxation time (inelastic) is much larger than the momentum relaxation time (elastic), that length scale is given by the energy diffusion length [73–77, 124, 125]

$$l = \sqrt{D\,[\tau_i]_\mathrm{F}} = \sqrt{l_e l_i/2} \quad , \tag{3.19}$$

with the diffusion coefficient of the Drude model in two-dimensions, $D = [v^2\tau_e/2]_\mathrm{F}$. The influence of finite-size effects on the thermoelectric transverse voltage for systems with dimensions comparable to the energy diffusion length have been discussed in Chap. 2 [2, 35].

This section deals with the effective solution of the isotropic distribution function, which is used to calculate the resulting current densities of arbitrary energy moments. A self-consistent balance equation is derived by taking account of $j_x = 0$. A discussion on boundary conditions concludes this section and, in principle, allows for an effective spatial solution of the distribution function. However, we have to discuss both, the position and the energy dependences of the distribution function. The latter is treated in context of the energy moment description and the Sommerfeld expansion which is discussed in detail in Secs. 3.2.6 and 3.2.7, respectively.

Effective solution

Equations (3.16) and (3.18) are of the type

$$\tilde{f} + \lambda_y \frac{\partial \tilde{f}}{\partial y} = \mathcal{I} \quad , \tag{3.20}$$

where both the length λ_y and the source term $\mathcal{I}$ are y-dependent. The general solution can be written as

$$\tilde{f}(y) = C \exp\left(-\int_{y_0}^{y} \frac{\mathrm{d}y'}{\lambda_y(y')}\right) + \int_{y_0}^{y} \mathrm{d}y''\, \mathcal{I}(y'') \frac{\exp\left(\int_{y}^{y''} \mathrm{d}y'\, \lambda_y^{-1}(y')\right)}{\lambda_y(y'')} \quad . \tag{3.21}$$

The constant y_0 is arbitrary and C has to be determined by boundary conditions [33, 115, 126, 127]. However, for the solution on a given interval in y (possibly of infinite length), we choose y_0 in a way that guarantees the decay of $\exp\Big\{-\int_{y_0}^{y} \mathrm{d}y'\, \lambda_y^{-1}(y')\Big\}$ within that interval. Therefore, we consider the motion

aligned with the direction given by λ_y starting from the interval's boundaries. In particular we set y_0 to be the left boundary for $\lambda_y > 0$ and the right boundary for $\lambda_y < 0$.

Since the dominating position-dependent contribution to the distribution function varies on the energy diffusion length, we consider the solution (3.21) in the *effective limit* $|y - y_0| \gg l_e$, where effects on length scales of l_e can be neglected. To be consistent, $\mathcal{I}$ must vary on length scales larger than l_e as well. Thus, the same statement applies for Φ_2 and $\langle f \rangle$. Variations of the external induced potential Φ_0 on length scales larger than l_e are described within this approximation. If Φ_0 changes on a range smaller than l_e, the problem is solved piecewise. To do so, we approximate the variation on that scale by a jump of the value of Φ_0, as discussed in Sec. 3.1. That is similar to the description of $E_x(y)$. Each step of E_x or Φ_0 is a boundary for the solution intervals.

We realize the effective description formally by introducing the dimensionless parameter $Y = \int_{y_0}^{y} \mathrm{d}y' \; \lambda_y^{-1}(y')$. Since $|\lambda_y|$ is of the order of l_e, we neglect terms proportional to $\exp\{-Y\}$. In addition, we use the approximation

$$\begin{aligned} \int_0^Y \mathrm{d}Y'' \, \mathcal{I}(Y'') e^{-Y''} &\approx \mathcal{I}(Y) - \frac{\partial \mathcal{I}(Y)}{\partial Y} + \dots \\ &= \mathcal{I} - \lambda_y \frac{\partial \mathcal{I}}{\partial y} + \dots \quad . \end{aligned} \tag{3.22}$$

That expansion is effectively an expansion with respect to $l_e \partial_y \ln \mathcal{I}$, i.e., the ratio of the elastic mean free path and the variation length of the quantities that describe the system. Thereby, the effective expansion in Eq. (3.22) is an expansion in τ_e/τ_i. That has to be taken into account while comparing the individual parts of $\mathcal{I}$.

To solve the balance equation (3.8), it is necessary to find expressions for $\boldsymbol{j}^{(n)}$ first. Therefore, we identify parts of $\tilde{f}$ that contribute to $\boldsymbol{j}^{(n)}$ and restrict the discussion to the dominating contribution in the effective expansion, i.e., we focus on the dominating contribution in τ_e/τ_i. The relevant contributions of $\tilde{f}$ have to be odd in $\boldsymbol{v}$, otherwise they are canceled out by multiplying with $\boldsymbol{v}$ and integrating over the momentum. Therefore, for each individual part of $\mathcal{I}$ the leading contribution can be found in the first or second term of the effective expansion (3.22). Thereby, we get

$$\tilde{f}_1 = -f_0' \left(\mathcal{E}_{\mathrm{el}} - \lambda_y \frac{\partial \mathcal{E}_{\mathrm{el}}}{\partial y} + \dots \right) \quad , \tag{3.23}$$

in first order and

$$\tilde{f}_2 = \left(1 - \lambda_y \frac{\partial}{\partial y} + \dots \right) \left[-\mathcal{E}_{\mathrm{el}} \left(\frac{\partial f_1}{\partial \epsilon_0} + \frac{\tau_e}{\lambda_x} \frac{\partial f_1}{\partial p_x} \right) + \lambda_y \frac{\partial (\Phi_2 f_0' - \langle f_2 \rangle)}{\partial y} - \frac{\tau_e}{\tau_i} \bar{f}_2 \right] \quad , \tag{3.24}$$

in second order.

Effective current density of the n-th energy moment

Using Eqs. (3.23) and (3.24), the x- and y-component of the current density for the n-th energy moment can be expressed by the effective solutions in Eqs. (3.23) and (3.24). The y-component of $\boldsymbol{j}^{(n)}$ vanishes in first order in E_x as expected from the symmetry arguments that have been applied before. The leading contribution in the effective expansion, i.e., l_e being small compared to the variation length, is given by

$$j_{1,x}^{(n)} = eE_x\ \rho \int \mathrm{d}\epsilon_0\ (\epsilon_0 - \epsilon_{\mathrm{F},0})^n D_{\epsilon_0} f_0' \quad , \tag{3.25}$$

$$j_{1,y}^{(n)} = 0 \quad , \tag{3.26}$$

with the energy-dependent diffusion coefficient $D_{\epsilon_0} = D_{\epsilon_0}(\epsilon_0, y) = \frac{v^2}{2}\tau_e$.

In second order, the x-component vanishes and the leading contribution to the current density yields

$$j_{2,x}^{(n)} = 0 \quad , \tag{3.27}$$

$$j_{2,y}^{(n)} = \rho \int \mathrm{d}\epsilon_0\ (\epsilon_0 - \epsilon_{\mathrm{F},0})^n D_{\epsilon_0} \frac{\partial(\Phi_2 f_0' - \langle f_2 \rangle)}{\partial y} \quad . \tag{3.28}$$

Terms of higher order in $\tau_\mathrm{e}/\tau_\mathrm{i}$ or $l_\mathrm{e}\partial_y I/I$ are neglected.[1] The balance equation (3.8) in second order in E_x reads

$$\frac{\partial j_{2,y}^{(n)}}{\partial y} = -\rho\ (eE_x)^2 \int \mathrm{d}\epsilon_0\ (\epsilon_0 - \epsilon_{\mathrm{F},0})^n \frac{\partial(D_{\epsilon_0} f_0')}{\partial \epsilon_0} - \rho \int \mathrm{d}\epsilon_0\ (\epsilon_0 - \epsilon_{\mathrm{F},0})^n \frac{\bar{f}_2}{\tau_i} \quad . \tag{3.29}$$

Comparing contributions proportional to $\mathcal{E}_\mathrm{el}^2$ in $j_{2,y}^{(n)}$ with the force term of Eq. (3.29) (the first one on the right-hand side) shows that the latter dominates with respect to the effective expansion. Thus, contributions proportional to $\mathcal{E}_\mathrm{el}^2$ are neglected in Eq. (3.28) already.

Effective balance equation

The electric transverse voltage is measured in case of vanishing charge current in transverse direction, $j_y^{(0)} = 0$. Therefore, using Eq. (3.28), $\frac{\partial \Phi_2}{\partial y}$ can be expressed by

$$\frac{\partial \Phi_2}{\partial y} = \frac{\int \mathrm{d}\epsilon_0\ D_{\epsilon_0} \frac{\partial \langle f_2 \rangle}{\partial y}}{\int \mathrm{d}\epsilon_0\ D_{\epsilon_0} f_0'} \quad . \tag{3.30}$$

[1] As the energy moment is originally defined by $(\epsilon_p - \mu)^n$. This heat factor includes higher-order contributions of the applied electric field. However, the first order correction of the chemical potential vanishes due to the symmetry of the system and the second order correction is relevant for higher than second order only. Therefore, we can use $(\epsilon_p - \epsilon_{\mathrm{F},0})^n$ instead.

That relation cancels the local-equilibrium contribution $\hat{f}_2$ in Eq. (3.29) since

$$\frac{\partial \left(\Phi_2 f_0' - \langle f_2 \rangle\right)}{\partial y} = \frac{\int \mathrm{d}\epsilon_0 \; D_{\epsilon_0} \frac{\partial \bar{f}_2}{\partial y}}{\int \mathrm{d}\epsilon_0 \; D_{\epsilon_0} f_0'} f_0' - \frac{\partial \bar{f}_2}{\partial y} \quad . \tag{3.31}$$

Here, we used the result that the energy dependence of $\hat{f}_2$ is already defined by Eq. (3.14), $\hat{f}_2 = -f_0' \hat{\mu}_2$. The y-dependence of the local-equilibrium contribution $\hat{\mu}_2$ is unimportant regarding the calculation of the transverse voltage since the chemical contributions vanish for $\pm\infty$ and steps of $\hat{\mu}_2$ cancel each other.

Taking Eq. (3.30) into account, Eq. (3.29) can be formulated as a self-consistent equation for $\bar{f}_2$

$$\bar{f}_2 - \frac{l_{\epsilon_0}^2}{D_{\epsilon_0}} \frac{\partial}{\partial y} \left[D_{\epsilon_0} \left(\frac{\partial \bar{f}_2}{\partial y} - \frac{\int \mathrm{d}\epsilon_0 \; D_{\epsilon_0} \frac{\partial \bar{f}_2}{\partial y}}{\int \mathrm{d}\epsilon_0 \; D_{\epsilon_0} f_0'} f_0' \right) \right] = \bar{f}_2^{\mathrm{bulk}} \quad . \tag{3.32}$$

Here, we set the moment prefactor, $(\epsilon_0 - \epsilon_{\mathrm{F},0})^n$, and the energy integration, $\int \mathrm{d}\epsilon_0 \; (\epsilon_0 - \epsilon_{\mathrm{F},0})^n$, aside for clarity. That is valid because the balance equation has to be solved for arbitrary n. Equation (3.32) is an ordinary differential equation of $\bar{f}_2$ with respect to y. However, to find an analytical expression for $\bar{f}_2$ is analytically non-trivial since the y-dependence of the potential Φ_0 leads to a y-dependence of D_{ϵ_0}, $l_{\epsilon_0} = l(\epsilon_0, y)$, and $\bar{f}_2^{\mathrm{bulk}} = \bar{f}_2^{\mathrm{bulk}}(\epsilon_0, y)$ in Eq. (3.32). The contribution $\bar{f}_2$ of the non-equilibrium distribution function in second order represents corrections to f_0 which are isotropic and by that, together with $\hat{f}_2$, the dominating contribution to f_2. Moreover, $\bar{f}_2$ relaxes by inelastic scattering, see Eq. (3.29), and, thereby, accounts for additional energy of the electronic system in case of non-equilibrium.

The spatial variation length of $\bar{f}_2$ is given by the energy diffusion length, l. Here, we define the energy-dependent energy diffusion length by

$$l_{\epsilon_0} = \sqrt{\frac{\epsilon_0 - \Phi_0}{m} \tau_e \tau_i} \quad . \tag{3.33}$$

In case that any y-dependence of $\bar{f}_2$ can be neglected, as in a bulk material for $\Phi_0 = \text{const.}$, that part of the distribution function equals to

$$\bar{f}_2^{\mathrm{bulk}} = (e E_x l_{\epsilon_0})^2 \left(f_0'' + \frac{\partial \ln D_{\epsilon_0}}{\partial \epsilon_0} f_0' \right) \quad . \tag{3.34}$$

That inhomogeneity of Eq. (3.32) results from the electric force which drives the system out of equilibrium. Thereby, $\bar{f}_2$ tends to reach the bulk value. On the other hand, that behavior is limited by the variation length, l_{ϵ_0}, and, thereby, by finite size effects on the same length scale.

We discussed earlier in Sec. 2.1.5 that each region with a finite electric field applied contributes to the temperature profile in a way such that the overall profile is the sum the individual profiles generated by each source region with a finite electric

field. That superposition principle can be extended to the entire non-equilibrium distribution function in second order, f_2. In particular, assuming that E_x is finite in a distinct number of regions with respect to y, we define one contribution by setting $E_x = 0$ in all but one region and calculate the corresponding distribution function. Then, the total distribution function as well as the measured transverse voltage is the sum of all these single contributions.

Studying again Eq. (3.24) and taking Eq. (3.30) into account allows for a direct comparison regarding the order in τ_e/τ_i of $\tilde{f}_2$ and $\bar{f}_2$. Both vary on the energy diffusion length. Then, the leading contribution of $\tilde{f}_2$ is proportional to $\tau_e\sqrt{\tau_e\tau_i}$ which is smaller by $\sqrt{\tau_e/\tau_i}$ compared to the order of $\bar{f}_2$ given by $l^2 \propto \tau_e\tau_i$.

Boundary conditions

As discussed previously, we solve Eq. (3.32) on intervals with respect to y where E_x is constant and Φ_0 changes on a length scale larger than l_e. External parameters varying on a length scale much smaller than or of the order of l_e are treated by a step function at the corresponding interval boundary. Thereby, electrons entering the interface are reflected with conserved p_x or are transmitted without scattering events corresponding to elastic or inelastic scattering. As a consequence, we demand the continuity of all current densities of the energy moments at the boundary

$$j_{2,y}^{(n)}(0^-) = j_{2,y}^{(n)}(0^+) \quad . \tag{3.35}$$

For this section, we set the location of the boundary to $y = 0$. For $j_{2,y}^{n}(0^{\pm})$, we calculate the current density in second order in E_x by Eq. (3.28) on the left-hand side $(-)$ and on the right-hand side $(+)$ of the boundary in the limit of $y \to 0$, respectively.

In addition, we may calculate the current for $y = 0$ exactly. At the boundary angle-dependent transmission probabilities have to be taken into account [103,123]. We split the integral over the momentum phase space into two half-space integrals depending on the momentum's direction. For contributions going to the right, f_2 has to be taken on the left side and vice versa. In contrast to Eq. (3.35), the isotropic contribution, $\langle f \rangle$, survives and dominates in τ_e/τ_i compared to $\tilde{f}$. Therefore, to be consistent, we neglect the contribution of the latter and get for the leading contribution [102, 128, 129]

$$\int \mathrm{d}\epsilon_0 \, (\epsilon_0 - \epsilon_{\mathrm{F},0})^n \, \mathcal{T}(\epsilon_0) \, \left[\langle f_2 \rangle (\epsilon_0, 0^-) - \langle f_2 \rangle (\epsilon_0, 0^+) \right] = 0 \quad . \tag{3.36}$$

The exact form of the energy-dependent transmission function $\mathcal{T}(\epsilon_0)$ is not needed in the following. Again, since n is arbitrary, that condition leads to the continuity of $\langle f_2 \rangle (\epsilon_0, y)$ by $\langle f_2 \rangle (\epsilon_0, 0^-) = \langle f_2 \rangle (\epsilon_0, 0^+)$ [130].

In the limit $y \to \pm\infty$, all non-equilibrium corrections to f will vanish in the voltage probes and, thus, $\langle f_2 \rangle (\epsilon_0, \pm\infty) = 0$. Thereby, the boundary conditions

for the balance equation (3.32) are well defined by the continuity of the moment current density, $j_{2,y}^{(n)}$, and the continuity of $\langle f_2 \rangle$.

3.2.6 Introduction of energy moments

Equation (3.32) is an integro-differential equation with respect to ϵ_0 and y. Since all quantities of interest, e.g. current density or particle density, are based on an integration in phase space, we introduce energy moments of the distribution function to describe those. First the n-th energy moment of the isotropic non-equilibrium correction (without the local-equilibrium contribution) reads

$$\bar{M}_n(y) = \int \frac{\mathrm{d}^2 p}{2(\pi\hbar)^2} \; (\epsilon_0 - \epsilon_{\mathrm{F},0})^n \bar{f}_2 \quad . \tag{3.37}$$

To treat the energy dependence of l_{ϵ_0} and D_{ϵ_0}, we expand both quantities or combinations of those in Taylor series with respect to $\epsilon_0 = \epsilon_{\mathrm{F},0}$. We define derivatives at the Fermi level by $F^{(k)} = F^{(k)}(y) = \partial_{\epsilon_0}^k F_{\epsilon_0}\big|_{\epsilon_0=\epsilon_{\mathrm{F},0}}$ and use the abbreviations $F = F^{(0)}, F' = F^{(1)}, \ldots$. Here, F can be replaced by either D, l, or functions of both. In addition, we will use the following expressions, which basically describe energy moments of f_0' or f_0''

$$M_n^{f_0'}(y) = \int \frac{\mathrm{d}^2 p}{2(\pi\hbar)^2} \; (\epsilon_0 - \epsilon_{\mathrm{F},0})^n f_0' \quad , \tag{3.38}$$

$$\bar{M}_n^{\mathrm{bulk}}(y) = \int \frac{\mathrm{d}^2 p}{2(\pi\hbar)^2} \; (\epsilon_0 - \epsilon_{\mathrm{F},0})^n \bar{f}_2^{\mathrm{bulk}} \quad . \tag{3.39}$$

Thereby, the balance equation (3.32) can be formulated energy-resolved by multiplying $(\epsilon_0 - \epsilon_{\mathrm{F},0})^n$ and integrating over the momentum degree of freedom,

$$\int \frac{\mathrm{d}^2 p}{2(\pi\hbar)^2} \; (\epsilon_0 - \epsilon_{\mathrm{F},0})^n \; \ldots \quad .$$

In addition, we express Φ_2 and the boundary conditions by energy moments in the same manner.

First, the continuity of $\langle f_2 \rangle$ at a boundary leads to the continuity of the corresponding energy moments. Since $\hat{\mu}_2$ is independent of ϵ_0, we can write

$$\int \frac{\mathrm{d}^2 p}{2(\pi\hbar)^2} \; (\epsilon_0 - \epsilon_{\mathrm{F},0})^n f_2 = \bar{M}_n - \hat{\mu}_2 M_n^{f_0'} \quad , \tag{3.40}$$

which is the continuous quantity at the boundary for the n-th energy moment. For the continuity of the energy-moment's current density, on the other hand, an expression of $j_{2,y}^{(n)}$ in terms of $\bar{M}_n$ and $M_n^{f_0'}$ is needed. Based on Eq. (3.28), the

y-component of the generalized current density in second order is given by

$$j_{2,y}^{(n)}(y) = \sum_{m=0}^{\infty} \frac{1}{m!} D^{(m)} \left(\frac{\sum_{k=0}^{\infty} \frac{1}{k!} D^{(k)} M_{k+n}^{f_0'}}{\sum_{k=0}^{\infty} \frac{1}{k!} D^{(k)} M_k^{f_0'}} \frac{\partial \bar{M}_m}{\partial y} - \frac{\partial \bar{M}_{m+n}}{\partial y} \right) \quad . \tag{3.41}$$

In Eq. (3.41) we use the condition that the y-component of the charge current density vanishes (see Eq. (3.30)). In Sec. 3.1 we motivated that the measured transverse voltage, U_y, is given by the step of the electrochemical potential between $y = -\infty$ and $y = +\infty$. The electric contribution in second order is given by Φ_2. Although, we argued that the chemical contributions cancel each other in U_y, they are still of interest for a general expression of the electrochemical potential. Therefore, we need to identify the chemical contribution in second order in E_x, $\mu_2(y)$. As defined in Sec. 3.1, that is done via the carrier density n_e. The expansion of the carrier density with respect to the electric field is given by

$$n_e = n_0(y) + n_2(y) + \mathcal{O}\left(E_x^3\right) \quad . \tag{3.42}$$

In the equilibrium state ($E_x = 0$), the carrier density is $n_0(y) = \rho\, \epsilon_\mathrm{F}$. Based on the arguments in Sec. 3.2.4, the contribution in first order of the electric field E_x vanish. The second order correction to the carrier density is given by

$$n_2(y) = \int \frac{\mathrm{d}^2 p}{2(\pi\hbar)^2}\, f_2 = \bar{M}_0 + \rho\, \hat{\mu}_2 \quad , \tag{3.43}$$

and we set

$$n_2(y) = \rho\, \mu_2(y) \quad . \tag{3.44}$$

Note that $M_0^{f_0'} = -\rho$ and we define $\bar{\mu}_2 = \bar{M}_0/\rho$ with $\mu_2 = \hat{\mu}_2 + \bar{\mu}_2$. Therefore, the gradient of the electrochemical potential in second order of E_x reads

$$-e\frac{\partial \phi_2}{\partial y} = \frac{\partial\left(\Phi_2 + \mu_2\right)}{\partial y} = \frac{\sum_{k=0}^{\infty} \frac{1}{k!} D^{(k)} \partial_y \bar{M}_k}{\sum_{k=0}^{\infty} \frac{1}{k!} D^{(k)} M_k^{f_0'}} - \frac{\partial_y \bar{M}_0}{M_0^{f_0'}} \quad . \tag{3.45}$$

To guarantee that the transverse charge current density vanishes, i.e. $j_y = 0$, diffusive and electric contributions have to cancel each other. That is formulated intrinsically by Eq. (3.45). Thus, the relation between the potential Φ_2, which is of electric origin, and the diffusive contribution can be written as

$$\frac{\partial \Phi_2}{\partial y} = \frac{\sum_{k=0}^{\infty} \frac{1}{k!} D^{(k)} \partial_y \bar{M}_k}{\sum_{k=0}^{\infty} \frac{1}{k!} D^{(k)} M_k^{f_0'}} - \frac{\partial \hat{\mu}_2}{\partial y} \quad . \tag{3.46}$$

The diffusive force on the right side equals to the electric force on the left-hand side. The second term on the right-hand side of Eq. (3.46), which is the gradient of the local-equilibrium chemical potential, $\hat{\mu}_2$, is a free parameter within the self-consistent Boltzmann equation approach. The first term on the right-hand side of Eq. (3.46), on the other hand, leads to the relation of the y-component of the electric field to the energy moments. That accounts for the non-equilibrium situation. Thereby, a given diffusive force leads to a finite electric force by Eq. (3.46), which in turn is related to a charge accumulation by the Poisson equation. Again, that charge accumulation leads to a diffusive force which enters Eq. (3.46) by the chemical potential of the local-equilibrium distribution, $\hat{\mu}_2$. A total self-consistent solution involves, thus, a solution of the Poisson equation as well [103, 131]. The second order correction to the charge-carrier density is given by $n_2 = \bar{M}_0 + \rho\,\hat{\mu}_2$. For given $\bar{M}_0$, finding a solution for the carrier density $n_2(y)$ means solving the local-equilibrium contribution at the same time. The relation between the carrier density and the electric potential Φ_2 for the two-dimensional electron gas is given by

$$\frac{\partial \Phi_2}{\partial y} = \frac{-e^2}{2\pi\varepsilon} \int \mathrm{d}y' \, \frac{n_2(y')}{y - y'} \quad . \tag{3.47}$$

The dielectric constant is given by ε. In combination with Eq. (3.46), that yields

$$-\frac{e^2}{2\pi\varepsilon} \int \mathrm{d}y' \, \frac{n_2(y')}{y - y'} = \frac{\sum_{k=0}^{\infty} \frac{1}{k!} D^{(k)} \partial_y \bar{M}_k}{\sum_{k=0}^{\infty} \frac{1}{k!} D^{(k)} M_k^{f_0'}} + \frac{\partial_y \bar{M}_0}{\rho} - \frac{\partial_y n_2(y)}{\rho} \quad . \tag{3.48}$$

which is an integro-differential equation for $n_2(y)$. Assuming that the y-dependence of the energy moments, which we study more in detail in the following, is known, Eq. (3.48) determines the profile of the carrier density.

However, the transverse voltage is independent of the functional dependence of $\hat{\mu}$ on y since the charge accumulation vanishes for $y \to \pm\infty$. Therefore, it is an appealing advantage that the calculation of the transverse voltage can be conducted without solving the Poisson equation. The steps of $\hat{\mu}$ are needed at the boundaries only. Those guarantee the continuity of the isotropic distribution function $\langle f \rangle$.

By Eq. (3.45) the electrochemical potential is given by all energy moments of the isotropic non-equilibrium correction in second order, $\bar{f}_2$. Using Eq. (3.45) we can write the balance equation (3.32) for the n-th energy moment as

$$\begin{aligned} \bar{M}_n^{\mathrm{bulk}} = \bar{M}_n - \sum_{m=0}^{\infty} \sum_{k=0}^{m} \frac{1}{m!} \binom{m}{k} \left(\frac{l^2}{D} \right)^{(k)} \\ \times \frac{\partial}{\partial y} \left[D^{(m-l)} \left(\frac{\partial \bar{M}_{n+m}}{\partial y} - \frac{\partial (\bar{\mu}_2 - e\phi_2)}{\partial y} M_{n+m}^{f_0'} \right) \right] \quad . \end{aligned} \tag{3.49}$$

An alternative formulation convenient for calculation can be found in App. A. All quantities in this balance equation are y-dependent either via Φ_0 or by representing

$\bar{f}_2$. The amplitude of the moments is given by $\bar{M}_n^{\mathrm{bulk}}$, which underlines that the isotropic distribution function can be described by derivatives of f_0 and polynomials of $(\epsilon_0 - \epsilon_{\mathrm{F},0})$ (see Ref. [114] for an equivalent statement or Refs. [38, 43]). The n-th energy moment, $\bar{M}_n^{\mathrm{bulk}}$, is coupled to the first or second spatial derivative of all energy moments of $\bar{f}_2$. To break down the series of coupled differential equations, we need to identify a criteria to achieve that goal, which is described in the following section.

3.2.7 Sommerfeld expansion

To limit the number of coupled differential equations arising from Eq. (3.49), we perform a Sommerfeld expansion [34] of the moments $\bar{M}_n$, $M_n^{f_0'}$, and $\bar{M}_n^{\mathrm{bulk}}$. We use the expansion

$$(-1)^k \int \mathrm{d}\epsilon_0 \; H(\epsilon_0) \frac{\partial^k f_0}{\partial \epsilon_0^k} = \sum_{j=0}^{\infty} a_j (k_B T_0)^{2j} H^{(2j+k)} \tag{3.50}$$

for a function $H(\epsilon_0)$, with $a_j = \left(2 - 2^{2(1-j)}\right) \zeta(2j)$, where ζ labels the Riemann zeta function. Equation (3.50) is an expansion in the dimensionless temperature $\Theta = k_B T_0 / \epsilon_{\mathrm{F},0}$. The energy moment corresponding to the derivative of the Fermi function, $M_n^{f_0'}$, can be related to a_j by $M_{2n}^{f_0'} = -a_n \, \rho \, (2n)! \, (k_B T_0)^{2n}$ and $M_{2n+1}^{f_0'} = 0$. We define $\bar{M}_{n,2j}$ and $\bar{M}_{n,2j}^{\mathrm{bulk}}$ to be of the order of Θ^{2j} in terms of the Sommerfeld expansion. Expressions for $\bar{M}_{n,2j}^{\mathrm{bulk}}$ up to the order Θ^2 can be found in App. B. Energy moments $\bar{M}_{n,2j}^{\mathrm{bulk}}$ that are more than one order higher than their order in Θ vanish, i.e. if $n > 2j + 1$. That results from the fact that $\bar{f}_2^{\mathrm{bulk}}$ is a linear combination of f_0' and f_0'' only.

In order to limit the number of coupled equations, we assume a similar restriction to $\bar{M}_{n,j}$. Without a finite bulk moment the corresponding energy moment of the non-equilibrium distribution function vanishes. Therefore, $\bar{M}_{n,2j}$ is finite if $n \leq 2j + 1$ and it vanishes for $n > 2j + 1$. With that relation, the effective balance equation of the energy moments can be solved systematically starting in lowest order, which is proportional to Θ^0. The necessary balance equations are given by Eq. (B.2) in App B. The boundary conditions discussed in Sec. 3.2.5 can be expressed in terms of the energy moments as well. To be consistent, an expansion of $\hat{\mu}$ in terms of the Sommerfeld expansion is necessary. The continuity of $\langle f_2 \rangle$ has to be fulfilled in each order of the Sommerfeld expansion, which leads automatically to the continuity of $\bar{M}_{n,2j} - \sum_{k=0}^{j} \hat{\mu}_{2,2k} \, M_{2(j-k)}^{f_0'}$. The boundary condition in Eq. (3.35) requires an expression for the current density of the n-th energy moment in terms of the Sommerfeld expansion. The corresponding expansion of Eq. (3.41) results in Eq. (B.6), which determines the y-component of the current density of the n-th energy moment of the order T_0^{2j}, $j_{2,y,2j}^{(n)}$. The position dependence of the energy moments determines the transversal variation of the electrochemical poten-

tial (second order in E_x), $\phi_{2,2j}$, in arbitrary order Θ^{2j} of the Sommerfeld expansion, see Eq. (B.5).

In the following two sections, we discuss the lowest order contribution and the first correction, which is proportional to Θ^2, explicitly. We show that the lowest order contribution can equally calculated by the application of a quasi-equilibrium ansatz for the distribution function. The latter is characterized by an effective, position-dependent temperature and chemical potential. For the analysis of higher-order contributions with respect to the Sommerfeld expansion, however, the moment description is necessary to fulfill the validity of the energy-dependent Boltzmann equation.

3.2.8 Sommerfeld expansion: effective balance equation in lowest order

In lowest order, i.e., the order Θ^0 of the Sommerfeld expansion, the relevant energy moments are $n = 0$ and $n = 1$. The particle current density is $\boldsymbol{j}^{(0)}$ while the energy flux is given by $\boldsymbol{j}^{(1)}$. Thus, the corresponding balance equations to those moments conserve the particle number and energy, respectively. Starting with the balance equation for the moment $n = 1$, we get

$$\bar{M}_{1,0}^{\text{bulk}} = \bar{M}_{1,0} - \frac{l^2}{D}\frac{\partial}{\partial y}\left[D\frac{\partial \bar{M}_{1,0}}{\partial y}\right] \quad . \tag{3.51}$$

Since

$$\int \frac{\mathrm{d}^2 p}{2(\pi\hbar)^2}\,(\epsilon_0 - \epsilon_{\mathrm{F},0}) f_2 = \bar{M}_1 \quad , \tag{3.52}$$

the first moment is the energy per volume of the two-dimensional electron gas in second order of the applied electric field, E_x. The source of energy in Eq. (3.51) is given by $\bar{M}_{1,0}^{\text{bulk}}$.

If the potential Φ_0 is constant (i.e. D is constant) for a certain y-range comparable to the energy diffusion length, the general analytic solution for $\bar{M}_{1,0}$ is given by

$$\bar{M}_{1,0} = \rho\,\mathcal{E}^2 + \bar{M}_{1,0}^{-}\,e^{-y/l} + \bar{M}_{1,0}^{+}\,e^{y/l} \quad , \tag{3.53}$$

with $\mathcal{E} = -eE_x l$, which is the energy gained by an electron in the electric field E_x from moving the distance of the energy diffusion length. The quantity $\bar{M}_{1,0}$ is the energy per volume in the two-dimensional electron gas. Hence, the non-equilibrium bulk energy density in second order in E_x and in lowest order with respect to the Sommerfeld expansion is given by $\rho\,\mathcal{E}^2$. Moreover, boundary conditions determine the constants $\bar{M}_{1,0}^{\pm}$. Equation 3.53 shows that $\bar{M}_{1,0}$ decays or rises in y-direction on the length scale of the energy diffusion, l.

The heat current density proportional to Θ^0 is given by

$$j^{(1)}_{2,y,0} = -D\frac{\partial \bar{M}_{1,0}}{\partial y} \quad , \tag{3.54}$$

which is needed to formulate the boundary condition of continuous heat flux. Particle conservation coincides with a constant particle flux $\boldsymbol{j}^{(0)}$. For $n = 0$, the energy relaxation term vanishes in Eq. (3.8), which in turn gives rise to a condition for $\bar{f}$ which can be formulated by the relation

$$0 = \int \mathrm{d}\epsilon_0 \, \tau_i^{-1} \bar{f} \quad . \tag{3.55}$$

The latter expression is valid for all orders in E_x. Expressed in terms of energy moments, this condition can be transformed to

$$0 = \sum_{k=0}^{\infty} \frac{1}{k!} \left[\frac{\partial \tau_i^{-1}}{\partial \epsilon_0}\right]_{\mathrm{F}} \bar{M}_k \quad , \tag{3.56}$$

which is evidently equivalent to the case $n = 0$ of Eq. (3.49) due to the origin of that balance equation. In lowest order of the Sommerfeld expansion that reads

$$\bar{M}_{0,0} - \bar{M}^{\mathrm{bulk}}_{0,0} = \left[\frac{\tau_i'}{\tau_i}\right]_{\mathrm{F}} \left(\bar{M}_{1,0} - \bar{M}^{\mathrm{bulk}}_{1,0}\right) \quad , \tag{3.57}$$

with $\tau_i' = \frac{\partial \tau_i}{\partial \epsilon_0}$.

In general, the inelastic relaxation of the isotropic correction, $\bar{f}$, to the equilibrium distribution function is energy dependent. Therefore, states of higher energy will relax faster. That results in the shift $\bar{\mu}_2$ of the chemical potential in second order in E_x or, equivalently, in a correction of the particle density in second order of E_x, $n_2 = \bar{M}_0 + \rho\,\hat{\mu}_2$. That shift is proportional to the energy derivative of the inelastic relaxation time multiplied by the additional amount of energy in the electronic system, see Eq. (3.57). In higher order of the Sommerfeld expansion, higher energy moments contribute to the shift of the chemical potential as well. In contrast to Eq. (3.51), Eq. (3.57) is an algebraic relation for the corresponding energy moment. The algebraic nature applies for the balance equations with $n = 0$ in arbitrary order of the Sommerfeld expansion. Thus, given the ansatz that $\bar{M}_{n,2j}$ vanishes for $n > 2j + 1$, $2j + 1$ differential equations are needed to be solved for the order Θ^{2j} of the Sommerfeld expansion.

The gradient of the electrochemical potential reads

$$-e\frac{\partial \phi_{2,0}}{\partial y} = -\frac{D'}{\rho D}\frac{\partial \bar{M}_{1,0}}{\partial y} \quad , \tag{3.58}$$

in lowest order of the Sommerfeld expansion. In fact, that relation describes the thermoelectric Seebeck effect by relating the gradient of the energy density (or heat), $\bar{M}_{1,0}$, to the variation of the electrochemical potential. That analogy is discussed in detail in the following section.

3.2.9 Quasi-equilibrium ansatz

The energy-moment ansatz for determining the non-equilibrium distribution function provides the possibility to treat the energy dependence of the distribution function by a systematic expansion. In this section, we see that in lowest order of the Sommerfeld expansion a quasi-equilibrium ansatz is applicable. Thereby, we derive the same balance equations as discussed in Chap. 2. That approach is equivalent to the systematic approach discussed here for the lowest order in Θ.

We assume that the isotropic distribution function, $\langle f \rangle$, can be written in terms of a Fermi function with a position-dependent chemical potential, $\mu(y)$, and a position-dependent temperature, $T(y)$, i.e.,

$$\langle f \rangle = \frac{1}{1 + \exp\left(\frac{\epsilon_p - \mu}{k_B T}\right)} \quad . \tag{3.59}$$

Thereby, $f = \langle f \rangle + \tilde{f}$ corresponds to a quasi-equilibrium description of f. Expanding $\langle f \rangle$ in E_x while assuming that both μ as well as T depend on y and E_x but not on ϵ_0 leads to

$$\langle f_2 \rangle = -f_0' \left(\mu_2 + (\epsilon_0 - \epsilon_{\mathrm{F},0}) \frac{T_2}{T_0} \right) \quad , \tag{3.60}$$

in second order of the applied electric field. Note that in case of equilibrium, i.e. $E_x = 0$, we get $\mu = \epsilon_\mathrm{F}$ and $T = T_0$. While the first order contributions vanish, the second order contributions in E_x to μ and T are given by $\mu_2(y)$ and $T_2(y)$, respectively. With this relation, we can express the energy moments of the order Θ^0 by the chemical potential and temperature. We find

$$\bar{M}_{0,0} = \rho \left(\mu_2 - \hat{\mu}_2 \right) \quad , \tag{3.61}$$

$$\bar{M}_{1,0} = \frac{\pi^2}{3} (k_B T_0)^2 \rho \, \frac{T_2}{T_0} \quad . \tag{3.62}$$

For the quasi-equilibrium ansatz, the electrochemical potential reads

$$\frac{\partial \phi_{2,0}}{\partial y} = \frac{\pi^2}{3e} (k_B T_0)^2 \frac{D'}{D} \frac{\partial}{\partial y} \frac{T_2}{T_0} \quad , \tag{3.63}$$

where $\frac{\pi^2 k_B^2 T_0}{3e} \frac{D'}{D}$ is the Mott expression for the Seebeck coefficient [41]. The fact that this thermoelectric response coefficient is the same as for a bulk situation with an externally applied temperature gradient accounts for the regime $\tau_i \gg \tau_e$. In this limit, the current is given by the dominating relaxation processes, which are the elastic ones. The effect of inelastic scattering enters the temperature profile by the energy diffusion length.

In order to get a finite solution, we need to consider not only the order Θ^0 for the quasi-equilibrium ansatz but Θ^2, too. That procedure incorporates that T_2 is of the order Θ^{-1}. Using the balance equations (3.57) and (3.51) we get

$$\mu_2 = \frac{\pi^2}{3}(k_B^2 T_0)\left[\frac{\tau_i'}{\tau_i}\right]_{\mathrm{F}} T_2 + \hat{\mu}_2 \quad , \tag{3.64}$$

$$\left(\frac{3\,\mathcal{E}}{\pi k_B T_0}\right)^2 = \frac{T_2}{T_0} - \frac{l^2}{D}\frac{\partial}{\partial y}\left(D\frac{\partial}{\partial y}\frac{T_2}{T_0}\right) \quad . \tag{3.65}$$

The first equation (3.64) is an expression for the chemical potential, while the second equation (3.65) is a heat balance equation. The latter is valid in case that elastic scattering dominates compared to inelastic scattering, as discussed in Sec. 3.1. The heat continuity equation is equivalent to the one discussed in Sec. 2.1.1 for setting $\delta T = T_2$. Both describe the same, the deviation from the equilibrium temperature T_0. In Sec. 2.1.1 the starting point is a heat balance equation which is simply given by Eq. (3.8) for $n = 1$ which reads

$$\partial_y j^{(1)}_{2,y,0} = -eE_x\, j^{(0)}_{1,x,0} - \frac{c_V}{[\tau_{\mathrm{i}}]_{\mathrm{F}}} T_2 \quad , \tag{3.66}$$

in second order of E_x. The last term on the right-hand side is the energy relaxation rate due to inelastic scattering,

$$\frac{c_V}{[\tau_{\mathrm{i}}]_{\mathrm{F}}} T_2 = \int \frac{\mathrm{d}^2 p}{2(\pi\hbar)^2}\,(\epsilon_0 - \epsilon_{\mathrm{F},0})^2 f_0' \frac{T_2/T_0}{\tau_i} \quad , \tag{3.67}$$

with the heat capacity $c_V = \rho\frac{\pi^2}{3}(k_B T_0)^2$ [2, 14, 74, 132]. Lohvinov *et al.* applied Eq. (3.66) to study nonlinear size effects in semiconductor thin films in case of a constant potential and high temperature [75].

In contrast to the goal of this part of the thesis, the application of the quasi-equilibrium distribution function is totally sufficient if the discussion is restricted to the lowest order contribution in Θ only. The results discussed in Chap. 2 can be reproduced exactly in lowest order of the Sommerfeld expansion. That can be done easily by using the quasi-equilibrium ansatz shown above. Therefore, we do not need to discuss the lowest order contribution any further. However, for higher-order contribution with respect to the Sommerfeld expansion, where higher energy moments as heat and particle number have to be taken into account, the quasi-equilibrium description leads to an inconsistent description of the Boltzmann equation. The moments $n > 1$ of Eq. (3.8) demand additional degrees of freedom with respect to the energy dependence of the isotropic distribution function. A generalization is necessary. Using the energy moment description is convenient and fulfills the coupled balance equations in arbitrary order of the Sommerfeld expansion. In addition, higher-order contributions to the transverse voltage will lead to deviations from the Mott relation (3.63). Other limitations to Mott's formula are discussed, e.g, by Buhmann *et al.* in case of strong electron-electron scattering [92].

3.2.10 Sommerfeld expansion: first correction to the effective balance equation

In this section, we present the first correction with respect to the Sommerfeld expansion. Starting from a rather technical point of view, we derive the analytic expressions which are the first correction to the discussion in Chap. 2. Section 3.3 shows the effects and characteristics of this first correction in terms of the Sommerfeld expansion.

There are three coupled differential equations, for $n = 3, 2, 1$, which are of the order Θ^2. The first two read

$$\bar{M}^{\text{bulk}}_{3,2} = \bar{M}_{3,2} - \frac{l^2}{D}\frac{\partial}{\partial y}\left(D\frac{\partial \bar{M}_{3,2}}{\partial y}\right) \quad , \tag{3.68}$$

$$\begin{aligned}\bar{M}^{\text{bulk}}_{2,2} = \bar{M}_{2,2} &- \frac{l^2}{D}\frac{\partial}{\partial y}\left(D\frac{\partial \bar{M}_{2,2}}{\partial y}\right) \\ &- \frac{l^2}{D}\frac{\partial}{\partial y}\left(D'\frac{\partial \bar{M}_{3,2}}{\partial y}\right) - \left(\frac{l^2}{D}\right)'\frac{\partial}{\partial y}\left(D\frac{\partial \bar{M}_{3,2}}{\partial y}\right) \\ &+ \frac{\pi^2}{3}(k_B T_0)^2\frac{l^2}{D}\frac{\partial}{\partial y}\left(D\frac{\partial \bar{M}_{0,0}}{\partial y} + D'\frac{\partial \bar{M}_{1,0}}{\partial y}\right) \quad .\end{aligned} \tag{3.69}$$

The balance equation for $n = 1$ and the algebraic equation that determines $\bar{M}_{0,2}$ can be found in App. B, Eqs. (B.3) and (B.4), respectively. We emphasize that the balance equation couples the related energy moment to higher moments and to energy moments that are of lower order in Θ, e.g. see Eq. (3.69).

The balance equation $n = 3$, i.e. $n = 2j + 1$, is the same as in Eq. (3.51) apart from the bulk value $\bar{M}^{\text{bulk}}_{1,0}$ and $\bar{M}^{\text{bulk}}_{3,2}$. Thereby, the ratio of the moments for $n = 2j + 1$ is given by the ratio of their bulk values, see Eq. (B.1). Equivalently, the ratio

$$\frac{\bar{M}_{2j+1,2j}}{a_j(2j+1)!(k_B T_0)^{2j}} = \text{const.} \tag{3.70}$$

is independent of the order in Θ, i.e., is a constant with respect to j. Thereby, the solution for $\bar{M}_{3,2}$ is given by $\bar{M}_{3,2} = \pi^2(k_B T_0)^2\bar{M}_{1,0}$. The reduced degree of independent parameters results from the restriction that $\bar{M}_{n>2j+1,2j}$ vanishes. The latter statement is equivalent to the assumption that the isotropic correction $\langle f_2 \rangle$ is a superposition of the first and second derivative of f_0 with coefficients that are independent of Θ. By that, we are able to derive a second relation

$$\frac{\bar{M}_{n,2j}}{a_j(2j)!(k_B T_0)^{2j}} = 2\,\frac{\bar{M}_{n-2,2j-2}}{a_{j-1}(2j-2)!(k_B T_0)^{2j-2}} - \frac{\bar{M}_{n-4,2j-4}}{a_{j-2}(2j-4)!(k_B T_0)^{2j-4}} \quad , \tag{3.71}$$

which becomes relevant starting from the order Θ^4 of the Sommerfeld expansion. In lowest order, the crucial position-dependent energy moment is the heat density,

$\bar{M}_{1,0}$. The zeroth energy moment is given by the particle conservation algebraically (in each order of the Sommerfeld expansion). In case of the first correction with respect to the Sommerfeld expansion, $\bar{M}_{2,2}$ and $\bar{M}_{1,2}$ are coupled, but still represent independent functions which are determined by the corresponding differential equations. The moment $\bar{M}_{3,2}$ is given by the relation (3.70). The number of finite independent energy moments that have to be determined by the balance equation is limited by three for the order Θ^4 and higher. For Θ^2 the moments $n = 1, 2$ are remain to be determined. Higher energy moments or the zeroth moment are given by either the moment relation Eq. (3.71) or the current conservation, respectively.

The first Sommerfeld correction of the order of Θ^2 to the electrochemical potential reads

$$\begin{aligned}
-e\rho\frac{\partial\phi_{2,2}}{\partial y} &= -\frac{D'}{D}\frac{\partial\bar{M}_{1,2}}{\partial y} - \frac{D''}{2D}\frac{\partial\bar{M}_{2,2}}{\partial y} - \frac{D'''}{6D}\frac{\partial\bar{M}_{3,2}}{\partial y} \\
&\quad + \frac{\pi^2}{6}(k_BT_0)^2\frac{D''}{D}\left(\frac{\partial\bar{M}_{0,0}}{\partial y} + \frac{D'}{D}\frac{\partial\bar{M}_{1,0}}{\partial y}\right) \\
&= -\frac{D'}{D}\frac{\partial\bar{M}_{1,2}}{\partial y} - \frac{D''}{2D}\frac{\partial\bar{M}_{2,2}}{\partial y} \\
&\quad + \frac{1}{6}\left(\frac{D''}{D}\frac{(l^2)'}{l^2} - \frac{D'''}{D}\right)\frac{\partial\bar{M}_{3,2}}{\partial y} \\
&\quad + \frac{\pi^2}{6}(k_BT_0)^2\frac{D''}{D}\left(\frac{\partial\bar{M}^{\text{bulk}}_{0,0}}{\partial y} - \left[\frac{\tau_i'}{\tau_i}\right]_{\text{F}}\frac{\partial\bar{M}^{\text{bulk}}_{1,0}}{\partial y}\right) . \qquad (3.72)
\end{aligned}$$

In addition to a Seebeck coefficient analogy with respect to the gradient of the heat density $\bar{M}_1$ in next order of the Sommerfeld expansion, the response on higher energy moments have to be considered as well. Therefore, a quasi-equilibrium, which describes the particle density and the heat of the electronic system only, leads to a fraction of the actual electrochemical potential. In addition, the following formulas for current densities of higher energy moments are beyond the quasi-equilibrium description with just a spatially dependent chemical potential and temperature:

$$j^{(3)}_{2,y,2} = -D\frac{\partial\bar{M}_{3,2}}{\partial y} \quad , \qquad (3.73)$$

$$\begin{aligned}
j^{(2)}_{2,y,2} &= -\left[D\frac{\partial\bar{M}_{2,2}}{\partial y} + D'\frac{\partial\bar{M}_{3,2}}{\partial y}\right] \\
&\quad + \frac{\pi^2}{3}(k_BT_0)^2\left[D\frac{\partial\bar{M}_{0,0}}{\partial y} + D'\frac{\partial\bar{M}_{1,0}}{\partial y}\right] \quad , \qquad (3.74)
\end{aligned}$$

$$\begin{aligned}
j^{(1)}_{2,y,2} &= -\left[D\frac{\partial\bar{M}_{1,2}}{\partial y} + D'\frac{\partial\bar{M}_{2,2}}{\partial y} + \frac{D''}{2}\frac{\partial\bar{M}_{3,2}}{\partial y}\right] \\
&\quad + \frac{\pi^2}{3}(k_BT_0)^2\frac{D'}{D}\left[D\frac{\partial\bar{M}_{0,0}}{\partial y} + D'\frac{\partial\bar{M}_{1,0}}{\partial y}\right] \quad . \qquad (3.75)
\end{aligned}$$

We demonstrated that the presented energy moment approach for the effective balance equation allows for a systematic Sommerfeld expansion. Thereby, the energy dependence of the Boltzmann equation can be treated correctly in an effective manner. That approach is beyond a quasi-equilibrium approximation, although the latter is sufficient in lowest order of the Sommerfeld expansion.

3.3 Thermoelectric transverse voltage beyond quasi-equilibrium

In this section, we discuss the differences of the transverse voltage characteristics regarding the energy moments and the Sommerfeld expansion in lowest order.

For a quantitative analysis, assumptions on the energy dependence of the elastic and inelastic relaxation time have to be made. We model the energy dependence of τ_e and τ_i by a power-law function

$$\tau_{\mathrm{e}}(\epsilon_0) \sim \left(\frac{\epsilon_0 - \Phi_0}{\epsilon_{\mathrm{F},0}}\right)^{\alpha_{\mathrm{e}}} , \tag{3.76}$$

$$\tau_{\mathrm{i}}(\epsilon_0) \sim \left(\frac{\epsilon_0 - \Phi_0}{\epsilon_{\mathrm{F},0}}\right)^{\alpha_{\mathrm{i}}} . \tag{3.77}$$

To quantify the obtained results, we use the following values for the exponents, $\alpha_{\mathrm{e}} = 0.88$ and $\alpha_{\mathrm{i}} = 1.45$ from Ref. [2], which are in good agreement with theoretical predictions [105, 133, 134]. We used the same approximation in Chap. 2. The magnitude of the elastic and inelastic relaxation time enter the transverse voltage via the energy diffusion length only. The latter determines, first, the relevant variation length of the energy moments, and, secondly, the amplitude of the measured signal. The leading order of the transverse voltage with respect to the Sommerfeld expansion is proportional to the additional energy provided by E_x per electron at $\Phi_0 = 0$. That energy has been introduced in Chap. 2 already and is given by $\omega_0 = (eE_x l_0)^2/\epsilon_{\mathrm{F},0}$ (see Sec. 2.1.3). We normalize the length in y by l_0. Here, l_0 is the energy diffusion length of the voltage probes, where $\Phi_0 = 0$. The transverse voltage itself is characterized by the quantity $s_0 = eU_y/\omega_0$ which describes the thermopower of the system under the influence of the mesoscopic device dimensions (see Chap. 2). As a consequence, the energy moment $\bar{M}_{n,2j}$ is proportional to $\omega_0 \Theta^{2j} \epsilon_{\mathrm{F},0}^{n-1}$.

This section is organized as follows: First, in Sec. 3.3.1, we discuss the response of the thermoelectric transverse voltage on variations of the energy moments. The general characteristics of the energy moments and the resulting transverse voltage are discussed in Sec. 3.3.2. Afterwards, we show an explicit, experimentally relevant situation in Sec. 3.3.3, where the first and second Sommerfeld correction influence the results significantly compared to the lowest order contribution.

3.3.1 Linear response to variations of the energy moments

In general, a spatially confined region in y with a finite applied electric field, E_x, works as a source for non-equilibrium energy moments. The amplitude is given by the energy $\omega = \mathcal{E}^2/\epsilon_\mathrm{F}$ which in turn is proportional to the square of the energy diffusion length. That length is small close to depletion ($\Phi_0 \to \epsilon_{\mathrm{F},0}$) and increases for enhanced carrier density, i.e., for $\Phi_0 < 0$. Therefore, the magnitude of the energy in this setup behaves accordingly with respect to the gate potential, Φ_0, of the region with finite E_x. Basically, that accounts for the transverse voltage, too. For comparison of other characteristics, we set aside that effect by considering the source region always to be at zero potential, i.e. $\Phi_0 = 0$ for $E_x \neq 0$.

In principle, the energy moments generated by the source in the system vary on the length scale of the energy diffusion length. Thus, in analogy to the temperature [2, 35], those energy moments relax on each side of the source region on that length scale to zero. The length of relaxation can be manipulated by tuning the potential Φ_0.

The gradient of the electrochemical potential (3.45) depends on the gradients of all contributing energy moments linearly. In general, all finite moments in the corresponding order of the Sommerfeld expansion contribute. The linear response coefficients that scale the contribution of a certain moment are labeled by $\mathcal{M}_n$ for the n-th moment. We use Eqs. (3.57) and the relation $\bar{M}_{3,2} = \pi^2 (k_B T_0)^2 \bar{M}_{1,0}$ to formulate the gradient of the electrochemical potential (Eqs. (3.58) and (3.72)) by

$$\frac{\partial \phi_{2,0}}{\partial y} = \mathcal{M}_1 \frac{\partial \bar{M}_{1,0}}{\partial y} \quad , \tag{3.78}$$

$$\frac{\partial \phi_{2,2}}{\partial y} = \mathcal{M}_1 \frac{\partial \bar{M}_{1,2}}{\partial y} + \mathcal{M}_2 \frac{\partial \bar{M}_{2,2}}{\partial y} + \mathcal{M}_3 \frac{\partial \bar{M}_{3,2}}{\partial y} \quad . \tag{3.79}$$

That description is valid in lowest order and for the first correction with respect to the Sommerfeld expansion. For simplicity, we assumed that the gate potential Φ_0 is piecewise constant. Thus, the gradient of the bulk term vanishes. Then, the linear response coefficients are given by

$$\mathcal{M}_1 = \frac{1}{e\rho} \frac{D'}{D} = \frac{S}{\frac{\pi^2}{3} k_B^2 T_0 \, \rho} \quad , \tag{3.80}$$

$$\mathcal{M}_2 = \frac{1}{2e\rho} \frac{D''}{D} \quad , \tag{3.81}$$

$$\mathcal{M}_3 = -\frac{1}{6e\rho} \left(\frac{D''}{D} \frac{(l^2)'}{l^2} - \frac{D'''}{D} \right) \quad . \tag{3.82}$$

Here, the Mott expression for the Seebeck coefficient, S, can be identified (see (3.80)). For corrections to $\partial_y \phi_2$ of the order Θ^2 or higher, contributions to $\mathcal{M}_i$ can be found that are proportional to Θ^{2j} itself. Thus, a linear response to the zeroth moment $\bar{M}_0$ will contribute to the electrochemical potential as well.

Note that $\mathcal{M}_1$ and $\mathcal{M}_2$ are always positive while the linear response to the third moment, characterized by $\mathcal{M}_3$, is negative. That originates from the substitution of the lowest order energy moments in Eq. (3.72) by moments of the order Θ^2. The contributions of the various energy moments may cancel each other partially due to an opposite sign.

The measured transverse voltage U_y of the order Θ^{2j} reads

$$U_{y,2j} = \int_{-\infty}^{\infty} \mathrm{d}y \, \frac{\partial \phi_{2,2j}}{\partial y} + \mathcal{O}(E_x^3) \quad . \tag{3.83}$$

We focus throughout this thesis on the contributions up to second order in E_x only. We introduce here the corresponding expansion of s_0 via

$$s_{0,2j} = \frac{eU_{y,2j}}{\omega_0} \quad . \tag{3.84}$$

Since all energy moments vanish for $y \to \pm\infty$, the left-right symmetry of $\mathcal{M}_n(y)$ with respect to the energy source has to be broken. That can be achieved by the modulation of the external potential Φ_0 on the left and/or right side of the energy source. The y-dependence of Φ_0 manipulates the amplitude of the linear response coefficients.

A simple setup that leads to a finite transverse voltage is described in the following: We consider a source region of width $l_0/2$ with a finite applied electric field, E_x, but vanishing external potential, $\Phi_0 = 0$. The electric field works as a source for non-equilibrium energy moments. That region is the heating channel (see Fig. 2.1). The energy moments drop to zero on both sides of the heating channel, which happens on the length scale of the energy diffusion length. On the right-hand side of the heating channel, we modulate the external potential (modulation channel). To guarantee that the energy moments drop approximately to zero within this region, we choose the width $3\,l_0$. On that range the potential is constant and takes the value $\Phi_0 = V_{\mathrm{mc}}$. That setup can be described by the tuples $\boldsymbol{V} = (0, V_{\mathrm{mc}})$ and $\boldsymbol{w} = (w_{\mathrm{hc}}, w_{\mathrm{mc}}) = (l_0/2, 3\,l_0)$ for the potential and the width of the channels, respectively.

Compared to $\Phi_0 = 0$, a low charge carrier density (or $\Phi_0 > 0$, equivalently) leads to larger response of the electrochemical potential on variations of the energy moments in the particular region of manipulated carrier density. Therefore, the contributions to the transverse voltage in lowest order, $U_{y,0}$, as well as the first correction, $U_{y,2}$, with respect to the Sommerfeld expansion, are enhanced close to depletion ($\Phi_0 \to \epsilon_{\mathrm{F},0}$). That can be seen in Fig. 3.1, where $s_{0,0}$ is represented by the dashed line and the vertical axis on the right side and $s_{0,2}$ by the solid line and the vertical axis on the left-hand side, respectively. The amount of both became infinitely large in the limit $V_R \to \epsilon_{\mathrm{F},0}$.

We define the contribution of the n-th energy moment to the transverse voltage

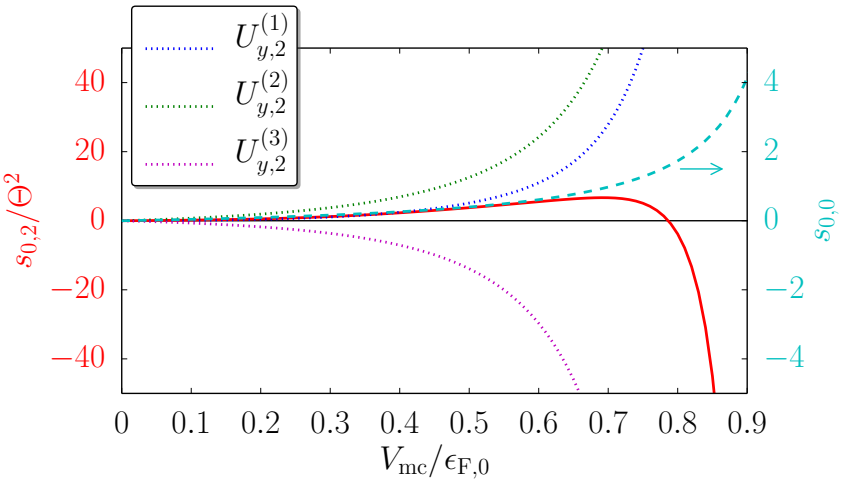

Figure 3.1: The setup consists of an energy source region (heating channel) with a finite electric field E_x and with $\Phi_0 = 0$. On the right side of that source region, the potential is modulated by a constant potential $\Phi_0 = V_{\mathrm{mc}}$. The extension of those two regions with respect to y are described by the tuple $\boldsymbol{w}/l_0 = (1/2, 3)$, where the figures in the tuple correspond to the width of the corresponding regions. These regions are in contact to the infinitely extended voltage probes on the most left and most right side. The right vertical axis scales the dashed line, which represents $s_{0,0}$. The left vertical axis scales the first Sommerfeld correction (solid line), $s_{0,2}$, and its resolved moment contributions (dotted lines), $eU_{y,2}^{(n)}/(\omega_0\Theta^2)$.

in the first Sommerfeld correction by

$$U_{y,2}^{(n)} = \int \mathrm{d}y \, \mathcal{M}_n \frac{\partial \bar{M}_{n,2}}{\partial y} \,, \tag{3.85}$$

with $U_{y,2} = U_{y,2}^{(1)} + U_{y,2}^{(2)} + U_{y,2}^{(3)}$. Those are shown in Fig. 3.1 by the dotted lines with respect to the left vertical axis. In principal, the higher the moment (according to n) the faster increases the amplitude of the contribution to the transverse voltage. For $V_{\mathrm{mc}} \lesssim 0.8\,\epsilon_{\mathrm{F},0}$, the contribution of the first and second moment together dominate over the negative contribution coming from the third moment. Therefore, $U_{y,2}$ is positive. Beyond that, close to $V_{\mathrm{mc}} = \epsilon_{\mathrm{F},0}$, the third moment gives the dominating contribution and $s_{0,2}$ becomes negative in total. From considering the power-law function of $\tau_{e/i}$ it follows that each energy derivative of D or l^2 leads to a factor $(V_{\mathrm{mc}}/\epsilon_{\mathrm{F},0} - 1)^{-1}$ in $\mathcal{M}_n$. In fact, that results in $\mathcal{M}_n \sim (V_{\mathrm{mc}}/\epsilon_{\mathrm{F},0} - 1)^{-n}$. Therefore, apart from prefactors, the higher the moment the faster increases the contribution to U_y with respect to $V_{\mathrm{mc}} \to \epsilon_{\mathrm{F},0}$.

Due to the superposition principal (see Sec. 3.2.5) with respect to energy sources, the setup discussed afore can be extended by further energy source regions to enhance the signal. Building a ratchet [76, 77, 106, 107, 135, 136] is possible. The setup consisting of a source region in combination with a potential-modulated region can be considered as a single device which forms the ratchet by contacting a finite number of devices of the same kind in transverse direction. Those are separated by a contact region, i.e., where $E_x = 0$ and $\Phi_0 = 0$. If this contact region is much larger than the energy diffusion length, the total transverse voltage equals to the transverse voltage of a single device times the number of devices. For a smaller separation length the total transverse voltage becomes smaller since then the profile of the energy moments is influenced by the neighboring devices. That effect has been discussed in Sec. 2.2.5 for a quasi-equilibrium ansatz. Since the focus of this part of the thesis is different, we restrict the discussion to the effects of one source region only.

3.3.2 Profile characteristics of the energy moments

In the previous section, the width of the modulation channel is as large as required to guarantee a total decay of the energy moments within this region. If the width of the right region is of the order of the energy diffusion length, the transverse voltage is affected by finite size effects. The latter can influence the transverse voltage either by a reduction of the modulation channel's width or by a negative potential, which increases the energy diffusion length. Then, the transverse voltage contributions are affected crucially by the spatial characteristics of the energy moments. In fact, those depend on the order of the moment and the order in Θ. That can be studied in detail by Fig. 3.2. The setup equals to that of the previous section. The gray area marks the region with a finite electric field, E_x. The dotted, blue

line depicts the profile of Φ_0 with respect to the right vertical axis. We choose $\Phi_0 = V_{\mathrm{mc}} = \epsilon_{\mathrm{F},0}/2$ for the potential of the right region and $\Phi_0 = 0$ anywhere else. Thereby, the corresponding energy diffusion length is given by $l \approx 0.3\, l_0$ in the potential-modulated region. The width of that region exceeds the energy diffusion length with $w_{\mathrm{mc}} = 3\, l_0$ by a factor of 10.

The other lines in Fig. 3.2 depict the profiles of the finite energy moments. The upper panel shows the lowest order contribution (Θ^0) and the lower panel the first Sommerfeld correction (Θ^2). The finite energy moments are generated in the heating channel and diffuse into the neighboring potential-modulated channel on the right-hand side and into the voltage probe on the left-hand side. The dashed, red line depicts the zeroth energy moment. As described in Sec. 3.2.8, that is the contribution to the chemical potential arising from the energy-dependent inelastic relaxation time, τ_i. Together with the local-equilibrium contribution they form the chemical potential, $\bar{M}_0/\rho + \hat{\mu}_2 = \mu_2$, in each order of the Sommerfeld expansion.

To guarantee that the transverse charge current density vanishes, i.e. $j_y = 0$, diffusive and electric contributions have to cancel each other. That is formulated intrinsically by Eq. (3.30). Using the moment description, a given diffusive force leads to a finite electric force by Eq. (3.46), which in turn is related to a charge accumulation by the Poisson equation. Again, that charge accumulation leads to a diffusive force which enters Eq. (3.46) by the chemical potential of the local-equilibrium distribution, $\hat{\mu}_2$. That argumentation holds for each order of the Sommerfeld expansion. A total self-consistent solution involves, as discussed in Sec. 3.2.6, a solution of the Poisson equation which determines $\hat{\mu}_2(y)$ in this case. However, it is an appealing advantage that the calculation of the transverse voltage can be conducted without solving the Poisson equation. The steps of $\hat{\mu}_2$ are needed at the boundaries only. Those compensate the visible steps of the even order energy moments in Fig. 3.2, and, thereby, guarantee the continuity of the isotropic distribution function $\langle f_2 \rangle$.

Although the variation length of the moments is given by the energy diffusion length, the spatial characteristics of each moment are clearly different. Qualitatively, the lower the order of the moment, n, but the higher the order in Θ, the longer takes the spatial relaxation of the moment. Therefore, if the width of the potential-modulated region is reduced, the highest moments still reach approximately zero, but the lower moments are still finite at the end of the modulated region. A strong dependence of the moment's relative contribution to the transverse voltage on w_{mc} is, thus, expected. That can be seen in Fig. 3.3. The contributions to $s_{0,2}$, which refer to the first Sommerfeld correction, are scaled by the left vertical axis. The red, solid line visualizes $s_{0,2}$. The moment resolved contributions to the transverse voltage, i.e. $U_{y,2}^{(n)}$, on the other hand, are depicted by the dotted lines. Here, especially the contribution by $U_{y,2}^{(1)}$ shows nontrivial characteristics up to $w_{\mathrm{mc}} = l_0$. At approximately $w_{\mathrm{mc}} \approx 0.75\, l_0$, the contribution vanishes. Comparison to the corresponding value of y in Fig. 3.2 allows for a qualitative argument. At

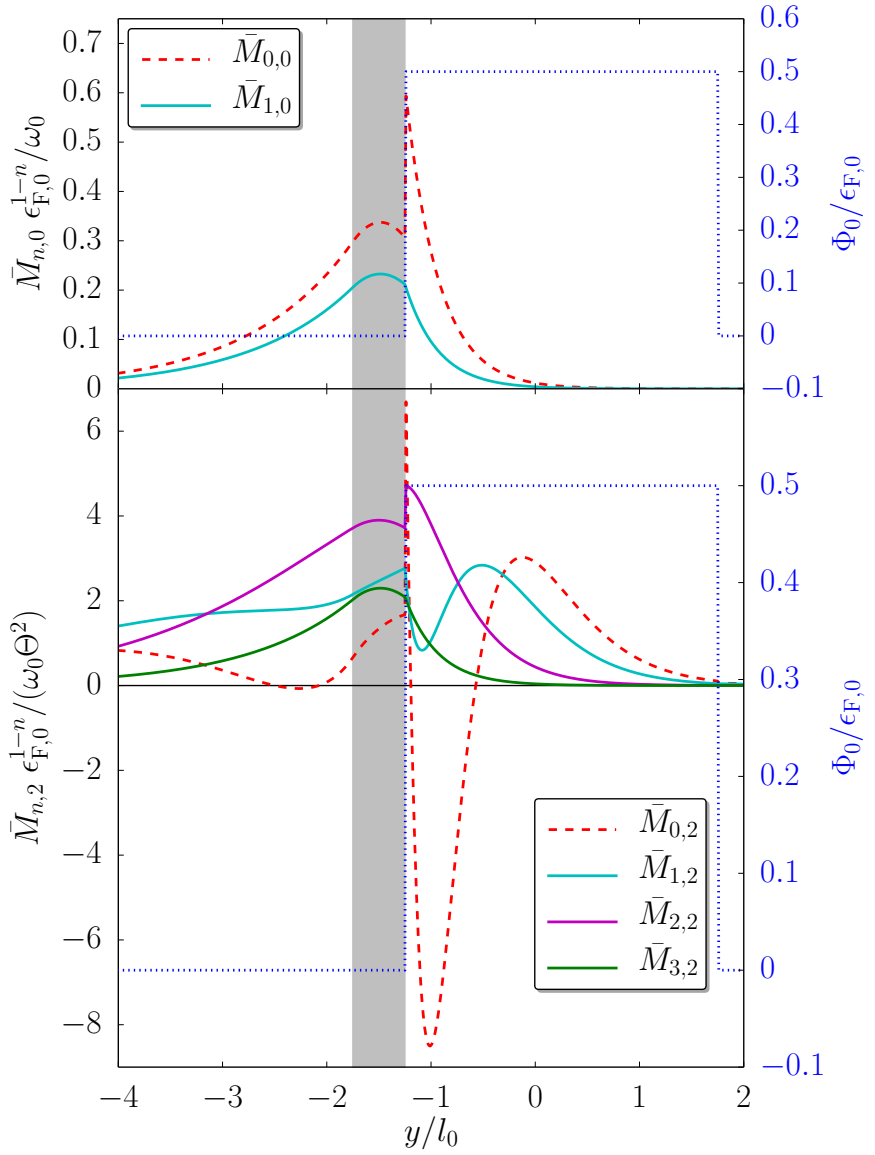

Figure 3.2: The setup consists of a heating and a modulation channel. The heating channel with a finite applied electric field E_x is indicated by the gray area. The potential and width of the two regions are described by $V_{\mathrm{mc}} = \epsilon_{\mathrm{F},0}/2$ and $\boldsymbol{w} = (l_0/2, 3\,l_0)$, respectively. The external potential is depicted by the dotted line with respect to the right vertical axes. The upper panel shows the spatial profiles of the energy moments in lowest order (Θ^0) and the lower panel those of the order Θ^2. Their values are given by the vertical scale on the left-hand side.

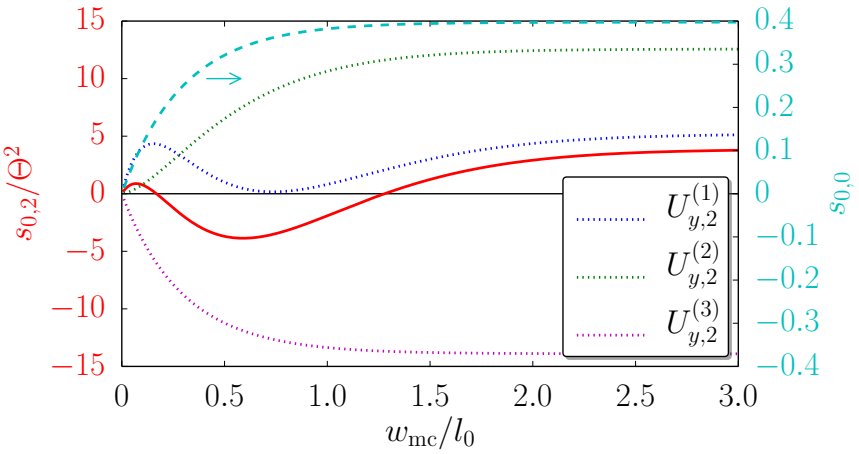

Figure 3.3: The setup consists of an energy-source region with a finite electric field E_x. On the right-hand side of that source region, there is a potential-modulated region with the constant potential $V_{\mathrm{mc}} = \epsilon_{\mathrm{F},0}/2$ ($\Phi_0 = 0$ anywhere else). The dimensions with respect to y are described by $\boldsymbol{w} = (l_0/2, w_{\mathrm{mc}})$. The right vertical axis scales the dashed line, which represents $U_{y,0}$. The left vertical axis scales the first Sommerfeld correction (solid line) and the resolved moment contributions (dotted lines) coming from $U_{y,2}^{(n)}$.

$0.75\,l_0$ on the right side of the boundary to the source region, the value of the first energy moment is the same as at the boundary. Therefore, the integration over that interval is approximately zero. That influences $U_{y,2}$ as well. The Sommerfeld correction to the transverse voltage changes its sign twice. The transverse voltage of the lowest order in the Sommerfeld expansion, which is depicted by the dashed line with respect to the vertical axis on the right side, reaches its constant value on a relatively small length, which is of the order of the energy diffusion length.

In summary, there are two effects regarding the dependence of the transverse voltage on the gate potential. First, higher moments enter the electrochemical potential with a factor that in(de)creases faster with $\Phi_0 \to \epsilon_{\mathrm{F},0}$ compared to those of lower moments. Therefore, the higher moment contributions dominate in that regime. Secondly, lower moments of higher order in the Sommerfeld expansion decay on a larger length scale (but of the order of the energy diffusion length) compared to either higher moments or moments of lower order in the Sommerfeld expansion. Those two effects in superposition can lead to situations in which, especially, the first Sommerfeld correction gives rise to a significant contribution. We discuss such a setup in the next section.

3.3.3 Higher-order contributions regarding the Sommerfeld expansion

The results of the previous discussion in Secs. 3.3.1 and 3.3.2 can be formulated as follows. The first energy moment ($n = 1$), which dominates the transverse voltage in lowest order of the Sommerfeld expansion, relaxes on a shorter length scale than the moments of the first Sommerfeld correction. One exception is $\bar{M}_{3,2}$ which is proportional to $\bar{M}_{1,0}$. Therefore, if we introduce a second potential modulation on the left side of the heating channel, there is the possibility to reduce the lowest order contribution, while the first correction is still equally strong. In particular, we choose the width of the left modulation channel to be the same as the width of the heating channel ($l_0/2$) and the potential is always the same in the left and right modulation channel. We consider the case, that the width of the right region is given by $w_\mathrm{R} = 3\,l_0$ and the external potential reads $V_\mathrm{mc} = \epsilon_{\mathrm{F},0}/2$ in both potential-modulated regions. In that constellation, the left region leads to an enhanced contribution with respect to the first Sommerfeld correction and, simultaneously, it reduces the lowest order contribution. In comparison to the setup without the left region, $s_{0,0}$ is decreased by 80% while the first Sommerfeld correction $s_{0,2}$ is approximately twice as large. The latter results dominantly from a reduction (by 80% as well) of the $U^{(3)}_{y,2}$ contribution.

In Fig. 3.4, the contributions to the transverse voltage are depicted in case of the above discussed setup. The width of the right potential-modulated region is changed along the horizontal axis. The lower panel shows s_0 in lowest order, $s_{0,0}$, the lowest order plus the first Sommerfeld correction, $s_{0,0} + s_{0,2}$, and the superposition of those and the second Sommerfeld correction, which is proportional to Θ^4, $s_{0,0} + s_{0,2} + s_{0,4}$. For comparison, we use $\Theta = 0.05$ which accounts for $T_0 = 4.2\,\mathrm{K}$ and $\epsilon_{\mathrm{F},0} = 0.74\,\mathrm{meV}$ approximately. If the width w_R is larger than $2\,l_0$, the first Sommerfeld correction leads to a correction by about 20%. That is certainly a significant effect and has to be taken into account in that setup. The next Sommerfeld correction is rather negligible in this case.

To illustrate the effects of the position dependence of the energy moments, the upper panel depicts the first Sommerfeld correction, $s_{0,2}$ only. For $w_\mathrm{R} = l_0/2$ all contributions vanish due to left-right symmetry. In comparison to Fig. 3.3 the contribution of the highest moment, $\bar{M}_{3,2}$, is relatively small, which results from the fact that contributions from the left and right modulation channel have an opposite sign and thus cancel each other. Mesoscopic effects influence $U^{(1)}_{y,2}$ on a larger length scale compared to the other moments. Especially, for $w_\mathrm{R} \approx l_0$ the contribution from the first moment changes sign.

The relative strength of the first Sommerfeld correction depends not only on the width of the regions, but on the gate potential as well. That is shown by Fig. 3.5, where the horizontal axis is labeled by the gate potential of the left and right region, V_mc. The width of the right region is $w_\mathrm{R} = 2\,l_0$ in this case. Two effects have to be distinguished. First, the potential varies the energy diffusion

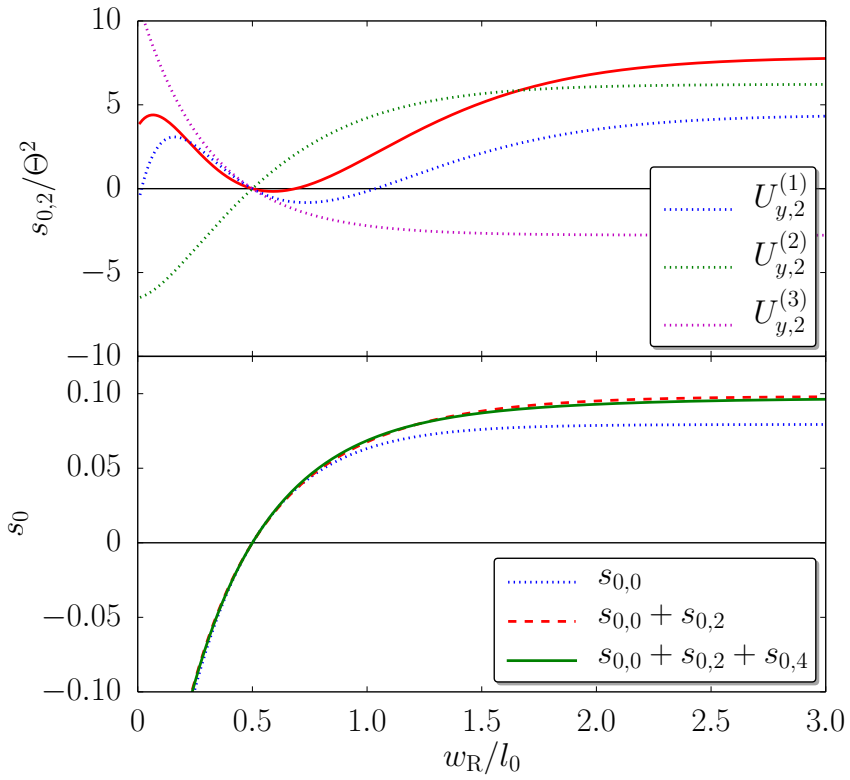

Figure 3.4: The setup consists of heating channel with a finite electric field E_x. On the left and right side of that channel potential-modulated regions are located with a constant potential $V_\mathrm{mc} = \epsilon_{\mathrm{F},0}/2$. The potential Φ_0 of the heating channel is kept at zero. The dimensions of each channel with respect to y are given by $\boldsymbol{w} = (l_0/2, l_0/2, w_\mathrm{R})$. The upper panel shows the dependence on the width of the right region, w_R. Depicted are the first Sommerfeld correction $s_{0,2}$ (solid line) and the corresponding moment contributions related to $U^{(n)}_{y,2}$ (dotted lines). The lower panel illustrates the dependence of s_0 on w_R up to the order Θ^{2j}.

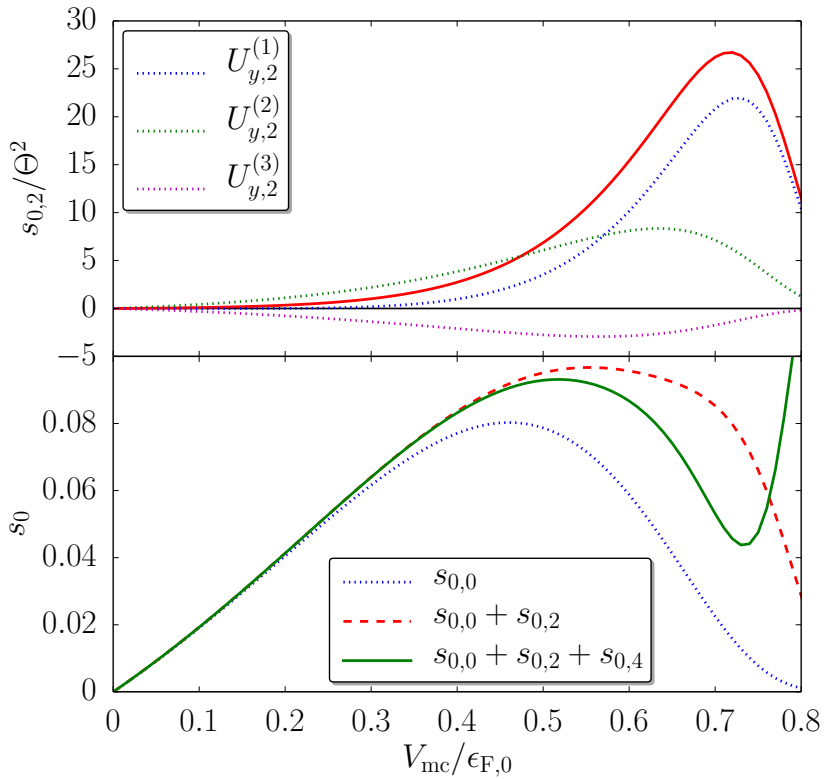

Figure 3.5: The setup consists of heating channel with a finite electric field E_x. On the left and right side of that channel potential-modulated regions are located with a varying potential V_{mc}. The potential Φ_0 of the heating channel is kept at zero. The dimensions of each channel with respect to y are given by $\boldsymbol{w} = (l_0/2, l_0/2, 2\,l_0)$. The upper panel shows the dependence on the potential V_{mc} of the modulation channels. Depicted are the first Sommerfeld correction $s_{0,2}$ (solid line) and the corresponding moment contributions related to $U_{y,2}^{(n)}$ (dotted lines). The lower panel illustrates the dependence of s_0 on V_{mc} up to the order Θ^{2j}.

length l. Therefore, the reduction of the transverse voltage contributions arising from moments that drop on a small length scale is less effective for $V \lesssim \epsilon_{\mathrm{F},0}/4$. Thus, the first Sommerfeld correction can be neglected in this regime. Close to depletion, $V \to \epsilon_{\mathrm{F},0}$, on the other hand, all moments drop totally to zero within the left and right modulated region. The contributions to the transverse voltage of the left and right side cancel each other completely and s_0 vanishes. Secondly, the gate voltage tunes the linear response coefficients that relate gradients of the moments to the electrochemical potential. Those are enhanced for large V_{mc}. Although, that enhances primarily the higher moments, the contribution of those are small compared to the lower moments in general. That can be seen in the upper panel of Fig. 3.5. The reason is again, that those contributions are canceled by an effective left-right symmetry for moments that change on a much smaller length than the width of the modulation channels.

However, to guarantee that the Sommerfeld expansion is applicable, the ratio of $\Theta/(1 - \Phi_{0,max}/\epsilon_{\mathrm{F},0})$ has to be much smaller than one, with $\Phi_{0,max}$ being the potential that is closest to $\epsilon_{\mathrm{F},0}$. Thereby, here, $\Theta/(1 - V_{\mathrm{mc}}/\epsilon_{\mathrm{F},0})$ is an indicator for the Sommerfeld expansion's figure of merit. For small V_{mc} it is as well small and Sommerfeld corrections can be neglected. If V_{mc} is larger, even for $V \approx 0.3\,\epsilon_{\mathrm{F},0}$, the Sommerfeld corrections influence the results significantly and have to be taken into account. As visible in the lower panel of Fig. 3.5, at approximately $V_{\mathrm{mc}} = 0.5\,\epsilon_{\mathrm{F},0}$, the second Sommerfeld correction has to be taken into account as well. The concept of the Sommerfeld expansion breaks down if $\Theta/(1 - V_{\mathrm{mc}}/\epsilon_{\mathrm{F},0}) = 1$, which is the case for $V_{\mathrm{mc}} = 0.95\,\epsilon_{\mathrm{F},0}$ if $\Theta = 0.05$.

The lower panel of Fig. 3.5 emphasizes that contributions to the transverse voltage of higher order with respect to the Sommerfeld expansion are significant when the external potential reduces the carrier density of the two-dimensional electron gas. Simultaneously, as shown in the upper panels of Figs. 3.4 and 3.5, in principle, all energy moments are equally relevant and have to be taken into account.

In this part of the thesis, we discussed and applied a semiclassical method for the calculation of the thermoelectric transverse voltage. That method is beyond the usual description by an effective temperature and chemical potential. The applied technique allows for a systematic calculation of the non-equilibrium contributions to the distribution function of the charge carriers. We discussed when and how higher-order contribution with respect to the Sommerfeld expansion influence the thermoelectric transverse voltage. Especially, close to depletion of a potential-modulated region, higher-order contributions in the Sommerfeld expansion and higher energy moments of the distribution function have to be taken into account.

Conclusion

The characteristic length scales that determine the properties of charge transport and energy diffusion by electrons in two-dimensional electron gases strongly differ from each other at low temperature. Compared to the elastic mean-free path (that marks the crossover from ballistic to diffusive charge transport), the energy diffusion length may be substantially larger. The latter defines the scale for spatial variations of the local electron temperature in non-equilibrium situations evoked by local Joule heating. In this thesis, we considered the following type of devices: metallic gates, with a length in x-direction that is much larger than the width, modulate the electric potential of a 2DEG in y-direction. That changes the local thermopower as well as the characteristics of energy diffusion. An electric current I_x driven through the 2DEG in x-direction heats up the electron system which, in turn, generates a transverse thermoelectric output voltage U_y.

On length scales comparable to this energy diffusion length, mesoscopic effects become important and give rise to mesoscopic features of the diffusion thermopower. Both, the temperature profile and the value of electric voltage, induced by local Joule heating, depend on geometric dimensions of a specific device, including the width of heating channels (regions with finite I_x), the width of modulation channels (modulation of the electric potential), and the separation between the two. Since in such a mesoscopic all-electric setup, heat generation and heat diffusion have to be treated on the same footing. Thus, we characterize the thermopower by relating the output voltage U_y to the input heating current or voltage. That relation is given by the dimensionless quantity

$$s = \frac{eU_y}{\omega} \quad , \tag{3.86}$$

where ω is the application of energy per electron provided by the heating current.

The measured transverse signal characterized by s can be understood within a diffusion thermopower model taking the temperature profile into account. That description is based on a quasi-equilibrium distribution function with spatially dependent temperature and chemical potential, where the linear transport coefficients are given by the lowest order contribution of the Sommerfeld expansion. In Chap. 2 we discussed the necessary qualitative and quantitative characteristics of the quantity s that result from Joule heating and potential modulation. That is especially relevant for engineering the transverse voltage and using such a device, e.g., as a tunable rectifier [2]. The relevance of the mesoscopic effects in the diffusive low-temperature regime are emphasized by a theoretical analysis related to

recent experiments [2,3]. Since those effects strongly depend on the energy diffusion length, it is crucial to analyze that parameter for a certain system. We discussed a method and the necessary theoretical background to measure that length by studying the dependence of the transverse voltage on the external potential.

The above mentioned diffusion thermopower model allows for an appropriate description of the mesoscopic effects in a low temperature regime. However, the results in Chap. 3 show that there are simple geometries in a density-modulated two-dimensional electron gas where a systematic Sommerfeld expansion is necessary. Especially, close to the depletion of a potential-modulated region, higher-order contributions in the Sommerfeld expansion and higher energy moments of the distribution function have to be taken into account. That demands an energy description of the distribution function, which is beyond the quasi-equilibrium ansatz consisting of a spatially dependent temperature and chemical potential only.

Starting from a semi-classical transport equation, we derived an effective differential equation for the (isotropic) distribution function regarding a perturbation expansion in the applied electric field and taking only length scales into account which are large compared to the elastic mean free path. Thereby, we considered elastic and inelastic scattering in an energy-dependent relaxation-time approximation of the Boltzmann equation. The characteristic length scale is again the energy diffusion length. To find a solution, we introduced energy moments of the distribution function which leads to a set of balance equations for those energy moments. The balance equations describe the energy dependence of the distribution function entirely. Within a systematic Sommerfeld expansion, the profiles of the energy moments can be calculated. Those characterize contributions to the chemical potential and to the temperature profile.

In lowest order of the Sommerfeld expansion, this generalized approach is equivalent to a quasi-equilibrium ansatz. The first correction to the lowest order in the Sommerfeld expansion already modifies the well known Mott formula for the Seebeck coefficient. Even at a low temperature, that correction can become significant if the electron density of the two-dimensional electron gas is reduced by an external potential.

The characteristics of the energy moment's profiles are, in principle, nontrivial and depend on the order of the moment and on the order of the Sommerfeld expansion. One aspect concerns the characteristic length on which finite size effects influence the transverse voltage. In principle, that length is larger for contributions of higher order with respect to the Sommerfeld expansion compared to lower-order contributions. That leads to the possibility of a strongly enhanced influence on the transverse voltage by those moments of higher order. Since the consideration of a systematic Sommerfeld expansion exceeds the validity of a quasi-equilibrium ansatz, the electrochemical potential is formulated in linear response to all energy moments.

Moreover, the systematic treatment of the energy moments of the distribution function allows for a better understanding of the non-equilibrium transport char-

acteristics which are important for device geometries as analyzed in this thesis. Especially the limits of a pure temperature description within a quasi-equilibrium ansatz can be understood in that context. This generalized ansatz has the opportunity to be extended to other systems and other regimes. A generalization to three dimensions is imaginable. However, the two-dimensional setup will still be easier to vary and modulate by using top-gates on a structured electron gas. Another extension of the discussed theory can be the determination of the non-equilibrium corrections to the electron density. As discussed in Sec. 3.2.6, the Poisson equation has to be solved self-consistently with the other non-equilibrium contributions which define the transverse voltage. For the motivation of this thesis the corrections to the electron density are not relevant. However, for a full solution of the spatial dependence in terms of the presented expansion, the electron density is left to determine.

In summary, this thesis presents an analytical approach to determine the non-equilibrium contributions which are necessary to understand mesoscopic effects in a certain regime. This regime is characterized by a low temperature, weak electric fields and, more importantly, by length scales comparable to the energy diffusion length. A systematic expansion provides higher-order contributions. The results are relevant for various experimental setups. The derived theory describes mesoscopic effects on thermoelectric transport in a density-modulated two-dimensional electron gas where a temperature gradient is created by Joule heating.

A Balance equations

A matrix-like formulation of the balance equation (3.49) with respect to the first and second derivative of the energy moments reads

$$\bar{M}_n^{\text{bulk}} = \bar{M}_n + \sum_{m=0}^{\infty} \left(A_{mn}\, \partial_y \bar{M}_m + B_{mn}\, \partial_y^2 \bar{M}_m \right) \quad . \tag{A.1}$$

For the definition of abbreviations see Sec. 3.2.6 and following. The coefficients are defined by

$$\begin{aligned} A_{mn} =& - \frac{\left(l^2 \frac{\partial_y D}{D} \right)^{(m-n)}}{(m-n)!} + \frac{\partial_y D^{(m)}}{m!} \frac{\sum_{k=0}^{\infty} \frac{1}{k!} (l^2)^{(k)} M_{n+k}^{f_0'}}{\sum_{k=0}^{\infty} \frac{1}{k!} D^{(k)} M_k^{f_0'}} \\ &+ \frac{D^{(m)}}{m!} \left(\frac{\sum_{k=0}^{\infty} \frac{1}{k!} \left(l^2 \frac{\partial_y D}{D} \right)^{(k)} M_{n+k}^{f_0'}}{\sum_{k=0}^{\infty} \frac{1}{k!} D^{(k)} M_k^{f_0'}} - \frac{\sum_{k,k'=0}^{\infty} \frac{1}{k'!} \frac{1}{k!} \left(l^2 \right)^{(k)} \left(\partial_y D \right)^{(k')} M_{n+k}^{f_0'} M_{k'}^{f_0'}}{\sum_{k,k'=0}^{\infty} \frac{1}{k'!} \frac{1}{k!} D^{(k)} D^{(k')} M_k^{f_0'} M_{k'}^{f_0'}} \right) , \\ B_{mn} =& - \frac{(l^2)^{(m-n)}}{(m-n)!} + \frac{D^{(m)}}{m!} \frac{\sum_{k=0}^{\infty} \frac{1}{k!} (l^2)^{(k)} M_{n+k}^{f_0'}}{\sum_{k=0}^{\infty} \frac{1}{k!} D^{(k)} M_k^{f_0'}} \quad , \end{aligned} \tag{A.2}$$

where the characteristics of various Taylor expansions are visible. Note, that $B_{mn} = 0$ for $m = 0 = n$. In addition, if the index, k, of the derivative of an arbitrary function $F^{(k)}$ becomes negative, we define $F^{(k<0)} = 0$.

B Balance equations in Sommerfeld expansion

In this section, we present the formal expressions of the balance equation and current densities in terms of the Sommerfeld expansion as discussed in Sec. 3.2.7. For the bulk energy moment we get the following results up to order Θ^2

$$\begin{aligned}
\bar{M}^{\text{bulk}}_{0,0} &= \rho\,\mathcal{E}^2\left(\frac{(l^2)'}{l^2}-\frac{D'}{D}\right) \quad , \\
\bar{M}^{\text{bulk}}_{0,2} &= \rho\,\mathcal{E}^2\,\frac{\pi^2}{6}(k_BT_0)^2\left(2\frac{(l^2)'}{l^2}\left(\frac{D'}{D}\right)^2-2\left(\frac{D'}{D}\right)^3-\frac{D'}{D}\frac{(l^2)''}{l^2}-2\frac{D''}{D}\frac{(l^2)'}{l^2}\right. \\
&\qquad\left.+3\frac{D'}{D}\frac{D''}{D}+\frac{(l^2)'''}{l^2}-\frac{D'''}{D}\right) \quad , \\
\bar{M}^{\text{bulk}}_{1,0} &= \rho\,\mathcal{E}^2 \quad , \\
\bar{M}^{\text{bulk}}_{1,2} &= \rho\,\mathcal{E}^2\,\frac{\pi^2}{6}(k_BT_0)^2\left(2\left(\frac{D'}{D}\right)^2-2\frac{D'}{D}\frac{(l^2)'}{l^2}+3\frac{(l^2)''}{l^2}-2\frac{D''}{D}\right) \quad , \\
\bar{M}^{\text{bulk}}_{2,2} &= \rho\,\mathcal{E}^2\,\frac{\pi^2}{3}(k_BT_0)^2\left(\frac{(l^2)'}{l^2}-\frac{D'}{D}\right) \quad , \\
\bar{M}^{\text{bulk}}_{3,2} &= \rho\,\mathcal{E}^2\,\pi^2(k_BT_0)^2 \quad . \qquad \text{(B.1)}
\end{aligned}$$

The n-th balance equation of the order Θ^{2j} expressed in terms of the energy moments $\bar{M}_{n,2j}$ reads

$$\begin{aligned}
\bar{M}^{\text{bulk}}_{n,2j} = \bar{M}_{n,2j} &- \sum_{m=0}^{2j+1-n}\sum_{m'=0}^{m}\frac{1}{m!}\binom{m}{m'}\left(\frac{l^2}{D}\right)^{(m')}\frac{\partial}{\partial y}\left[D^{(m-m')}\frac{\partial\bar{M}_{n+m,2j}}{\partial y}\right] \\
&+\sum_{m=0}^{2j+1-n}M^{f_0'}_{n+m}\sum_{m'=0}^{m}\frac{1}{m!}\binom{m}{m'}\left(\frac{l^2}{D}\right)^{(m')} \\
&\times\frac{\partial}{\partial y}\left[D^{(m-m')}\sum_{j'=0}^{j-\frac{n+m}{2}}\frac{\mathcal{A}_{2j'}(k_BT_0)^{2j'}}{\rho}\mathcal{S}_{2(j-j')-(n+m)}\right] \quad , \qquad \text{(B.2)}
\end{aligned}$$

with the recursive coefficients

$$\mathcal{A}_{2k} = -\sum_{k'=0}^{(k-1)}\mathcal{A}_{2k'}\frac{D^{(2k-2k')}}{D}a_{k-k'}$$

starting with $\mathcal{A}_0 = -1/D$ and

$$\mathcal{A}_2 = \frac{\pi^2}{6}\frac{D''}{D^2} \quad .$$

The first moments $M_n^{f_0'}$ are given by $M_0^{f_0'} = -\rho$, $M_1^{f_0'} = 0$, $M_2^{f_0'} = -\rho\,\frac{\pi^2}{3}(k_B T_0^2)$, and $M_3^{f_0'} = 0$. Moreover, we introduced the definition

$$\mathcal{S}_{2j} = \sum_{m=0}^{2j+1} \frac{D^{(m)}}{m!}\frac{\partial \bar{M}_{m,2j}}{\partial y} \quad .$$

In addition to the balance equations of the order Θ^2 in Sec. 3.2.10 for $\bar{M}_{1,2}$ and $\bar{M}_{0,2}$, Eqs. (3.68) and (3.69), respectively, we get

$$\begin{aligned}
\bar{M}_{1,2}^{\text{bulk}} = \bar{M}_{1,2} &- \frac{l^2}{D}\frac{\partial}{\partial y}\left(D\frac{\partial \bar{M}_{1,2}}{\partial y}\right) - \frac{l^2}{D}\frac{\partial}{\partial y}\left(D'\frac{\partial \bar{M}_{2,2}}{\partial y}\right) - \left(\frac{l^2}{D}\right)'\frac{\partial}{\partial y}\left(D\frac{\partial \bar{M}_{2,2}}{\partial y}\right) \\
&- \frac{1}{2}\frac{l^2}{D}\frac{\partial}{\partial y}\left(D''\frac{\partial \bar{M}_{3,2}}{\partial y}\right) - \frac{1}{2}\left(\frac{l^2}{D}\right)''\frac{\partial}{\partial y}\left(D\frac{\partial \bar{M}_{3,2}}{\partial y}\right) - \left(\frac{l^2}{D}\right)'\frac{\partial}{\partial y}\left(D'\frac{\partial \bar{M}_{3,2}}{\partial y}\right) \\
&+ \frac{\pi^2}{3}(k_B T_0)^2\left[\frac{l^2}{D}\frac{\partial}{\partial y}\left(D'\frac{\partial \bar{M}_{0,0}}{\partial y} + \frac{(D')^2}{D}\frac{\partial \bar{M}_{1,0}}{\partial y}\right)\right. \\
&\left.+ \left(\frac{l^2}{D}\right)'\frac{\partial}{\partial y}\left(D\frac{\partial \bar{M}_{0,0}}{\partial y} + D'\frac{\partial \bar{M}_{1,0}}{\partial y}\right)\right] \quad . \qquad \text{(B.3)}
\end{aligned}$$

The zeroth order energy moment $\bar{M}_{0,2}$ is given by the following relation

$$\begin{aligned}
\bar{M}_{0,2} - \bar{M}_{0,2}^{\text{bulk}} = &\left(\frac{l^2}{D}\right)'\frac{\partial}{\partial y}\left(D\frac{\partial \bar{M}_{1,2}}{\partial y}\right) + \left(\frac{l^2}{D}\right)'\frac{\partial}{\partial y}\left(D'\frac{\partial \bar{M}_{2,2}}{\partial y}\right) \\
&+ \frac{1}{2}\left(\frac{l^2}{D}\right)''\frac{\partial}{\partial y}\left(D\frac{\partial \bar{M}_{2,2}}{\partial y}\right) + \frac{1}{2}\left(\frac{l^2}{D}\right)'\frac{\partial}{\partial y}\left(D''\frac{\partial \bar{M}_{3,2}}{\partial y}\right) \\
&+ \frac{1}{2}\left(\frac{l^2}{D}\right)''\frac{\partial}{\partial y}\left(D'\frac{\partial \bar{M}_{3,2}}{\partial y}\right) + \frac{1}{6}\left(\frac{l^2}{D}\right)'''\frac{\partial}{\partial y}\left(D\frac{\partial \bar{M}_{3,2}}{\partial y}\right) \\
&- \frac{\pi^2}{3}(k_B T_0)^2\left[\left(\frac{l^2}{D}\right)'\frac{\partial}{\partial y}\left(D'\frac{\partial \bar{M}_{0,0}}{\partial y}\right) + \left(\frac{l^2}{D}\right)'\frac{\partial}{\partial y}\left(\frac{(D')^2}{D}\frac{\partial \bar{M}_{1,0}}{\partial y}\right)\right. \\
&\left.+\frac{1}{2}\left(\frac{l^2}{D}\right)''\frac{\partial}{\partial y}\left(D\frac{\partial \bar{M}_{0,0}}{\partial y}\right) + \frac{1}{2}\left(\frac{l^2}{D}\right)''\frac{\partial}{\partial y}\left(D'\frac{\partial \bar{M}_{1,0}}{\partial y}\right)\right] \quad . \qquad \text{(B.4)}
\end{aligned}$$

In terms of a systematic Sommerfeld expansion, the electrochemical potential in second order in E_x (3.45) and of the order Θ^{2j} can be formulated by

$$-e\frac{\partial \phi_{2j}}{\partial y} = \frac{1}{\rho}\left(\sum_{j'=0}^{j}\mathcal{A}_{2(j-j')}(k_B T_0)^{2(j-j')}\frac{\partial \mathcal{S}_{2j'}}{\partial y} + \frac{\partial \bar{M}_{0,2j}}{\partial y}\right) \quad . \qquad \text{(B.5)}$$

Accordingly, the current for $n > 0$ is given by

$$j^{(n)}_{2,y,2j} = -\sum_{j'=n/2}^{j} (k_B T_0)^{2j'} \left(\sum_{k=n/2}^{j'} \frac{(2k)! a_k D^{(2k-n)}}{(2k-n)!} \mathcal{A}_{2(j'-k)} \right) \mathcal{S}_{2(j-j')} - \sum_{m=0}^{2j+1-n} \frac{D^{(m)}}{m!} \frac{\partial \bar{M}_{m+n,2j}}{\partial y} \quad . \tag{B.6}$$

Bibliography

[1] A. Ganczarczyk, C. Notthoff, M. Geller, A. Lorke, D. Reuter, and A. D. Wieck, AIP Conf. Proc. **1199**, 143 (2009).

[2] A. Ganczarczyk, S. Rojek, A. Quindeau, M. Geller, A. Hucht, C. Notthoff, J. König, A. Lorke, D. Reuter, and A. D. Wieck, Phys. Rev. B **86**, 085309 (2012).

[3] W. E. Chickering, J. P. Eisenstein, and J. L. Reno, Phys. Rev. Lett. **103**, 046807 (2009).

[4] A. M. Song, A. Lorke, A. Kriele, J. P. Kotthaus, W. Wegscheider, and M. Bichler, Phys. Rev. Lett. **80**, 3831 (1998).

[5] K. Hieke and M. Ulfward, Phys. Rev. B **62**, 16727 (2000).

[6] I. Shorubalko, H. Q. Xu, I. Maximov, P. Omling, L. Samuelson, and W. Seifert, Appl. Phys. Lett. **79**, 1384 (2001).

[7] L. Worschech, H. Q. Xu, A. Forchel, and L. Samuelson, Appl. Phys. Lett. **79**, 3287 (2001).

[8] B. Hackens, L. Gence, C. Gustin, X. Wallart, S. Bollaert, A. Cappy, and V. Bayot, Appl. Phys. Lett. **85**, 4508 (2004).

[9] M. Knop, U. Wieser, U. Kunze, D. Reuter, and A. D. Wieck, Appl. Phys. Lett. **88**, 082110 (2006).

[10] D. Salloch, U. Wieser, U. Kunze, and T. Hackbarth, Appl. Phys. Lett. **94**, 203503 (2009).

[11] M. Wiemann, U. Wieser, U. Kunze, D. Reuter, and A. D. Wieck, Appl. Phys. Lett. **97**, 062112 (2010).

[12] D. Salloch, U. Wieser, U. Kunze, and T. Hackbarth, Microelectron. Eng. **88**, 2386 (2011).

[13] J. Matthews, D. Sánchez, M. Larsson, and H. Linke, Phys. Rev. B **85**, 205309 (2012).

[14] L. W. Molenkamp, H. van Houten, C. W. J. Beenakker, R. Eppenga, and C. T. Foxon, Phys. Rev. Lett. **65**, 1052 (1990).

[15] L. W. Molenkamp, T. Gravier, H. van Houten, O. J. A. Buijk, M. A. A. Mabesoone, and C. T. Foxon, Phys. Rev. Lett. **68**, 3765 (1992).

[16] A. Bulusu and D. Walker, Superlattices Microstruct. **44**, 1 (2008).

[17] T. M. Tritt, Annu. Rev. Mater. Res. **41**, 433 (2011).

[18] F. Giazotto, T. Heikkilä, A. Luukanen, A. Savin, and J. Pekola, Rev. Mod. Phys. **78**, 217 (2006).

[19] V. G. Kantser, in *Nanoscale Devices - Fundamentals and Applications*, Vol. 233, edited by R. Gross, A. Sidorenko, and L. Tagirov (Springer Netherlands, Dordrecht, 2006) pp. 291–307.

[20] D. Sánchez and R. López, C. R. Phys. **17**, 1060 (2016).

[21] B. Sothmann, R. Sánchez, and A. N. Jordan, Nanotechnology **26**, 032001 (2015).

[22] S. Maximov, M. Gbordzoe, H. Buhmann, L. W. Molenkamp, and D. Reuter, Phys. Rev. B **70**, 121308 (2004).

[23] G. Granger, J. P. Eisenstein, and J. L. Reno, Phys. Rev. Lett. **102**, 086803 (2009).

[24] W. E. Chickering, J. P. Eisenstein, L. N. Pfeiffer, and K. W. West, Phys. Rev. B **81**, 245319 (2010).

[25] K. Fujita, A. Endo, S. Katsumoto, and Y. Iye, Physica E **42**, 1030 (2010).

[26] F. L. Bakker, A. Slachter, J.-P. Adam, and B. J. van Wees, Phys. Rev. Lett. **105**, 136601 (2010).

[27] A. Gold and V. T. Dolgopolov, Europhys. Lett. **96**, 27007 (2011).

[28] M. Schmidt, G. Schneider, C. Heyn, A. Stemmann, and W. Hansen, Phys. Rev. B **85**, 075408 (2012).

[29] V. Narayan, M. Pepper, J. Griffiths, H. Beere, F. Sfigakis, G. Jones, D. Ritchie, and A. Ghosh, Phys. Rev. B **86**, 125406 (2012).

[30] V. Narayan, M. Pepper, J. Griffths, H. Beere, F. Sfigakis, G. Jones, D. Ritchie, and A. Ghosh, J. Low Temp. Phys. **171**, 626 (2013).

[31] V. Narayan, E. Kogan, C. Ford, M. Pepper, M. Kaveh, J. Griffiths, G. Jones, H. Beere, and D. Ritchie, New J. Phys. **16**, 085009 (2014).

[32] J. Billiald, D. Backes, J. König, I. Farrer, D. Ritchie, and V. Narayan, Applied Physics Letters **107**, 022104 (2015).

[33] J. Ziman, *Electrons and Phonons* (Clardendon Press, Oxford, 1960).

[34] N. W. Ashcroft and N. D. Mermin, *Solid State Physics* (Saunders College, Philadelphia, 1976).

[35] S. Rojek and J. König, Phys. Rev. B **90**, 115403 (2014).

[36] K. Bløtekjær, *High-frequency Conductivity, Carrier Waves, and Acoustic Amplification in Drifted Semiconductor Plasmas* (Defense Technical Information Center, 1966).

[37] K. Bløtekjær and E. B. Lunde, Phys. Status Solidi B **35**, 581 (1969).

[38] J. J. Duderstadt and W. R. Martin, *Transport Theory* (John wiley and Sons, New York, 1979).

[39] S. Taschini, M. Rudan, and R. Brunetti, Phys. Rev. B **60**, 13582 (1999).

[40] T. Christen, Europhys. Lett. **89**, 57007 (2010).

[41] M. Cutler and N. F. Mott, Phys. Rev. **181**, 1336 (1969).

[42] T. T. Heikkilä, *The Physics of Nanoelectronics: Transport and Fluctuation Phenomena at Low Temperatures* (Oxford University Press, 2013).

[43] C. Jacoboni, *Theory of Electron Transport in Semiconductors* (Springer, 2010).

[44] J. J. Harris, J. A. Pals, and R. Woltjer, Rep. Prog. Phys. **52**, 1217 (1989).

[45] L. Esaki and R. Tsu, IBM J. Res. Dev. **14**, 61 (1970).

[46] T. Ando, A. B. Fowler, and F. Stern, Rev. Mod. Phys. **54**, 437 (1982).

[47] J. Tsao, *Materials Fundamentals of Molecular Beam Epitaxy* (Academic, San Diego, 1993).

[48] G. Stringfellow, *Organometallic Vapor-Phase Epitaxy: Theory and Practice* (Academic, San Diego, 1999).

[49] S. M. Sze and K. K. Ng, *Physics of Semiconductor Devices* (Wiley-Interscience, 2007).

[50] L. Pfeiffer, K. W. West, H. L. Stormer, and K. W. Baldwin, Appl. Phys. Lett. **55**, 1888 (1989).

[51] W. Walukiewicz, H. E. Ruda, J. Lagowski, and H. C. Gatos, Phys. Rev. B **30**, 4571 (1984).

[52] T. Seebeck, Proc. Prussian Acad. Sci., 265 (1822).

[53] J. Peltier, Ann. Chem. **LVI**, 371 (1834).

[54] G. S. Nolas, J. Sharp, and J. Goldsmid, *Thermoelectrics: Basic Principles and New Materials Developments*, Springer series in materials science No. v. 45 (Springer, Berlin Heidelberg, 2001).

[55] G. E. W. Bauer, E. Saitoh, and B. J. van Wees, Nat. Mater. **11**, 391 (2012).

[56] K. Uchida, S. Takahashi, K. Harii, J. Ieda, W. Koshibae, K. Ando, S. Maekawa, and E. Saitoh, Nature **455**, 778 (2008).

[57] J. Flipse, F. L. Bakker, A. Slachter, F. K. Dejene, and B. J. van Wees, Nat. Nanotechnol. **7**, 166 (2012).

[58] N. T. Hung, E. H. Hasdeo, A. R. T. Nugraha, M. S. Dresselhaus, and R. Saito, Phys. Rev. Lett. **117** (2016).

[59] A. Sommerfeld, Zeitschrift für Physik **47**, 1 (1928).

[60] A. Sommerfeld and N. H. Frank, Rev. Mod. Phys. **3**, 1 (1931).

[61] D. Salloch, U. Wieser, U. Kunze, and T. Hackbarth, Physica E **42**, 2618 (2010).

[62] R. Fleischmann and T. Geisel, Phys. Rev. Lett. **89**, 016804 (2002).

[63] S. de Haan, A. Lorke, J. P. Kotthaus, W. Wegscheider, and M. Bichler, Phys. Rev. Lett. **92**, 056806 (2004).

[64] S. de Haan, A. Lorke, J. P. Kotthaus, M. Bichler, and W. Wegscheider, Physica E **21**, 916 (2004).

[65] H. Q. Xu, Appl. Phys. Lett. **78**, 2064 (2001).

[66] H. Irie, Q. Diduck, M. Margala, R. Sobolewski, and M. J. Feldman, Appl. Phys. Lett. **93**, 053502 (2008).

[67] A. N. Jordan and M. Büttiker, Phys. Rev. B **77**, 075334 (2008).

[68] F. X. Bronold, in *Computational Many-Particle Physics*, Vol. 739, edited by H. Fehske, R. Schneider, and A. Weiße (Springer, Berlin Heidelberg, 2008) pp. 223–254.

[69] T. Kawamura and S. Das Sarma, Phys. Rev. B **45**, 3612 (1992).

[70] A. Kreschuk, M. Martisov, T. Polyanskaya, I. Savel'ev, I. Saidashev, A. Shik, and Y. Shmartsev, Solid State Commun. **65**, 1189 (1988).

[71] W. T. Kelvin, *Collected Papers I* (Cambridge University Press, 1882).

[72] L. Onsager, Phys. Rev. **37**, 405 (1931).

[73] F. G. Bass and Y. G. Gurevich, Sov. Phys. Usp. **14**, 113 (1971).

[74] P. W. Anderson, E. Abrahams, and T. V. Ramakrishnan, Phys. Rev. Lett. **43**, 718 (1979).

[75] H. Lohvinov, Y. Gurevich, and O. Titov, Rev. Mex. Fis. **49**, 482 (2003).

[76] E. L. Ivchenko and S. D. Ganichev, JETP Lett. **93**, 673 (2011).

[77] P. Olbrich, J. Karch, E. L. Ivchenko, J. Kamann, B. März, M. Fehrenbacher, D. Weiss, and S. D. Ganichev, Phys. Rev. B **83**, 165320 (2011).

[78] A. A. M. Staring, L. W. Molenkamp, B. W. Alphenaar, H. v. Houten, O. J. A. Buyk, M. A. A. Mabesoone, C. W. J. Beenakker, and C. T. Foxon, Europhys. Lett. **22**, 57 (1993).

[79] A. S. Dzurak, C. G. Smith, C. H. W. Barnes, M. Pepper, L. Martín-Moreno, C. T. Liang, D. A. Ritchie, and G. A. C. Jones, Phys. Rev. B **55**, R10197 (1997).

[80] M. C. Llaguno, J. E. Fischer, A. T. Johnson, and J. Hone, Nano Lett. **4**, 45 (2004).

[81] R. Scheibner, H. Buhmann, D. Reuter, M. N. Kiselev, and L. W. Molenkamp, Phys. Rev. Lett. **95**, 176602 (2005).

[82] S. F. Svensson, A. I. Persson, E. A. Hoffmann, N. Nakpathomkun, H. A. Nilsson, H. Q. Xu, L. Samuelson, and H. Linke, New J. Phys. **14**, 033041 (2012).

[83] O. Entin-Wohlman, Y. Imry, and A. Aharony, Phys. Rev. B **82**, 115314 (2010).

[84] S. Juergens, F. Haupt, M. Moskalets, and J. Splettstoesser, Phys. Rev. B **87**, 245423 (2013).

[85] B. Sothmann, R. Sánchez, A. N. Jordan, and M. Büttiker, New J. Phys. **15**, 095021 (2013).

[86] F. Mazza, R. Bosisio, G. Benenti, V. Giovannetti, R. Fazio, and F. Taddei, New J. Phys. **16**, 085001 (2014).

[87] S. Washburn and R. A. Webb, Rep. Prog. Phys. **55**, 1311 (1992).

[88] C. M. Marcus, A. J. Rimberg, R. M. Westervelt, P. F. Hopkins, and A. C. Gossard, Phys. Rev. Lett. **69**, 506 (1992).

[89] H. Predel, H. Buhmann, L. W. Molenkamp, R. N. Gurzhi, A. N. Kalinenko, A. I. Kopeliovich, and A. V. Yanovsky, Phys. Rev. B **62**, 2057 (2000).

[90] S. F. Fischer, G. Apetrii, S. Skaberna, U. Kunze, D. Reuter, and A. D. Wieck, Appl. Phys. Lett. **81**, 2779 (2002).

[91] A. Javey, J. Guo, M. Paulsson, Q. Wang, D. Mann, M. Lundstrom, and H. Dai, Phys. Rev. Lett. **92**, 106804 (2004).

[92] J. M. Buhmann and M. Sigrist, Phys. Rev. B **88**, 115128 (2013).

[93] C. Hua and A. J. Minnich, Phys. Rev. B **89**, 094302 (2014).

[94] J.-S. Wang, J. Wang, and J. T. Lü, Eur. Phys. J. B **62**, 381 (2008).

[95] C. Possanzini, R. Fletcher, P. T. Coleridge, Y. Feng, R. L. Williams, and J. C. Maan, Phys. Rev. Lett. **90**, 176601 (2003).

[96] S. Faniel, E. Tutuc, E. P. De Poortere, C. Gustin, A. Vlad, S. Melinte, M. Shayegan, and V. Bayot, Phys. Rev. Lett. **94**, 046802 (2005).

[97] W. E. Chickering, J. P. Eisenstein, L. N. Pfeiffer, and K. W. West, Phys. Rev. B **81**, 245319 (2010).

[98] L. Moldovan, S. Melinte, V. Bayot, S. J. Papadakis, E. P. De Poortere, and M. Shayegan, Phys. Rev. Lett. **85**, 4369 (2000).

[99] S. Goswami, C. Siegert, M. Baenninger, M. Pepper, I. Farrer, D. A. Ritchie, and A. Ghosh, Phys. Rev. Lett. **103**, 026602 (2009).

[100] B. L. Gallagher, T. Galloway, P. Beton, J. P. Oxley, S. P. Beaumont, S. Thoms, and C. D. W. Wilkinson, Phys. Rev. Lett. **64**, 2058 (1990).

[101] W. Hänsch and M. Miura-Mattausch, J. Appl. Phys. **60**, 650 (1986).

[102] U. Sivan and Y. Imry, Phys. Rev. B **33**, 551 (1986).

[103] B. Laikhtman and S. Luryi, Phys. Rev. B **49**, 17177 (1994).

[104] V. K. Dugaev, V. I. Litvinov, and P. P. Petrov, Phys. Rev. B **52**, 5306 (1995).

[105] E. H. Hwang and S. Das Sarma, Phys. Rev. B **77**, 235437 (2008).

[106] Y. M. Blanter and M. Büttiker, Phys. Rev. Lett. **81**, 4040 (1998).

[107] S. Sassine, Y. Krupko, J. C. Portal, Z. D. Kvon, R. Murali, K. P. Martin, G. Hill, and A. D. Wieck, Phys. Rev. B **78**, 045431 (2008).

[108] M. Büttiker, Z. Phys. B **68**, 161 (1987).

[109] G. Chen, J. Appl. Phys. **97**, 083707 (2005).

[110] K. Bløtekjær, IEEE T. Electron. Dev. **17**, 38 (1970).

[111] B. K. Ridley, *Quantum Processes in Semiconductors* (Oxford Science Publications, 1993).

[112] T. Kawamura and S. Das Sarma, Phys. Rev. B **42**, 3725 (1990).

[113] D. Mintzer, Phys. Fluids **8**, 1076 (1965).

[114] P. B. Allen, Phys. Rev. B **17**, 3725 (1978).

[115] V. Bezák, M. Kedro, and A. Pevala, Thin Solid Films **23**, 305 (1974).

[116] K. Fuchs, Math. Proc. Cambridge Philos. Soc. **34**, 100 (1938).

[117] R. B. Dingle, Proc. R. Soc. Lond. A **201**, 545 (1950).

[118] R. G. Chambers, Proc. R. Soc. Lond. A **202**, 378 (1950).

[119] M. N. Baibich, J. M. Broto, A. Fert, F. N. Van Dau, F. Petroff, P. Etienne, G. Creuzet, A. Friederich, and J. Chazelas, Phys. Rev. Lett. **61**, 2472 (1988).

[120] G. Binasch, P. Grünberg, F. Saurenbach, and W. Zinn, Phys. Rev. B **39**, 4828 (1989).

[121] R. E. Camley and J. Barnaś, Phys. Rev. Lett. **63**, 664 (1989).

[122] J. Barnaś, A. Fuss, R. E. Camley, P. Grünberg, and W. Zinn, Phys. Rev. B **42**, 8110 (1990).

[123] R. Q. Hood and L. M. Falicov, Phys. Rev. B **46**, 8287 (1992).

[124] D. J. Thouless, Phys. Rev. Lett. **39**, 1167 (1977).

[125] D. Thouless, Phys. Rep. **13**, 93 (1974).

[126] R. G. Chambers, Proc. R. Soc. Lond. A **65**, 458 (1952).

[127] E. Sondheimer, Adv. Phys. **1**, 1 (1952).

[128] R. Bosisio, G. Fleury, and J.-L. Pichard, New J. Phys. **16**, 035004 (2014).

[129] P. N. Butcher, J. Phys.: Condens. Matter **2**, 4869 (1990).

[130] D. Schroeder, Proc. of SISDEP **3**, 343 (1988).

[131] H. Lin, N. Goldsman, and I. Mayergoyz, Solid-State Electron. **35**, 769 (1992).

[132] R. T. Syme, M. J. Kelly, and M. Pepper, J. Phys.: Condens. Matter **1**, 3375 (1989).

[133] K. Hirakawa and H. Sakaki, Phys. Rev. B **33**, 8291 (1986).

[134] K. Hirakawa and H. Sakaki, Appl. Phys. Lett. **49**, 889 (1986).

[135] H. Linke, Appl. Phys. A: Mater. Sci. Process. A **75**, 167 (2002).

[136] P. Olbrich, E. L. Ivchenko, R. Ravash, T. Feil, S. D. Danilov, J. Allerdings, D. Weiss, D. Schuh, W. Wegscheider, and S. D. Ganichev, Phys. Rev. Lett. **103**, 090603 (2009).

Acknowledgments

At this point, I would like to thank all the people who contributed to this thesis. First of all, I want to thank my supervisor Prof. Dr. Jürgen König for the possibility to work in his group. He was always open to discussions and gave me the opportunity to attend various conferences and workshops. I learned a lot under his mentoring. After my time in his group, when I started working in the insurance industry, it was difficult for me to hold contact and keep working on my thesis. I am grateful for his patience during that time. Furthermore, I thank Prof. Dr. Tero Heikkilä for reviewing my thesis.

The research that led to this thesis was accompanied by discussions with Prof. Dr. Axel Lorke und Dr. Arkadius Ganczarczyk related to the interpretation of their experimental results. I thank both for the very interesting discussions and the opportunity working together. I would also like to thank Dr. Fred Hucht for his advises concerning numerical challenges.

When I started with my work, I was indirectly supported by Dr. Daniel Urban. I am honored to have worked on the same topic as he did during his last days.

I am very thankful for my time in the group of Prof. Dr. Jürgen König, not only for the scientific work, but also for the time with my colleges. I would like to thank them for that time. I especially want to thank Dr. Stephan Lindebaum, Dr. Bastian Hiltscher, Dr. David Futterer, Nina Winkler, Dr. Philipp Stegmann, Dr. Stephan Weiß and Prof. Dr. Björn Sothmann.

For their support during my studies, I want to warmly thank my parents, Hilke and Dr. Dieter Rojek. My father and my brother, Karsten Rojek, proof-read my thesis. I am very thankful for their comments and their time.

Since 2014 I have been working for the insurance company ARAG SE. I also thank my superiors for enabling me to keep working on my thesis.

My wife, Julia Rojek, supported me all the time with her love. I am grateful for sharing my life with her and for our unborn child. They finally made it possible to finish my thesis.

Stephan Rojek, November 2017

Publications

I. A. Ganczarczyk, S. Rojek, A. Quindeau, M. Geller, A. Hucht, C. Notthoff, J. König, A. Lorke, D. Reuter, and A. D. Wieck,
"Transverse rectification in density-modulated two-dimensional electron gases",
Phys. Rev. B **86**, 085309 (2012).

II. S. Rojek, J. König, and A. Shnirman,
"Adiabatic pumping through an interacting quantum dot with spin-orbit coupling",
Phys. Rev. B **87**, 075305 (2013).

III. S. Rojek, M. Governale, and J. König,
"Spin pumping through quantum dots",
Phys. Status Solidi B **251**, 1912 (2014).

IV. S. Rojek and J. König,
"Mesoscopic diffusion thermopower in two-dimensional electron gases",
Phys. Rev. B **90**, 115403 (2014).

The work presented in this thesis is motivated by an experiment published by Ganczarczyk *et al.* in Ref. I. The experimental results can be interpreted in the framework of the theory presented in Chapter 2 of this thesis. The results shown in Chapter 2 have been published in Ref. IV. However, this thesis goes beyond that publication, especially by the content of Chapter 3 which has not been published yet.